


1993

Mechanics of unsaturated granular media

Steven Mark Levorson
Iowa State University

Follow this and additional works at: <https://lib.dr.iastate.edu/rtd>

 Part of the [Civil Engineering Commons](#), and the [Materials Science and Engineering Commons](#)

Recommended Citation

Levorson, Steven Mark, "Mechanics of unsaturated granular media " (1993). *Retrospective Theses and Dissertations*. 10836.
<https://lib.dr.iastate.edu/rtd/10836>

This Dissertation is brought to you for free and open access by the Iowa State University Capstones, Theses and Dissertations at Iowa State University Digital Repository. It has been accepted for inclusion in Retrospective Theses and Dissertations by an authorized administrator of Iowa State University Digital Repository. For more information, please contact digirep@iastate.edu.

9 4

1 3 9 9 7

UMI

MICROFILMED 1994

INFORMATION TO USERS

This manuscript has been reproduced from the microfilm master. UMI films the text directly from the original or copy submitted. Thus, some thesis and dissertation copies are in typewriter face, while others may be from any type of computer printer.

The quality of this reproduction is dependent upon the quality of the copy submitted. Broken or indistinct print, colored or poor quality illustrations and photographs, print bleedthrough, substandard margins, and improper alignment can adversely affect reproduction.

In the unlikely event that the author did not send UMI a complete manuscript and there are missing pages, these will be noted. Also, if unauthorized copyright material had to be removed, a note will indicate the deletion.

Oversize materials (e.g., maps, drawings, charts) are reproduced by sectioning the original, beginning at the upper left-hand corner and continuing from left to right in equal sections with small overlaps. Each original is also photographed in one exposure and is included in reduced form at the back of the book.

Photographs included in the original manuscript have been reproduced xerographically in this copy. Higher quality 6" x 9" black and white photographic prints are available for any photographs or illustrations appearing in this copy for an additional charge. Contact UMI directly to order.

U·M·I

University Microfilms International
A Bell & Howell Information Company
300 North Zeeb Road, Ann Arbor, MI 48106-1346 USA
313/761-4700 800/521-0600



Order Number 9413997

Mechanics of unsaturated granular media

Levorson, Steven Mark, Ph.D.

Iowa State University, 1993

U·M·I

**300 N. Zeeb Rd.
Ann Arbor, MI 48106**



Mechanics of unsaturated granular media

by

Steven Mark Levorson

**A Dissertation Submitted to the
Graduate Faculty in Partial Fulfillment of the
Requirements for the Degree of
DOCTOR OF PHILOSOPHY**

**Department: Civil and Construction Engineering
Major: Civil Engineering
(Geotechnical Engineering)**

Approved:

Signature was redacted for privacy.

In Charge of Major Work

Signature was redacted for privacy.

For the Major Department

Signature was redacted for privacy.

For the Graduate College

Members of the Committee:

Signature was redacted for privacy.

**Iowa State University
Ames, Iowa**

1993

TABLE OF CONTENTS

	PAGE
1. INTRODUCTION	1
1.1 Scope and objectives	3
1.2 Explanation of format	4
2. REVIEW OF LITERATURE	5
2.1 The concept of effective stress	5
2.1.1 Effective stress in unsaturated soils	7
2.1.2 Unsaturated effective stress equations	8
2.1.3 Limitations to the effective stress equation	10
2.1.4 Major engineering problems in unsaturated materials	12
2.2 Total stress models of strength in unsaturated material	13
2.3 Packing density in dry materials	16
2.4 Packing density in partially saturated soils	19
3. MOISTURE-DENSITY RELATIONS IN SAND: EXPERIMENTAL RESULTS	23
3.1 Introduction	23
3.2 Materials	23
3.2.1 Gradation preparation and control	25
3.2.2 Impact of gradation variance	27
3.2.3 Particle density	27
3.3 Testing procedure	28
3.3.1 Minimum index density tests	30
3.3.2 Maximum index density tests	31
3.3.3 Modifications and additions to the standards	31
3.3.4 Calibration of equipment	33
3.3.5 Nonlinear least squares regression	35
3.4 Presentation of results	35
3.5 Discussion	37
3.5.1 Maximum index density	39
3.5.2 Bulking	42
3.6 Conclusions	43
4. MOISTURE-PRESSURE RELATIONS IN SAND: EXPERIMENTAL RESULTS	44
4.1 Introduction	44
4.1.1 Background	44
4.2 The moisture characteristic curve	47
4.3 Measurement techniques	53
4.4 Experimental procedure	58
4.4.1 Sample preparation	58
4.4.2 Pressure measurement	58

4.4.3	Density and moisture content measurements . . .	59
4.4.4	Measurement precision and accuracy	61
4.5	Curve fitting technique and results	63
4.5.1	Analysis of the parameters α , n , and m	64
4.6	Experimental results and discussion	66
5.	COMPARISON OF PARTICLE AND PORE SIZE DISTRIBUTIONS . . .	71
5.1	Introduction	71
5.2	Calculations of pore size distribution	71
5.2.1	Limitations of the capillary tube model	73
5.3	Discussion of pore size distributions	73
5.4	Conceptual model of pore and particle size distributions	80
6.	EQUIVALENT PORE PRESSURES IN PARTIALLY SATURATED SYSTEMS	82
6.1	Introduction	82
6.2	Continuum mechanics approach	83
6.3	Micromechanical approach	85
6.4	Resolution of effective and total stress concepts .	87
6.4.1	Equality of tensile stress and equivalent pore pressure	88
6.5	Equivalent pore pressure model	90
6.5.1	Capillary state model	91
6.5.2	Pendular state model	93
6.5.3	Funicular state model	95
6.5.4	Parameters for the equivalent pore pressure model	97
6.6	Estimates of specific surface mean diameter	98
6.6.1	Comparison of mean diameters	99
7.	COMPRESSIVE STRENGTH IN PARTIALLY SATURATED SYSTEMS .	101
7.1	Introduction	101
7.2	Shear strength as a function of negative pore pressure	101
7.2.1	Relationship between friction angle and initial density	103
7.2.2	Limitations of the model	106
7.3	Comparison of measured and predicted strengths .	107
7.3.1	Experimental method	108
7.3.2	Presentation of results	109
7.3.3	Modifications to model A	114
7.3.4	Direct comparison of predictions and data .	116
7.4	Discussion	118
8.	DISCUSSION OF EXPERIMENTAL AND MODELING RESULTS . . .	123
8.1	Shear strength	125
8.1.1	Empirical model	125

9. APPLICATION TO COAL HANDLING	127
9.1 Introduction	127
9.2 The handleability index	128
9.3 Summary of EPRI experimental project	129
9.4 Handleability classification	131
9.4.1 Modifications to the classification system	133
10. CONCLUSIONS	139
10.1 Recommendations for application and further development	142
REFERENCES	144
ACKNOWLEDGEMENTS	152
APPENDIX A: MOISTURE-DENSITY DATA	153
APPENDIX B: MOISTURE RETENTION DATA	155
APPENDIX C: UNCONFINED STRENGTH DATA	157

LIST OF TABLES

	PAGE
Table 3.1	Analysis of gradation variance 28
Table 3.2	Relative density classification 30
Table 3.3	Results of least squares regression 37
Table 3.4	Measured and predicted maximum and minimum dry densities (g/cc) 40
Table 4.1	Typical soil moisture parameters 51
Table 4.2	Relative density of moisture retention samples 61
Table 4.3	Regression analysis of moisture characteristic data 67
Table 4.4	Moisture characteristic data 69
Table 6.1	Comparison of predicted and measured values . 100

LIST OF FIGURES

	PAGE
Figure 2.1 Total stress representation of the Mohr-Coulomb failure criterion for unsaturated granular media	15
Figure 3.1 Target gradations used in this study	25
Figure 3.2 Calibration results for double amplitude control setting	34
Figure 3.3 Results of maximum density testing for the five gradations	36
Figure 3.4 Relative density versus saturation for the five gradations under conditions of maximum index density compaction	38
Figure 3.5 Dependence of maximum/minimum index densities on gradation exponent	41
Figure 4.1 Schematic of a general moisture characteristic curve	48
Figure 4.2 Schematic of the effect of compaction or desiccation on a moisture characteristic curve	54
Figure 4.3 Schematic of hanging water column	55
Figure 4.4 Schematic of mercury tensiometer	56
Figure 4.5 Schematic of a pressure plate cell	57
Figure 4.6 Sensitivity of van Genuchten's equation to changes in the parameter α	65
Figure 4.7 Sensitivity of van Genuchten's equation to changes in the parameter n	66
Figure 4.8 Sensitivity of van Genuchten's equation to changes in the parameter m	67
Figure 4.9 Moisture retention data and fitted drainage curves for five sand gradations	69

Figure 4.10	Semi-logarithmic presentation (pF) of moisture retention data and fitted drainage curves for five sand gradations	70
Figure 5.1	Cumulative pore size distributions according to equations 4.5 and 5.1	74
Figure 5.2	Particle size frequency distribution	75
Figure 5.3	Pore size frequency distribution	76
Figure 5.4	Relationship between equivalent pore diameters at the moisture characteristic curve flex points and gradation exponents	78
Figure 5.5	Fraction of pore volume attributable to the pendular, funicular, and capillary moisture ranges	80
Figure 6.1	Total and effective stress representation of unconfined compressive strength for non-cohesive materials	89
Figure 6.2	Diagram of the equivalent pore pressure model as a function of saturation level	98
Figure 7.1	Relationship between initial void ratio and friction angle for a medium fine sand (Rowe, 1962)	104
Figure 7.2	Relationship between initial void ratio and friction angle for $n = 0.2$ and $n = 0.8$ gradations	105
Figure 7.3	Measured and predicted strengths ($n = 0.2$ & 0.4)	110
Figure 7.4	Measured and predicted strengths ($n = 0.5$ & 0.6)	111
Figure 7.5	Measured and predicted strengths ($n = 0.8$) .	112
Figure 7.6	Comparison of model predictions and data . .	117
Figure 7.7	Comparison of models and data for $10\% < S < 60\%$	119
Figure 7.8	Summary of failure mode observations from unconfined strength tests	121
Figure 9.1	Initial handleability classification (from Lohnes and Levorson, 1992)	132

Figure 9.2	Comparison of predicted (eq. 9.3) and experimentally determined values of handleability index (HI)	135
Figure 9.3	Handleability index classification flowchart for topsize less than 8 mm (n = gradation exponent, UW = unit weight-kN/cu.m., w = moisture content-%)	137
Figure 9.4	Handleability index classification flowchart for topsize greater than 8 mm (n = gradation exponent, UW = unit weight-kN/cu.m., w = moisture content-%)	138

1. INTRODUCTION

Engineers deal with both natural and manufactured granular materials everyday. Soils and foundation engineers routinely design foundation systems on sandy alluvium to support structures or embankments. They also specify granular material as a construction material for structural fill, road bases, filters, and drainage layers. Granular material is not limited to soils, however. Engineers often work with particulates either as raw material or finished product in processing plants. For example, processing ore is based on size reduction in order to better separate valuable metals from the host rock. In cases where an entire formation is mined as the finished product (e.g., limestone and coal) size reduction is necessary to enhance handling and transportation. But, when dealing with very fine powders (e.g., pharmaceuticals, plastics, coal filter cake) the particle size may be increased by agglomeration, pelletization, or briquetting to reduce handling problems associated with fine particles. In all of these materials, the behavior during handling, transportation, compaction, and flow plays varying roles. In other words, the mechanical characteristics of the material controls the behavior of the material in different applications.

Part of the variability in mechanical behavior of particulate systems stems from the range and frequency of particle sizes. Naturally occurring particulates owe their gradation

properties to the geologic processes which formed and deposited them. Depending on the processes, this can result in gradations ranging from very uniform to multi-modal to well graded. Particulates manufactured from geologic materials owe some of their gradation properties to the processes of formation and deposition of their parent material. These processes control the abundance and orientation of fractures, cracks and other weaknesses within the parent material which are exploited during size reduction operations. Different crushing operations leave a signature on the resulting material in the form of controlled top size and particle size distribution. In addition, the environment contributes variations in moisture content that limit or enhance storage, handling, and transportation practices.

Taking the coal fired power industry as an example; coal is alternately compacted for storage in stockpiles, reclaimed for handling, expected to flow under gravity forces through chutes and hoppers, allowed to consolidate under both self weight and vibratory forces in bunkers, silos and bins, again expected to flow under gravity forces, segregated by size or mixed to reduce segregation before finally being pulverized for injection into boilers. For these reasons, the compaction and shear strength behavior of the coal is of vital importance at various points in the handling circuit.

As moisture contents fluctuate during handling and storage, the strength and compaction characteristics of the material fluctuate as well. In essence, changes in moisture content, particle size distribution, or density create a new material with a totally different mechanical behavior. Similarly, the range of mechanical behavior in any remolded granular medium is a function of changes in moisture level either during or subsequent to the remolding process.

1.1 Scope and objectives

The objective of this research is to investigate the effect of particle size distribution on the mechanics of remolded, unsaturated, granular materials. The compaction and shear strength behavior of the material is explained in terms of the effect of the interparticle forces due to the gas and liquid phases. This analysis is supported by experimental evidence of the interaction and distribution of the three phases on the compacted density, the moisture retention capacity, pore size distribution, and shear strength for five controlled gradations of sand and silt.

Further, the effect of the pore phases on the mechanics of the material is analyzed in terms of the effective stress concept for partially saturated materials. In this analysis, the actual pressures in each phase are taken into account when explaining the behavior of the material.

Finally, the various aspects of the research are drawn together to formulate an explanation for the behavior of crushed coal during handling, storage, and transportation in coal fired power plants. This approach is then used to develop recommendations and strategies to reduce operating problems associated with coal handling.

1.2 Explanation of format

Chapter two provides a literature review on the subjects of effective and total stress modeling of unsaturated materials and an overview of existing compaction theories. Further references which are particularly significant to specific aspects of the studies are provided in applicable sections.

Chapters three through seven present five experimental and/or analytical studies dealing with the interrelationship of moisture, density, moisture tension, pore and particle size distribution, and shear strength in unsaturated particulates. The results of these studies are synthesized into an empirical theory in chapter eight. This is followed by an examination of the mechanical behavior of unsaturated, crushed coal in light of the conclusions drawn in chapter eight. Chapter ten presents the conclusions of this research and recommendations for its application and further development.

2. REVIEW OF LITERATURE

2.1 The concept of effective stress

The concept of effective stresses was first proposed by Terzaghi in 1923 to provide a rational basis for describing changes in volume and changes in shear strength in soils subject to fluid pressures. In 1936, Terzaghi restated the principle of effective stress as:

The stresses in any point of a section through a mass of soil can be computed from the *total principal stresses* $\sigma_1, \sigma_2, \sigma_3$ which act in this point. If the voids of the soil are filled with water under stress, u , the total principal stresses consist of two parts. One part, u , acts in the water and in the solid in every direction with equal intensity. It is called the *neutral stress* [or pore water pressure]. The balance $\bar{\sigma}_1 = \sigma_1 - u, \bar{\sigma}_2 = \sigma_2 - u, \bar{\sigma}_3 = \sigma_3 - u$ represents an excess over the neutral stress, u , and it has its seat exclusively in the solid phase of the soil.

This fraction of the total principal stresses will be called the *effective principal stress* A change in the neutral stress, u , produces practically no volume change and has practically no influence on the stress conditions for failure Porous materials (such as sand, clay and concrete) react to a change in u as if they were incompressible and as if their internal friction were equal to zero. All the measurable effects of a change in stress, such as compression, distortion and a change of shearing resistance are exclusively due to changes in the effective stresses $\bar{\sigma}_1, \bar{\sigma}_2, \bar{\sigma}_3$. Hence every investigation of the stability of a saturated body of soil requires the knowledge of both the total and the neutral stresses (as cited by Bishop and Blight, 1963, pp. 177-178).

Bishop and Eldin (1950), Bishop (1959), and Skempton (1960) have shown that Terzaghi's effective stress expression, $\bar{\sigma} = \sigma - u$, holds rigorously for both volume change and shear strength if the following two conditions are imposed (Bishop and Blight, 1963):

- 1) The soil grains are incompressible.
- 2) The yield strength of the solids, which controls both particle to particle contact area and shearing resistance, is independent of confining pressure ... (178).

In reality, soils do not fulfill these conditions rigorously. However, in general engineering applications where the range of stresses is not great, the differences between observable and theoretical behavior are so small that they are not experimentally evident. Bishop and Blight (1963) proposed that the departure of real soil behavior from the conditions stated above does not invalidate the principle of effective stress. They distinguish between the principle itself and the algebraic expressions used to represent the relationships between total stress and pore pressures.

On this basis, the effective stress is, by definition, that function of total stress and pore pressure which controls the mechanical effects of a change in stress, such as volume change and a change in shear strength. The principle of effective stress is the assertion that such a function exists, with determinate parameters, under a given set of conditions (Bishop and Blight, 1963, p. 178).

2.1.1 Effective stress in unsaturated soils

Aitchison and Donald (1956) state that an implicit assumption in Terzaghi's effective stress concept as applied to unsaturated soils is that the principle of effective stress is not invalidated by changes in the physical state of the pore fluid or by changes in the degree of saturation as a function of the pore pressures. However, Terzaghi's equation, as originally written, assumes that the pore pressures act equally over the entire plane of interest. This is not the case in partially saturated soils where both water and air pressures act on different areas. Aitchison (1960a) advocated that the effective stress could be calculated if the water phase is treated differently depending on the nature of the pore water geometry.

Aitchison (1956) further proposed that unsaturated soil be defined as soil, which at a specific condition of external stresses, can absorb air-free water supplied at atmospheric pressure. This would include three phase (gas, liquid, solid) soils, and saturated swelling soils which can increase their void volume at constant external stress and atmospheric pressure. It would not, however, include soils with large pores which are drainable under atmospheric conditions such as permeable, crushed stone, base courses.

In order to clarify the terminology used to describe the concept of equivalent pore pressures in unsaturated soils,

Croney and Coleman (1960) promoted using suction to describe the pressure deficiency in an unsaturated soil sample free from external stresses. The equivalent negative pore pressure was then defined as the pressure deficiency existing at the stress regime relevant to the situation under consideration.

Matyas and Radhakrishna (1968) stated that any form of an effective stress equation should be able to satisfy:

- (a) the boundary cases for full saturation and for a completely dry state.
- (b) the behavior (volume change and shear strength) of a soil element exposed to a change in stress should be predictable in terms of effective stresses and should be independent of the manner in which the total stresses and the pore pressures change.
- (c) the correctness of the form of such an effective stress equation should be verified experimentally (434).

2.1.2 Unsaturated effective stress equations

Bishop and Eldin (1950), introduced an equation for the computation of effective stress in unsaturated soils:

$$\bar{\sigma} = \sigma - u_a + X(u_a - u_w) \quad (2.1)$$

where $\bar{\sigma}$ is the effective normal stress, σ is the total normal stress, u_a is the pressure in the gas phase, u_w is the pressure in the liquid phase, and X is a proportionality parameter. In this form, two stress state parameters ($\sigma - u_a$ and $u_a - u_w$) as well as one material state parameter (X) provide the basis for

analysis of experimental results. It is generally agreed that this form of the effective stress equation provides a practical basis for defining those stress state parameters which have proved most useful in interpreting experimental results.

Skempton (1960) proposed that Bishop's equation be restated as:

$$\sigma' = \sigma - [u_a + X(u_a - u_w)] \quad (2.2)$$

which could be written as:

$$\sigma' = \sigma - S_x \cdot u_w \quad (2.3)$$

where,

$$S_x = 1 + (1 - X) \frac{u_a - u_w}{u_w} \quad (2.4)$$

Therefore, $S_x u_w$ could be considered as an equivalent pore pressure.

Fredlund (1979) suggested that the traditional view of unsaturated soil as a three phase system be amended to include the liquid-gas interface as a fourth phase and that the effective stress equation be modified to include this term. Allam and Sridharan (1987) also proposed a more comprehensive effective stress equation which included terms for the contribution of the liquid-gas interface as well the osmotic pressure.

2.1.3 Limitations to the effective stress equation

Aitchison (1960a) cautioned against trying to reconcile effective or intergranular stress at the microstructure level with the mechanistic or macrostructure level. He suggested that effective stress in unsaturated soils be redefined as the combination of three phase stresses necessary to cause a change in the shear strength or volume of a soil equivalent to that of an externally applied effective stress in a saturated soil.

Jennings and Burland (1962) argued that the principle of effective stress could not explain cases of collapse or swell in unsaturated soils and that the expressions for effective stress had to be limited to application in certain ranges of saturation only. They further suggest that the structural changes in unsaturated soils due to changes in suction are very different from the structural changes due to consolidation by external loading.

Griffiths and Joshi (1989) present the results of Mercury Intrusion Porosimetry investigations on samples consolidated to different stress levels in an odometer which indicate that the pore structure is not brittle, but that collapse of large pores occurs in increments. Griffiths and Joshi (1989) went further, using a double intrusion technique, and conclude that increases in the external consolidation stress do not tend to create aggregation of clay particles; rather, the increased

consolidation is the result of reduction of the interaggregate pore volume. In their discussion of Griffith and Joshi's work, Nagaraj et al. (1990) generally support the authors' conclusions but add that dehydration can cause a reduction in very fine pore volume. They suggest that this is due to higher suction pressures in very fine pores than can be achieved in conventional consolidation tests.

Aitchison (1956) shows that highly compressible soils (mainly clays) can exhibit large void ratio changes as moisture is removed, and yet remain almost completely saturated. Aitchison and Donald (1956) further demonstrate a functional relationship between void ratio and pressure deficiency in high clay content soils which remain saturated while exhibiting high degrees of shrinkage.

In incompressible soils (sands) which exhibit no volume change, only drainage, as suction increases, the pressure deficiency can be stated as a function of the saturation level and the initial density (Aitchison, 1956). In these soils, the maximum suction generally occurs at saturation levels near 10% and exceeds 1000 kPa (Aitchison and Donald, 1956). The moisture characteristic curve in this case represents the initial pore size distribution of the soil (Aitchison, 1956).

Aitchison (1956) concludes that for a moisture characteristic curve to be useful in soil mechanics applications, such information as the stress-strain characteristics dependent on

the circumstances of desaturation must be included. Thus, in most naturally occurring soils, the saturation level, pressure deficiency, and void ratio of the soil are mutually dependent (Aitchison and Donald, 1956).

Jennings and Burland (1962) conclude that the occurrence of collapse and heave in soils cannot be explained in terms of effective stresses. They propose that there is a "critical" saturation level below which the effective stress law is not valid and that this limiting saturation level can be correlated to the particle size of the soil. In their observations, collapse will not occur upon wetting for materials compacted above saturation levels of 20% for crushed rock (-3/8" to +48 mesh), to 45 to 60% for sandy silts and silts, to 90% for silty clays. The argument for these conclusions stems from a series of double odometer and isotropic consolidation tests conducted by Jennings and Burland.

2.1.4 Major engineering problems in unsaturated materials

Jennings (1960) listed the following as major engineering problems associated with unsaturated soils which can not yet be predicted with any accuracy:

- a) The magnitude and time rate of settlements due to the compressibility of the air phase.
- b) The time rate of heave due to swelling of desiccated clays.
- c) The time rate and physical mechanism of settlement due to collapse of sands and silts under-

going saturation. Here, time rate can not be predicted, however, collapse is usually instantaneous.

- d) Variations in soil shear strength due to variable moisture content over the life of a structure.

2.2 Total stress models of strength in unsaturated material

Research into the interaction of three phase (solid, liquid, gas) systems originally grew out of work done in soil science to explain moisture holding capacity of agronomic soils. Recognition of the importance of these findings by soils engineers led to the development of the effective stress theory for unsaturated soils. However, this theory was preceded by total stress theories in which the bonding effect of the liquid phase was simply added to the frictional resistance of the solid phase and incorporated in the cohesion term of Coulomb's shear strength equation:

$$\tau = c + \sigma \tan\phi \quad (2.5)$$

where τ is the shear strength, c is cohesion, ϕ is the angle of internal friction, and $\tan\phi$ is the coefficient of friction. In the total stress approach cohesion becomes a function of moisture level rather than an inherent property of the material and is therefore commonly referred to as "apparent" cohesion.

The branches of chemical and mechanical engineering which are involved in designing systems to handle industrial particulates and in developing agglomeration, briquetting, and pelletization processes originally drew on the total stress theory developed by soil mechanics and agronomy researchers. However, the close ties among the three disciplines which are evident in pre-1950's literature are not evident in more recent research. Where soil mechanics researchers turned to the effective stress concept in order to describe the mechanics of unsaturated materials, researchers in industrial powder and particulate applications turned to elaborate micromechanistic models of shear strength. These models predict the apparent tensile strength caused by the negative pressures in the moisture and incorporate this tensile strength into equation 2.1 as part of the apparent cohesion.

Just as Bishop, Aitchison, Coleman and others pioneered the effective stress concept for unsaturated soils, Rumpf (1958, 1962), Rumpf and Turba (1964), Newitt and Conway-Jones (1958), and Schubert (1975, 1984) have led the way in total stress modeling. The basic premise in these models is that the bonding forces between particles due to moisture tension, solid interlocking, viscous binding, short range electrical forces, and cementation of chemical precipitates create a tensile strength in the material. This tensile strength is the normal stress intercept of the Mohr-Coulomb relationship in

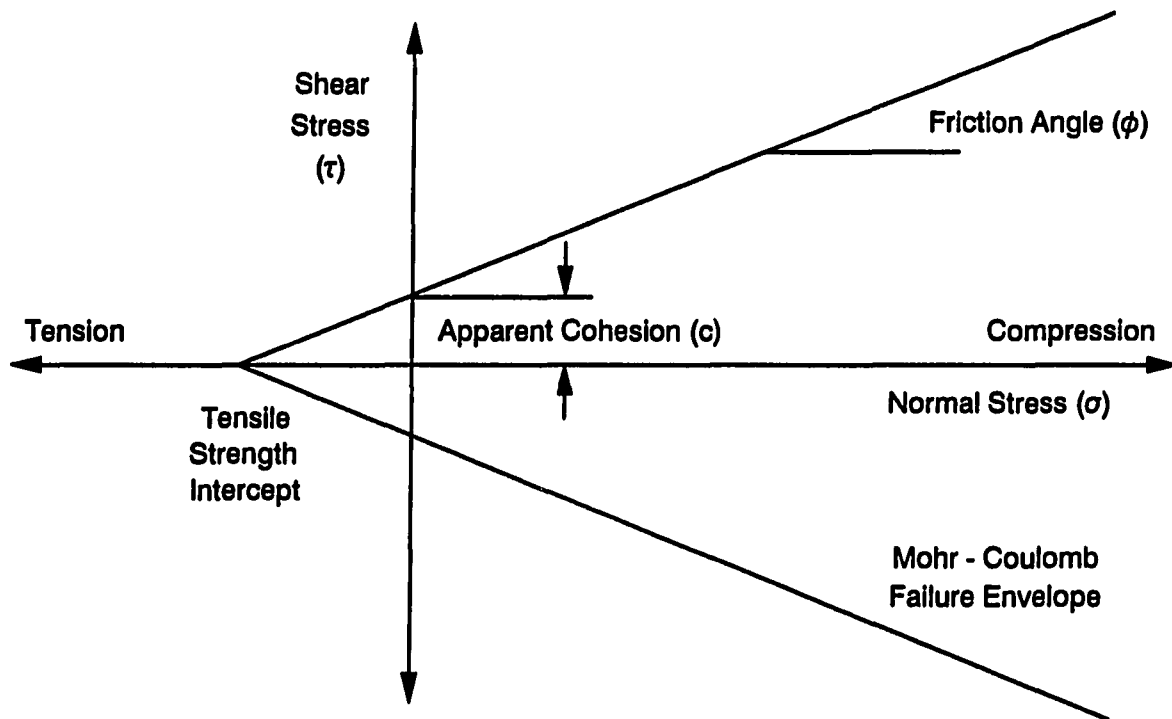


Figure 2.1 Total stress representation of the Mohr-Coulomb failure criterion for unsaturated granular media

Figure 2.1. The magnitude of the tensile strength directly affects the shear strength of the material under compressive normal stresses and can be related to the apparent cohesion (Fig. 2.1). Because the tensile strength is a function of the amount of moisture in the material, the shear strength becomes a function of the moisture content, with different Mohr envelopes for each moisture content. This necessitates experimen-

tal determination of separate Mohr envelopes for each moisture content (Jenike, 1961 and 1964).

In application, these tensile strength models depend on many of the relations developed to relate gradation, coordination number, and packing geometry described in the next section. From these, idealized geometries of the microstructure are developed and statistical theory is used to expand the basic, interparticle force equations from the micromechanical to macromechanical scale. In final form, the models become functions of the following primary variables: particle size and shape, porosity, and moisture content. In addition to the models of Rumpf and Schubert, other similar models have been developed by: Ashton et al. (1965), Cheng (1968), Kočova and Pilpel (1973), Shinohara and Tanaka (1969; reported by Schubert, 1975), and Tsunakawa and Aoki (1972).

2.3 Packing density in dry materials

Considerable effort has gone into the study of the packing state of dry, granular materials. Theoretical studies of ordered packing of monosized spheres were conducted by Manegold, Hoffman, and Solf (1931), Manegold and von Engelhardt (1933), and Graton and Fraser (1935). These studies established relationships between porosity, packing mode, and number of contacts between particles (coordination number).

The results of these studies are confirmed by experimental studies of monosized lead, steel, and bronze balls conducted by Westman and Hugill (1930), and Macrae and Gray (1960 reported by Gray, 1960). These studies also established empirical relationships between porosity and coordination number for randomly ordered systems that allow interpolation and limited extrapolation of the results to other systems.

McGreary (1961) experimentally investigated the effect of size on the packing density of monosized spheres and found that decreasing size decreased the poured, or loosest possible, density of the system. Decreasing size was also shown to influence the final, vibrated density of the system because of the effect on initial packing density. The explanation is that the decreased size of the individual particles increases the surface area of the system, making the adhesion and frictional properties of individual particles more pronounced.

Carman (1938) and Coulson (1949) extended the experimental data base with their work in non-spherical, monosized systems. Evans and Millman (1956) and Orr (1966) showed that non-spherical particles exhibited looser packing arrangements in cascaded deposition but attained denser packing arrangements than spherical particles when subjected to vibration or pressure.

Andreasen and Andersen (1930), White and Walton (1937), and Heywood (1946 reported by Gray, 1960) extended the theo-

retical work done on packing density by studying the effects of particle size distribution. These efforts provided various relationships between void volume and multimodal mixtures of monosized particles. They did not produce general relationships describing density in continuous particle size distributions which occur in nature or in most industrial production of particulates.

These studies were enhanced by the experimental work of Bell (1958), McGreary (1961), Linger (1963), Bo, Freshwater, and Scarlett (1965), and Ayer and Soppett (1965 and 1966). These researchers worked with multimodal mixtures of both spherical and nonspherical particles. The emphasis in most of these studies was to determine parameters for production of industrial particulates with optimum packing properties. Again, the results did not produce general relationships which could be used to predict density from particle size distribution information due to the immense number of variables which affect the relationship between particle size distribution and density.

The previously mentioned research has provided some specific equations applicable to very specific materials and gradations. Despite the lack of a general, predictive model, there is agreement that particle size distributions where each consecutively smaller mode of particles has a diameter approximately the square root of the diameter of the next larger

mode produce the maximum achievable packing density. The general form of this relation is:

$$P = \left(\frac{d}{D}\right)^n \quad (2.6)$$

where P is the percentage of the total mass finer than any particle diameter, d , for a gradation with a maximum size particle, D , and a gradation exponent, n . This is generally referred to as the Talbot equation (National Stone Assoc., 1991). The value of the exponent defines the curvature of the gradation. Values of n less than 0.5 indicate highly distributed particle sizes, while values approaching 1.0 produce very uniform gradations. Gradations with exponent values of approximately 0.5 achieve higher packing densities than gradations with higher or lower exponent values. However, the actual magnitude of the packing density can not be predicted from this equation.

2.4 Packing density in partially saturated soils

Proctor (1933) observed and described the relationship between soil density, moisture content, and compactive energy in which the maximum packing density occurs at some intermediate moisture content between the dry and saturated states. To date, this relationship must be empirically derived for each material to determine optimum packing density. Proctor concluded that capillary forces in the moisture at contact

points caused increased frictional resistance between grains and that this caused the reduction in density seen at low moisture contents. Importantly, Proctor's theory regarding the influence of capillary forces predates the effective stress principle in unsaturated materials. Mistakenly, he placed more emphasis on the theory that the liquid at high moisture contents acted as a lubricant and thus increased the packing density. It is now recognized that nonclay minerals like quartz actually have higher sliding friction wet than dry (Horn, 1960).

Hogentogler (1936) postulated that liquid, adsorbed to solid particles, decreased in viscosity with increasing distance from the solid (increasing moisture content). This variation in fluid viscosity was assumed to explain decreased shearing resistance with increasing moisture content up to the maximum packing density. At moisture contents above that of the maximum packing density, Hogentogler depended on the lubrication theory to describe reductions in density.

Lambe (1960) introduced a theory based on the surface chemistry of the clay fraction of the soil. This theory was founded on assumptions of the variation in electrolyte concentration in soil moisture and the effect this variability would have on the short range attractive and repulsive forces of the clay surfaces. This theory explained the shape of the moisture-density curves for some, but not all, clayey soils.

Olson (1963), in concluding a detailed review of these and other compaction theories, states that each theory was reasonably consistent with the state of knowledge at the time. Advances in supporting fields of science exposed limitations in each theory which were not apparent at the time they were developed. In addition, none of the theories were subjected to rigorous experimental validation, nor were they extended to explain variability in shearing strength or stress-strain behavior.

Olson (1963) proposed an effective stress theory of compaction which takes into account variations in pore water and pore gas pressure, confining and shear stresses, and compaction energy for kneading and impact compaction. In summary, the theory states that during impact of the compactive force, the increase in pore pressures reduce the strength of the material, allowing densification. This continues until the increases in residual (that remaining after removal of the compacting force) total lateral stresses, residual negative pore pressure, and shear stresses between layers have increased the effective stress state in the material to a degree that additional impacts cause only minor, local densification.

As moisture content is increased, the decrease in air permeability due to the decreasing continuity of the gas phase causes significant gas pressures to develop. Olson proposes that the saturation level at which maximum density is attained

is equivalent to the state at which the gas phase becomes discontinuous and the gas permeability becomes zero. These high gas pressures then resist the impact stresses causing maximum attainable density to occur at less than full saturation.

Olson's theory is qualitative, presenting a mechanistic explanation of the compaction process, based on existing scientific knowledge. The theory was not subjected to rigorous experimental validation, nor is it a predictive model of attainable density. As with Proctor's original theory, the actual moisture-density relation must be determined experimentally for each material.

3. MOISTURE-DENSITY RELATIONS IN SAND: EXPERIMENTAL RESULTS

3.1 Introduction

A considerable body of research has been published on the relation between maximum achievable packing density and particle size distribution. Most of this research has been conducted for the completely dry state. Those studies which have addressed the effect of moisture on the packing density of particulates have been aimed at special situations, not at general or fundamental relationships. The objective of this phase of the study was to explore the interrelationship of moisture and density for five single curvature gradations. The parent materials, test procedures, and maximum particle size were held constant in order to limit the number of independent variables to moisture content, and particle size distribution.

A further objective of the study was to gain insights into the phenomenon commonly referred to as "bulking" in relation to the effective stress law. The results are presented and discussed phenomenologically in this chapter. The effective stress analysis is discussed in chapter six.

3.2 Materials

A single curvature, power function was chosen for the experimental particle size distributions. The function chosen was

$$P = \left(\frac{d}{D}\right)^n \quad (3.1)$$

where P is the cumulative fraction of material finer than a particle diameter, d , for a material with a maximum size, D . The maximum particle diameter was held constant at 4.75 mm in this study. The exponent, n , was the major independent variable of interest in this research.

The sand (0.75 to 4.75 mm) fractions of the different gradations used in this experimental work were prepared from commercially available concrete and mortar sands of fluvial origin. The grains vary in shape from subrounded to well rounded according to Pettijohn's 1949 classification provided in Lambe and Whitman (1969).

The power function gradations chosen for this work require larger quantities of very fine sand and silt (-0.15 mm) than were practical to prepare from the commercial sands. These fines were produced from western Iowa loess. The clay fraction was separated by cyclic sedimentation to remove clay chemistry and mineralogy from the list of potential variables in this study. The major mineral constituent in the fine material is quartz with small amounts of calcium carbonate, dolomite and feldspar (Badger, 1972). The particles are generally subangular to subrounded in shape.

3.2.1 Gradation preparation and control

Each gradation was constructed from the silt and sand fractions to exponent, n , values of: 0.2, 0.4, 0.5, 0.6, and 0.8. All gradations were truncated at the 0.002 mm particle size as a result of the removal of the clay fraction. Figure 3.1 presents the target cumulative particle size distributions.

A sieve analysis of each gradation was conducted (ASTM C-136) prior to testing to verify that each gradation met the experimental design criteria. Acceptance was based on a 95%

Cumulative Percent Finer for $P = (d/D)^n$

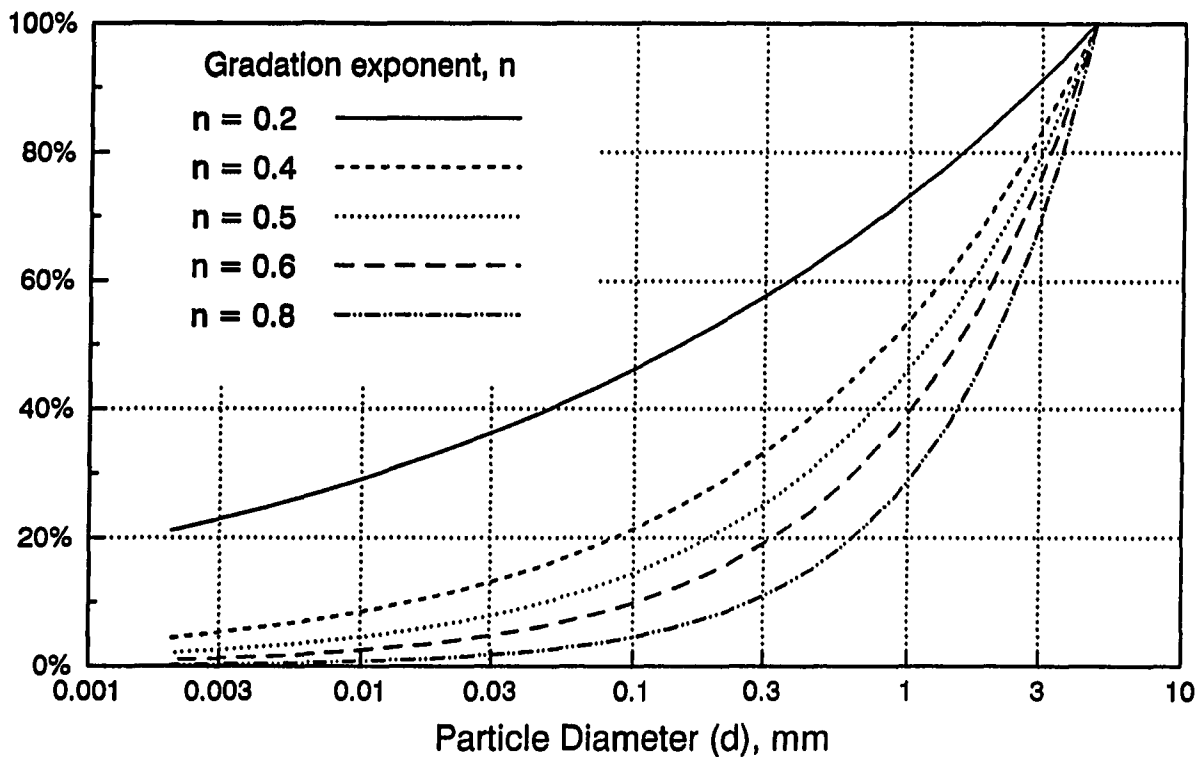


Figure 3.1 Target gradations used in this study

confidence interval for the gradation exponent as obtained by linear regression of the logarithmic transform of equation 3.1.

Because of the difficulty in producing silt sized material, samples one and one-half to two times the size required for testing were constructed. Repeated testing of samples introduced the possibility of sample degradation and loss of fines during testing. A sieve analysis of the $n = 0.4$ gradation was conducted after testing to verify the gradation. The post testing gradation deviated slightly from the original gradation. As a result, checks of the amount of #50 and #200 mesh (U.S. Standard Sieve Series) material were conducted between every second test and compared to the target gradations to provide quality control. The gradations with exponents of 0.5, 0.6, and 0.8 did not exhibit loss of coarse particles or fines during testing. The $n = 0.2$ gradation, however, exhibited loss of coarse material following testing at the hygroscopic moisture level. This sample was therefore regraded prior to continued testing. Following the first two tests at higher moisture contents, loss of fines became apparent in this gradation. It was thereafter necessary to regrade the sample between tests to maintain an exponent of 0.2 for the gradation.

3.2.2 Impact of gradation variance

Table 3.1 presents the results of statistical analyses conducted on the gradation results to evaluate the variance of the gradation exponents before and after testing. The gradation exponent for each gradation was determined by linear regression of the logarithmic transformation of equation 3.1. A t-test was then performed for each gradation with the null hypothesis that the slope determined by linear regression was equal to the target gradation exponent. Table 3.1 shows that the null hypothesis was only rejected at the 5% significance level for the 0.4 gradation. Further analysis of the 0.4 gradation indicates that it can be considered significant at the 5% level for the average exponent (before and after testing) of 0.3775. The 95% confidence intervals for all gradations are also shown in Table 3.1.

For ease of terminology, the gradations will be referred to by the target exponents. The actual values used for analysis will be those values shown in Table 3.1 which are not rejected at the 5% significance level.

3.2.3 Particle density

The specific gravity of each gradation was measured according to ASTM D-854. Three tests were conducted on each material and show that all gradations have a specific gravity of 2.69. The standard deviation for all tests was ± 0.013 .

Table 3.1 Analysis of gradation variance

Target Exponent	Null Hypothesis	Reject at 5% Significance Level?	95% Confidence Interval
0.2	n = 0.2	No	0.192 ± 0.014
0.2	n = 0.2	No	0.209 ± 0.019
0.2	n = 0.2	No	0.224 ± 0.040
0.4	n = 0.4	Yes	NA
0.4	n = 0.3775	No	0.355 ± 0.024
0.5	n = 0.5	No	0.491 ± 0.039
0.6	n = 0.6	No	0.585 ± 0.039
0.8	n = 0.8	No	0.810 ± 0.021

ASTM acceptance criteria for noncohesive soils are not available; however, a single operator acceptance criteria for cohesive soils of 0.021 is reported in the ASTM standard. This criterion can not be ascribed to the materials in this study; however, the magnitude of the standard deviation is reasonable in light of the value reported for cohesive soils.

3.3 Testing procedure

Maximum and minimum index density tests were conducted according to ASTM methods D-4253 and D-4254 respectively. The test methods are described in sections 3.3.1 and 3.3.2 and insured a constant, reproducible, experimental standard for comparison of results.

The following terminology will be used to differentiate various densities in subsequent sections. Minimum index

density, ρ_{dmin} , is the minimum density attained under index or standard conditions according to ASTM D-4254. This is the lowest, poured density attainable in the completely dry state. Maximum index density, ρ_{dmax} , is the maximum density attained according to ASTM D-4253. This is the maximum density associated with standard vibratory compaction in either a dry or completely saturated state. Relative density, D_r , is a measure of the dry density, ρ_d , of any material expressed as a percentage of the range in maximum and minimum index densities. Relative density can be calculated as:

$$D_r = \frac{\rho_{dmax} (\rho_d - \rho_{dmin})}{\rho_d (\rho_{dmax} - \rho_{dmin})} \times 100 \quad (3.2)$$

$$= \frac{e_{max} - e}{e_{max} - e_{min}} \times 100$$

in terms of either dry density, ρ_d , or void ratio, e . Table 3.2 provides a classification of relative density for granular soils. An intermediate density is any density between the maximum and minimum index densities. An intermediate moisture content is any moisture content greater than zero which produces less than full saturation. The minimum bulking density is the lowest density of a material due to bulking. Bulking is the phenomena of low density occurring at intermediate moisture contents under the same compaction energy which produces maximum index density.

Table 3.2 Relative density classification

Relative Density (%)	Description
0 - 15	Very Loose
15 - 35	Loose
35 - 65	Medium
65 - 85	Dense
85 - 100	Very Dense

3.3.1 Minimum index density tests

ASTM D-4254 minimum index density tests consist of determining the lowest density attained by the material in an oven dry state when placed loosely in a rigid mold. Method A, the preferred standard, was used throughout this study. This consists of gently pouring material into the density mold from a height of 13 mm above the surface of the sample until the mold is filled 6 to 13 mm above its rim, striking off the excess material, and measuring the weight of material in the control volume. Compliance with the standard has been shown to produce a standard deviation in multilab precision of ± 0.027 g/cc for fine sands with an acceptable range of two results of 7.0% of the mean value. Single operator precision is reported as 0.008 g/cc standard deviation and an acceptable range of two results as a percentage of the mean of 1.9%. A minimum of three tests were conducted on each material. The maximum range in results was 0.51%.

3.3.2 Maximum index density tests

ASTM D-4253 maximum index density tests consist of vibrating a sample in a rigid mold for a specified length of time under controlled vibration and surcharge conditions in both the oven dry and fully saturated states. For the electromagnetic, vertically vibrating table used in this study (a Syntron Vibrating Table, FMC Corporation), the standard calls for vibration at 60 Hz at a double amplitude of 0.33 ± 0.05 millimeters for 8 ± 0.25 minutes. The surcharge applied to the sample was 14 kPa.

Testing fine sands in compliance with the specifications produces a standard deviation in multilab precision of ± 0.038 g/cc with an acceptable range of two results of 8.3% of the mean value. Single operator precision is reported as 0.013 g/cc standard deviation with an acceptable range of two results of 2.7% as a percentage of the mean. Replicate tests conducted during this study yielded a maximum difference of 1.0%.

3.3.3 Modifications and additions to the standards

The greatest departures from standard methods occurred while determining maximum index density. ASTM D-4253 requires tests on oven dried samples. The minimum moisture content at which the $n = 0.4$ and 0.5 gradations were tested was air dry (approximately 0.3%). Oven dry maximum density for these two gradations was extrapolated from the nonlinear, least squares

regression equation for the relationship between moisture content and dry density, discussed in section 3.3.5 and summarized in Table 3.3. A comparison of the predicted and measured dry densities at zero moisture content for the other three gradations showed a maximum percentage difference (based on the measured value) of 2.64%. If we treat the least squares regression values as separate test values, this maximum percentage difference is acceptable since it is within the acceptable single operator precision range of 2.7%. The extrapolated values of maximum density for the $n = 0.4$ and 0.5 gradations were therefore used in determining relative density. In addition, because the focus of this research is to describe the full moisture-density relationship, tests at intermediate moisture contents were conducted to investigate the behavior between the oven dry and saturated states.

The amount of material chosen for moisture content determination was varied depending on the operator's qualitative observation of moisture distribution within the sample after testing. For evenly distributed moisture conditions, a vertical core sample of approximately 150 to 200 grams was taken from the center of the mold for moisture content determination. For stratified or otherwise nonuniform distribution of moisture, the entire sample was used for moisture content determination, as per the ASTM D-4253, wet method specification.

3.3.4 Calibration of equipment

The volume of the mold was checked by the direct measurement method (ASTM D-4253) and found to be 2831 cm³, compared to the nominal volume of 2830 cm³; well within the specified tolerance of $\pm 1.5\%$.

The double amplitude of vibration (maximum to minimum vertical displacement) of the vibratory table was calibrated to 0.33 ± 0.05 mm. This was done by setting a cathetometer outside of the range of vibration, focused on the tip of an upright bolt welded to the center of the vibrating table. A bright light was focused on a black line painted on the tip of the bolt. At rest, the cathetometer was focused on the black line and adjusted so that the horizontal cross hair covered the line. The table was then turned on and the cathetometer was raised until the line could no longer be seen vibrating above the cross hair. The difference between the initial and final readings was then recorded. This same procedure was duplicated to find the lower bound of vertical displacement. The upward and downward displacements were summed to yield an estimate of the double amplitude. This procedure was performed for the entire range of amplitude settings on the table's control box. The results for the range of interest are shown in Figure 3.2. Also shown in this figure is the allowable range of operating double amplitude. Even with the scatter associated with the crude method of calibration, it is

Double Amplitude, mm.

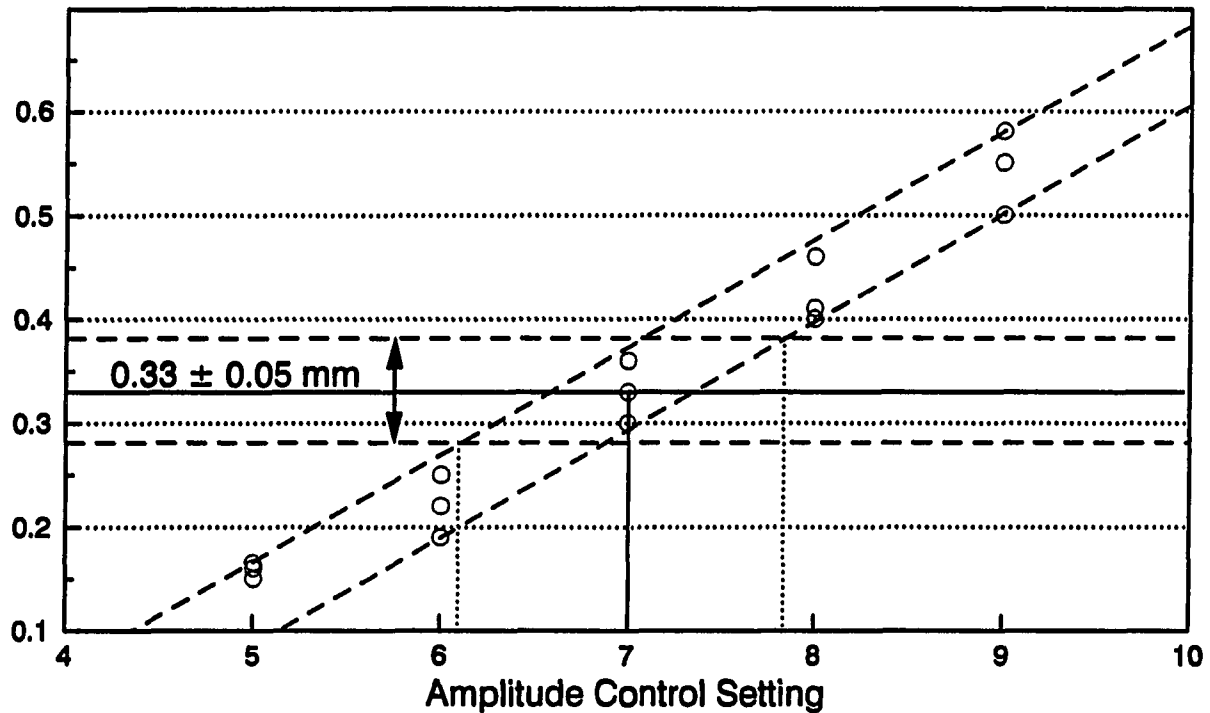


Figure 3.2 Calibration results for double amplitude control setting

apparent that a setting of seven on the amplitude control provides a double amplitude within the acceptable range. This setting was held constant throughout all testing. No attempt was made to ascertain the optimum double amplitude for any of the gradations, since a single, standard method was sought to minimize testing procedure variability.

3.3.5 Nonlinear least squares regression

To facilitate analysis of the moisture - density relationship, the data were fitted with a third order polynomial using nonlinear least squares regression with moisture content as the independent variable. The equation used was of the form:

$$\rho_{d_i} = A_1 + A_2 \omega_i + A_3 \omega_i^2 + A_4 \omega_i^3 \quad (3.3)$$

where ρ_{d_i} is the i^{th} dry density (g/cc) calculated from the i^{th} moisture content (ω_i), and $A_{1..4}$ are the regression parameters. A program based on the subroutine UNCMND, (Kahaner, Moler, and Nash, 1988) was used to minimize the function:

$$\sum (\rho_{d_{measured_i}} - \rho_{d_{predicted_i}})^2 \quad (3.4)$$

where the predicted dry density is from equation 3.3.

3.4 Presentation of results

Figure 3.3 presents the results of the modified maximum density-moisture content tests for the five gradations. The left ordinate displays the dry density and the right ordinate shows void ratio. Individual data points are grouped by gradation exponent as shown in the legend. The boundary line in the upper right quadrant of the figure is the zero air voids (ZAV) curve, or line of 100% saturation, based on a

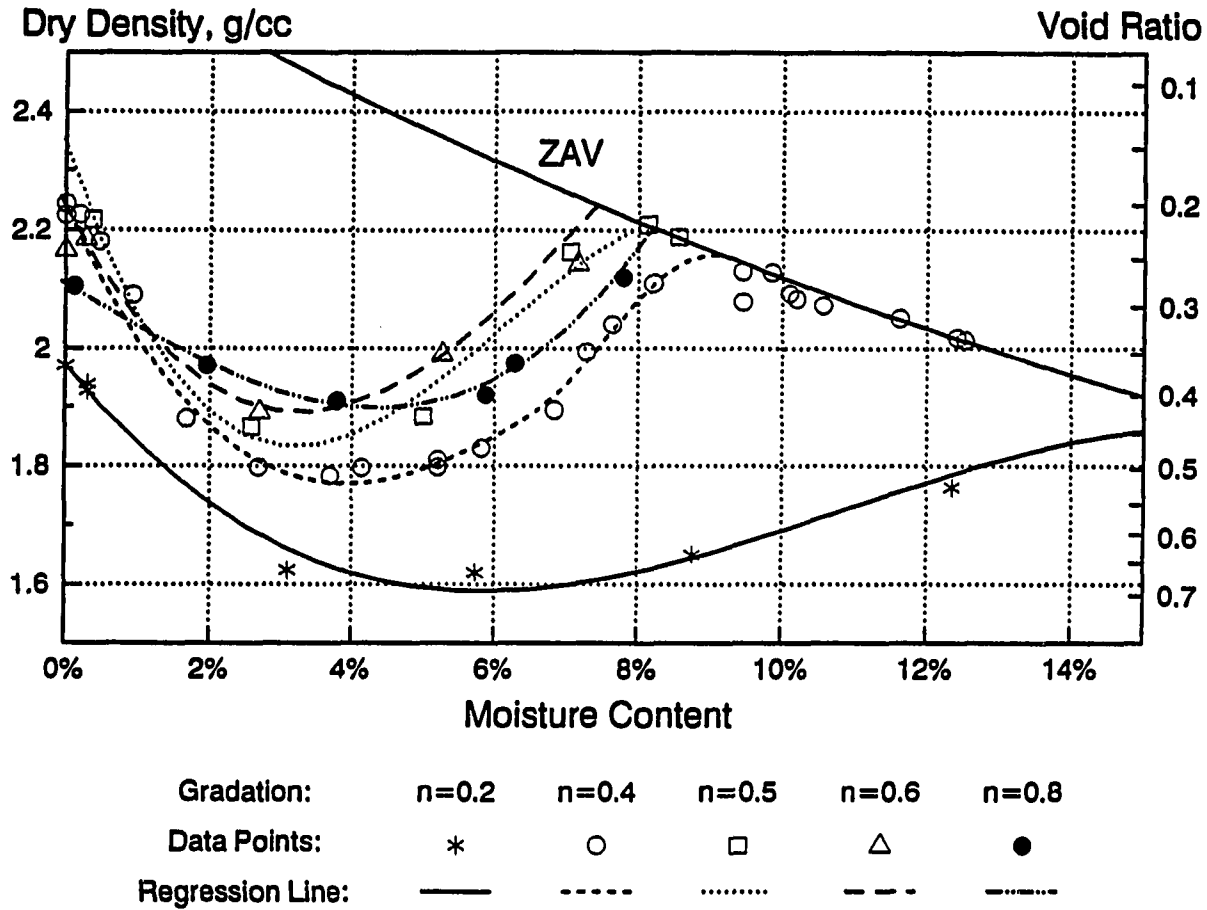


Figure 3.3 Results of maximum density testing for the five gradations

specific gravity of 2.69. The lines drawn through the data are calculated from equation 3.3 using the parameters generated by non-linear regression. The four curve fitting parameters ($A_{1..4}$) and the least squares residuals generated for each of the five gradations are presented in Table 3.3.

Table 3.3 Results of least squares regression

Target Exponent	A ₁	A ₂	A ₃	A ₄	Sum of Squares
0.2	1.9704	-14.920	174.46	-533	0.00303
0.4	2.2611	-27.653	467.14	-1991	0.01030
0.5	2.3480	-36.682	774.39	-4234	0.00340
0.6	2.2458	-23.661	442.16	-1686	0.00603
0.8	2.1110	-7.426	5.03	1199	0.00054

Figure 3.4 shows the relationship between the relative density of the material (in terms of the ASTM maximum and minimum index densities) and the saturation level. Saturation level normalizes the interaction of void ratio and moisture content. Relative density normalizes the magnitude of density or void ratio when assessing differences in material and gradation. Data points are grouped according to gradation and have the same symbols as in Figure 3.3. The lines drawn through the data are not regression lines; they are smooth curves drawn by the author. Superimposed on this figure is the classification of Table 3.2. Density classes are separated by dashed, horizontal lines.

3.5 Discussion

It is immediately obvious from Figure 3.3 that the 0.2 exponential gradation exhibited consistently lower dry densities (higher void ratios) than any other gradation. This gradation also had the highest percentage of fine material.

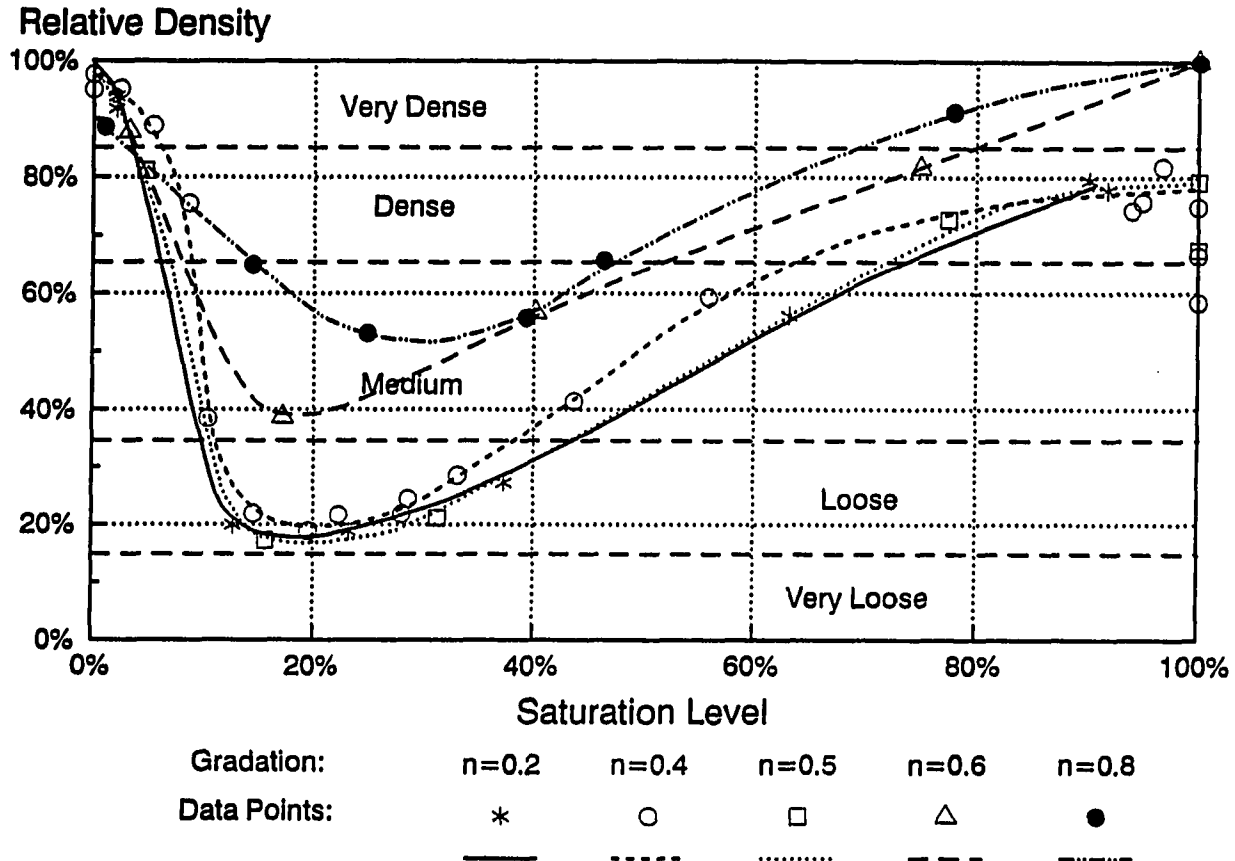


Figure 3.4 Relative density versus saturation for the five gradations under conditions of maximum index density compaction

A total of twenty tests were conducted on the $n = 0.4$ gradation (the first material tested) in order to provide a very clear picture of the trends to be expected in subsequent materials. Thereafter, larger moisture content intervals were chosen to expedite testing. Of particular interest in Figure

3.3 are the two $n = 0.5$ data points which lie on the zero air voids line and the nine $n = 0.4$ gradation tests conducted at moisture contents in excess of 9%. These tests, although saturated, show a decrease in density with increasing moisture content. This corroborates the caution stated in ASTM D-4253 that the wet method of determining maximum index density requires substantial care. It is not enough to prepare and test a saturated specimen. The sample must be brought just to the point of saturation; further increases in moisture content create excess void space since excess water is unable to drain due to the construction of the test mold.

Both Figures 3.3 and 3.4 demonstrate the bulking phenomena for all five gradations. At intermediate moisture contents, the compacted dry density is much less than at either end of the saturation spectrum. Figure 3.4 especially illustrates how drastic a reduction in dry density can occur due to bulking, with densities falling into the loose to nearly, very loose classifications. This figure also shows that, with the exception of the $n = 0.8$ gradation, the greatest reduction in dry density occurs in a very narrow range of saturation levels.

3.5.1 Maximum index density

According to the commentary in ASTM D-4253, the oven dry index density attained by this method is not necessarily the maximum attainable dry density. In some materials maximum dry

density can occur at full saturation. In this study, maximum dry density was obtained in the oven dry state for the 0.2, 0.4, and 0.5 exponential gradations and at saturation for the 0.8 exponential gradation. The 0.6 gradation exhibited almost exactly the same dry density at both oven dry and saturated moisture contents.

Table 3.4 presents a comparison of the measured dry densities and those predicted by equation 3.3 with the parameters in Table 3.3 for the five gradations at both zero moisture content and full saturation. It also presents the minimum index densities determined according to ASTM D-4254.

Table 3.4 Measured and predicted maximum and minimum dry densities (g/cc)

Target Exponent	Maximum Oven Dry Density Measured	Maximum Oven Dry Density Predicted	Maximum Saturated Density Measured	Maximum Saturated Density Predicted	Minimum Oven Dry Density Measured
0.2	1.97	1.97	1.83	1.82	1.55
0.4	2.19	2.26	2.04	2.06	1.70
0.5	2.16	2.35	2.08	2.18	1.78
0.6	2.16	2.25	2.22	2.23	1.74
0.8	2.13	2.11	2.19	2.19	1.68

Figure 3.5 presents these data and the minimum dry density due to bulking in graphical form. For the compaction conditions and materials used in this study, the 0.5 gradation produced the highest maximum density. This is consistent with the work done by many of those cited in chapter two who have

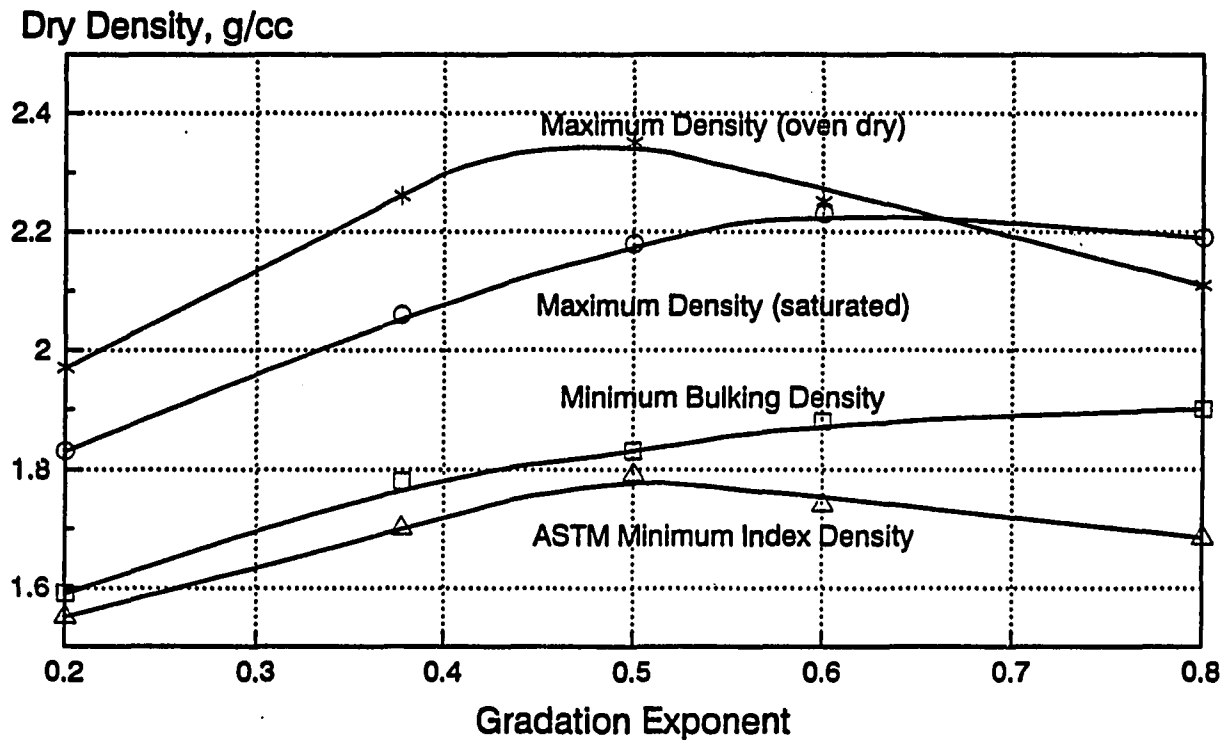


Figure 3.5 Dependence of maximum/minimum densities on gradation exponent

shown that a square root relationship (exponent, n , of 0.5) between successive particle sizes does indeed produce an optimum packing arrangement. What is perhaps more significant is that the maximum packing density is so much lower for the material with the highest silt content (\sim #200 mesh, 0.2 exponent) and varies less than those gradations with higher exponents. Also, maximum index density occurs at the oven dry state for gradations with exponents less than 0.6 and at full saturation for gradations with exponents greater than 0.6.

3.5.2 Bulking

All of the gradations exhibited some degree of bulking, or reduction in dry density due to the presence of capillary moisture forces which oppose compaction. This is illustrated in Figure 3.5 in which it is seen that the minimum dry densities due to bulking are only slightly higher than the minimum index density attained by ASTM D-4254. Examination of Figure 3.5 also indicates that increasing gradation exponents above $n = 0.5$ show a decrease in the magnitude of density reduction due to bulking.

The percentage difference in maximum and minimum index densities for these five gradations fall in a fairly narrow range (20 to 25%). This is consistent with results reported by Terzaghi and Peck (1948) for a wide variety of soils, sands, and gravels.

To examine the possible effect of top size on these relationships, maximum and minimum index density tests in an oven dry state were conducted on three nearly monosized sands: 4x8, 8x16, and 30x50 mesh (U.S. Standard Series). All three exhibited the same maximum and minimum index densities: 1.70 g/cc and 1.44 g/cc. This suggests that top size is not a factor in the moisture-density-gradation relationship and reaffirms the assertion that gradation curvature (as controlled by gradation exponent in this case) is the important, independent variable. These results also imply that the dry

density-gradation exponent relationships for maximum and minimum index density in Figure 3.5 have limiting values at very high gradation exponents equal to those of the three uniform sands. Thus, the more nearly monosized the gradation, the closer the maximum and minimum index density should approach 1.70 g/cc and 1.44 g/cc respectively.

3.6 Conclusions

The moisture-density relationships of particulate materials ranging in size from 0.002 mm to 4.75 mm obtained according to ASTM D-4253 are highly dependent on the particle size distribution of the material. Increasing the fineness of the gradation causes a substantial reduction in the maximum dry density. This is in agreement with the work cited in chapter two which found that very fine materials exhibit low density due to the high specific surface of the material. Lower proportions of fine sizes in the distribution minimizes the bulking effect at intermediate moisture contents. However, bulking can still reduce dry density to below thirty percent relative density. Slight amounts of moisture cause drastic reductions in relative density but 70% relative density is achievable at saturation levels greater than 60 - 70% depending on gradation. Bulking also appears to be a function of the gradation exponent, with lesser differences between maximum index density and minimum bulking density occurring as the gradation approaches a uniform size.

4. MOISTURE-PRESSURE RELATIONS IN SAND: EXPERIMENTAL RESULTS

4.1 Introduction

The objective of this phase of the study was to investigate the moisture content-pressure deficiency relationship (moisture characteristic curve) for the five gradations of sand presented in the previous chapter.

4.1.1 Background

Soils and other particulate materials consist of both solid and void space. Just as the solid fraction is composed of discrete particles of varying sizes and shapes, the void fraction is made up of various sizes and shapes of pores. So far, emphasis has been placed on the distribution and arrangement of the solid particles which is the conventional soils engineering approach; however, as Badger (1972) observed, much of soil engineering practice is founded on methods to manage and manipulate the soil voids and void fillers in order to control soil behavior. Therefore, in order to fully examine a particulate system, special attention must be given to the "holes" in the system. This can be difficult for when "looking into a hole, it is almost impossible not to look at the sides and bottom of the hole instead of the vacant space" (Badger, 1972, p. 2). The following three chapters emphasize the distribution of the void space and the pressure transmission characteristics of the fluid phase in the void space.

When liquid makes up part of the pore volume, the attractive forces between the solids and liquid and the surface tension effects at the gas-liquid interface produce pressures in the liquid phase that are less than atmospheric pressure. This phenomena is referred to as moisture tension, negative pore pressure, soil suction, matric potential, or capillary potential. The use of energy relationships by Buckingham (1907), Gardner (1920), Haines (1930), Edelfson and Anderson (1943) and others has gradually supplanted the earlier capillary tube concept. In terms of potential energy, matric potential is defined as "the energy per unit volume of water required to transfer an infinitesimal quantity of water from a reference pool of soil water at the elevation of the soil to the point of interest in the soil at reference air pressure" (Jury et al., 1991, p. 51).

The older capillary tube model of soil water interaction (Briggs, 1897) does not conflict with the energy concept however. The hypothesis is that soil water exists as continuous films around the soil particles and that the forces arising from this curvature provide the primary cause of moisture retention. This then is dependent on the number and size of the capillary tubes in the system (Jury et al., 1991). As the name implies, this model presupposes that the void space in a soil body can be thought of as a bundle of interwoven, continuous capillary tubes; each capable of producing pressures in-

versely related to the pore diameter according to the capillary rise equation:

$$P = - \frac{4T \cos \delta}{d} \quad (4.1)$$

where P is the pressure (Pa), T is the surface tension of water in contact with air (0.073 N/m at 18°C), δ is the wetting angle of water on the solids (assumed to be 0° during drainage), and d is the equivalent pore diameter (m).

Carman (1941) provides the following argument for describing the irregular pore structure of a sand bed as a bundle of interwoven capillary tubes. Any very thin cross section of a randomly packed bed should have the same volumetric porosity as the whole bed. As the thickness of the cross section approaches zero, the volumetric porosity becomes equal to the ratio of the void to total areas. Thus, the areal porosity may be used to represent the sum of the cross sectional areas of a bundle of capillary channels. The route of any single channel is tortuous and its cross section is not constant, yet the average area is constant. Individual channels in a random bed do expand and contract, but all void channels in a sand bed are so interconnected that no single channel can be treated as an isolated entity.

Further, assuming that the pore liquid completely wets the walls of the pores and that the cross section of the

capillary is small enough that the effect of gravitational force on the curvature of the menisci can be neglected compared to the surface tension force, a circular capillary of diameter, d , would have a hemispherical meniscus. Therefore, the pressure differential across the meniscus could be predicted by the capillary rise equation. At equilibrium, the matric potential or pressure differential is therefore a function of the largest pore size filled with liquid. Thus, exploration of the moisture characteristic relationship can yield significant insights into the interaction of the pore and solid fractions in partially saturated, particulate systems.

4.2 The moisture characteristic curve

The moisture characteristic curve describes the relationship between the potential or pressure of the moisture in a particulate system and the amount of liquid in the system. Figure 4.1 shows a generalized moisture characteristic curve. Typically, the potential or pressure is plotted on the ordinate in either arithmetic or logarithmic form and the moisture level is plotted on the abscissa in arithmetic scale. The moisture level can be expressed as gravimetric or volumetric moisture content, fraction of the pore volume filled with liquid (volumetric saturation), or relative fraction of the pore volume filled with liquid (ratio of the filled pore volume to the pore volume which can be drained).

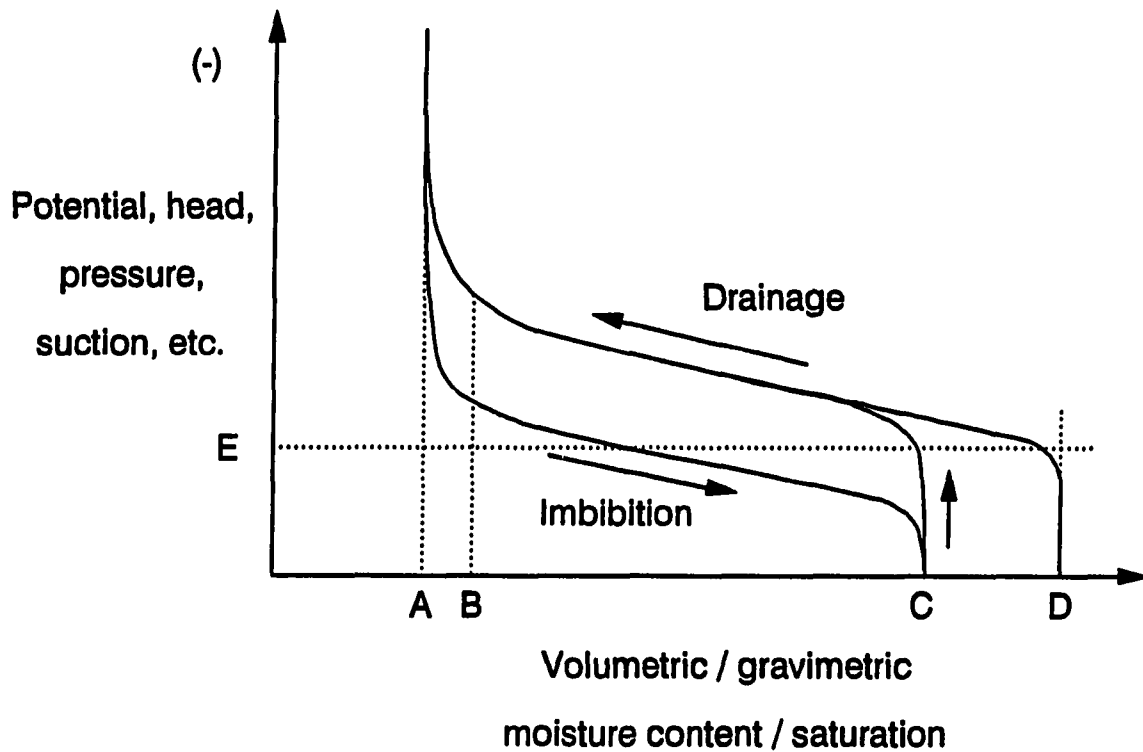


Figure 4.1 Schematic of a general moisture characteristic curve

Drainage of a fully saturated system initially at atmospheric pressure (Figure 4.1, point D) causes a rapid decrease in potential with very little change in the volume of liquid held in the pores. As the gas-liquid pressure difference increases, the meniscus at the exterior of the sample is pulled inward until the gas phase makes a general, wide spread breakthrough into the pore structure of the system. The gas entry or bubbling pressure associated with this breakthrough (E) is generally seen to occur at saturation levels (ratio of

liquid to pore volume) of approximately 90 to 100% in fine grained materials (Pietsch, 1984). This lower flex point in the moisture characteristic curve marks the transition from a fully saturated (capillary) to partially saturated (funicular) state (Versluys, 1917; Newitt and Conway-Jones, 1958). The potential at this point is also strongly related to the shear strength of partially saturated granular materials which have undergone drainage as is discussed in chapter seven.

As drainage continues, the moisture characteristic curve assumes a new, nearly linear, trend until it reaches the funicular-pendular transition (B) or the upper flex point of the moisture characteristic curve. The pendular moisture range is defined as the lower range of moisture contents in which the moisture exists as rings at the particle contact points and as adsorbed films on the surfaces of the particles. As such, the liquid phase is no longer continuous throughout the pore structure as it is in the funicular range. The pendular state, as defined here, is equivalent to the capillary state in Briggs' (1897) classification system for soil moisture, in which the nomenclature indicates the primary forces which act on the liquid phase. Thus, pendular moisture is subject primarily to capillary forces of attraction, while funicular or gravity water is primarily affected by gravitational forces, and therefore, can be drained by low tension heads. This interpretation of the upper flex point is sup-

ported by the writings of Haines (1930), Baver (1956), Newitt and Conway-Jones (1958), Rumpf (1962), and Schubert (1984). The slope and range of saturation levels covered by the moisture characteristic curve in the funicular range is indicative of the volume and size range of pores which are easily drainable. Very horizontal curves indicate nearly monosized pores in this range; conversely, a steep slope between the flex points indicates a wide range of pore sizes in the funicular range. The range of saturation levels which this portion of the curve covers is indicative of the number or volume of pores in the funicular range and also the expected natural range of moisture contents under field conditions. Livneh et al. (1970) and Russel and Mickle (1971) have also shown that the moisture contents at the upper and lower flex points correlate reasonably well with the plastic and liquid Atterberg limits.

Finally, the drainage curve becomes asymptotic at a point referred to as the residual moisture content or residual saturation level (Figure 4.1, point A). The moisture content at which this occurs is dependent on the particle and pore size distributions, state of packing, and surface charge of the particles and is therefore variable from material to material (Richards, 1928; Richards and Weaver, 1944; Salter and Williams, 1965) as is the entire moisture characteristic curve. Baver (1956) presents data for a number of sands and

soils that show that the residual saturation level can occur from five to 45% saturation. Materials with higher proportions of fine particles (particularly clays and colloids) and therefore higher fractions of fine pores exhibit high residual saturation levels. Table 4.1 presents some data for a range of natural soils and one controlled sand fraction. In general, increasing clay content causes increased air entry pressures, although this is also dependent on the density of the soil. As the soil becomes coarser textured, or less dense, these values decrease. The saturated (θ_s) and residual (θ_r) volumetric moisture contents (ratio of volume of water to total soil volume) are also given.

Table 4.1 Typical soil moisture parameters

Soil	θ_s^1	p_e^2	θ_r^1	Reference
40x60 mesh Quartz sand	0.36	14	0.05	Baver, 1956
Ramona sand	0.42	30	NA ³	Richards and Weaver, 1944
Guelph loam	0.52	55	0.32	van Genuchten, 1980
Indio loam	0.24	70	NA	Richards and Weaver, 1944
Touchet silt loam	0.47	150	0.19	van Genuchten, 1980
Hanford fine silty loam	0.29	150	NA	Richards and Weaver, 1944
Silt loam G.E.3	0.39	160	0.05	van Genuchten, 1980
Fresno loam	0.56	300	NA	Richards and Weaver, 1944

1 cm^3/cm^3

2 cm H₂O

3 Not Available

During imbibition of liquid, varying amounts of hysteresis occur due to contact angle hysteresis, differences in pore neck and body sizes, and the presence of gas entrapped in pore bodies. The potential of the liquid phase at a given level of saturation is less than that for the drainage case. As a result of entrapped gas in some pore bodies, the full pore volume is not saturated at the end of imbibition (Figure 4.1, point C).

This general description of the moisture characteristic curve does not address the effects of changes in density due either to naturally occurring shrinkage or swelling or to physical manipulation whether engineered or incidental. Baver (1956) presents an analysis of the effect of compaction on the shape of the moisture characteristic curve for a range of soils from sands to clays. In each case, an increase in the dry density of the soil resulted in lowering the saturated volumetric moisture content (equal to the gross porosity), increasing the residual moisture content, and increasing the pressure deficiency at both the upper and lower flex points. The explanation given was that compaction decreased both the size and volume of the largest pores (larger than 10 microns equivalent diameter) and increased the uniformity of the pore sizes. This has also been documented using mercury intrusion porosimetry by Badger and Lohnes (1973) for compacted western Iowa loess and Thompson et al. (1985) and McBride et al.

(1987) for B horizon samples of three common Iowa parent materials: till, loess, and paleosol.

Conversely, Tuncer (1976), Tuncer et al. (1977), McBride et al. (1987) and Kaspar (1988) have shown that volume change due to desiccation primarily affects the 0.1 to 10.0 micron diameter pores. This happens because the larger pores are subject to very low tensions which are not able to break down the large pore structure and the smaller pores possess greater structural stability (Tuncer et al., 1977). This produces higher percentage volumes of both smaller and larger diameter pores.

Based on these studies, it is concluded that the total reduction in pore volume would cause a decrease in the saturated volumetric moisture content and the increase in small pore volume would increase the residual moisture content. However, the relative increase in large pore volume would lower the pressure deficiency at the air entry point, raise the pressure at the upper flex point and cause more nonuniformity of the pore size distribution. A schematic of this hypothesis on the effects of compaction and desiccation on the moisture characteristic curve is given in Figure 4.2.

4.3 Measurement techniques

Since the moisture in the pore phase of a particulate system can exist over a wide range of pressure deficiencies (commonly between 0 and -300 kPa through the funicular range

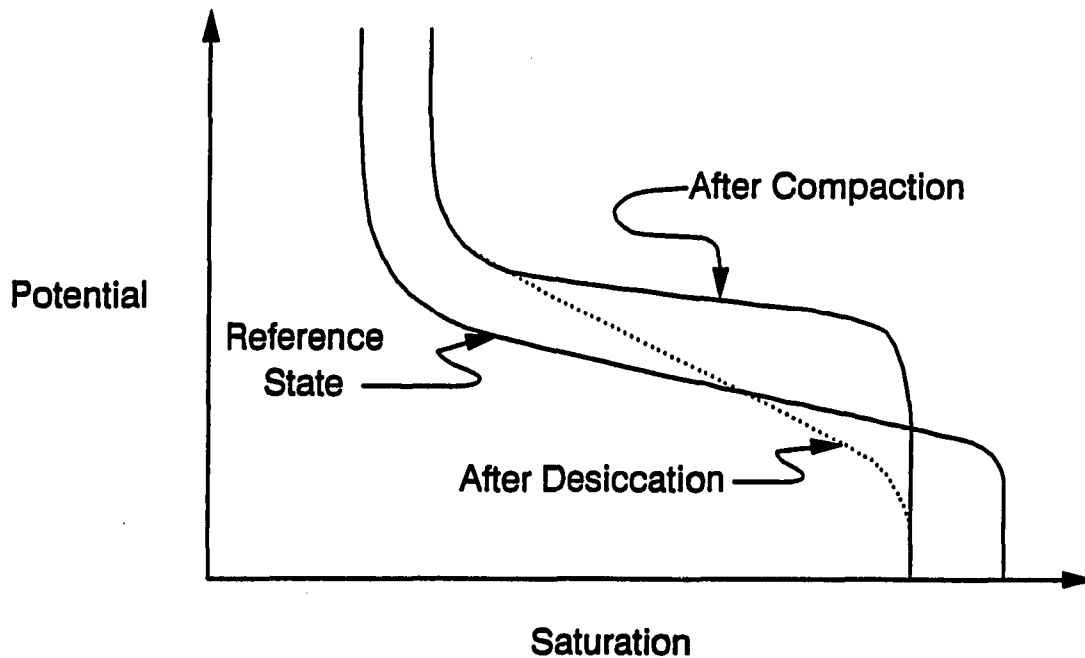


Figure 4.2 Schematic of the effect of compaction or desiccation on a moisture characteristic curve

and exceeding -1500 kPa in the pendular range), no one technique is suitable to measure the entire range of pressures associated with any one material.

In the 0 to -100 cm (0 to -10 kPa) range, a hanging water column (Figure 4.3) consisting of a saturated, highly permeable ceramic plate connected to a water column with its end open to the atmosphere can be used to produce equilibrium between the moisture in the sample and the tension induced by the difference in sample and outlet elevations. Different

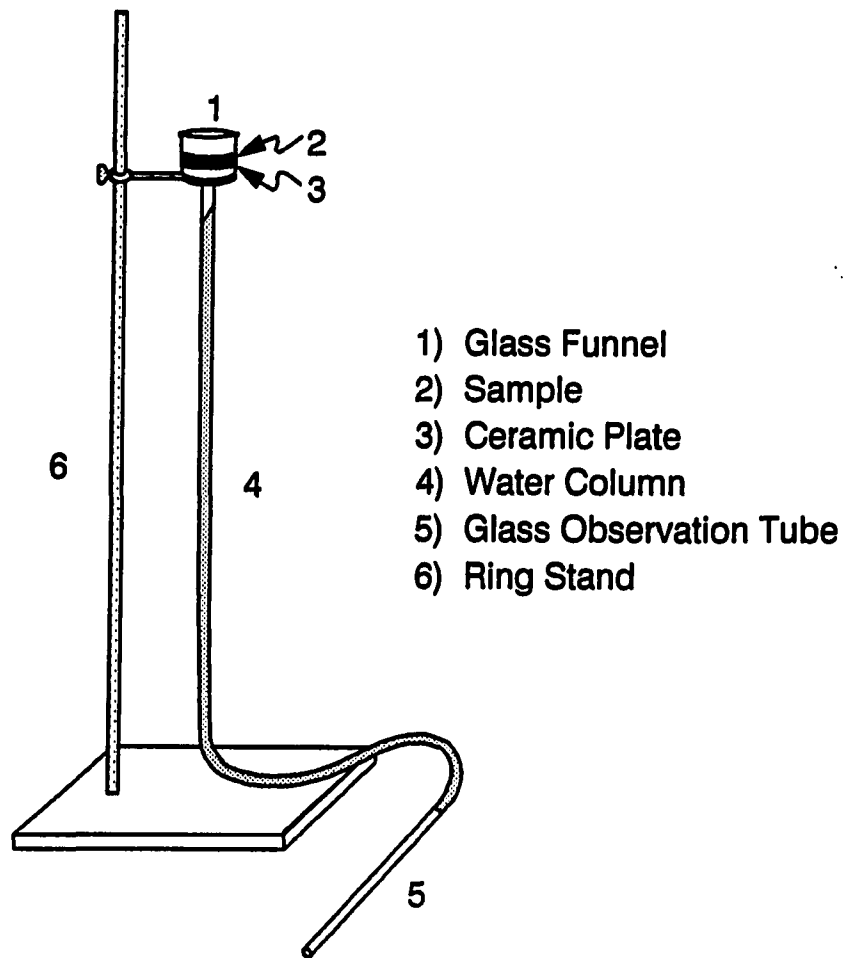


Figure 4.3 Schematic of a hanging water column

pressure deficiencies are produced by changing the elevation of the sample above the outlet datum. The observation tube at the outlet is used to gauge when flow between the column and sample has ceased and equilibrium has been attained.

A tensiometer (Figure 4.4) uses essentially the same principle as the hanging water column except that by using a mercury manometer the range of measurable potentials is

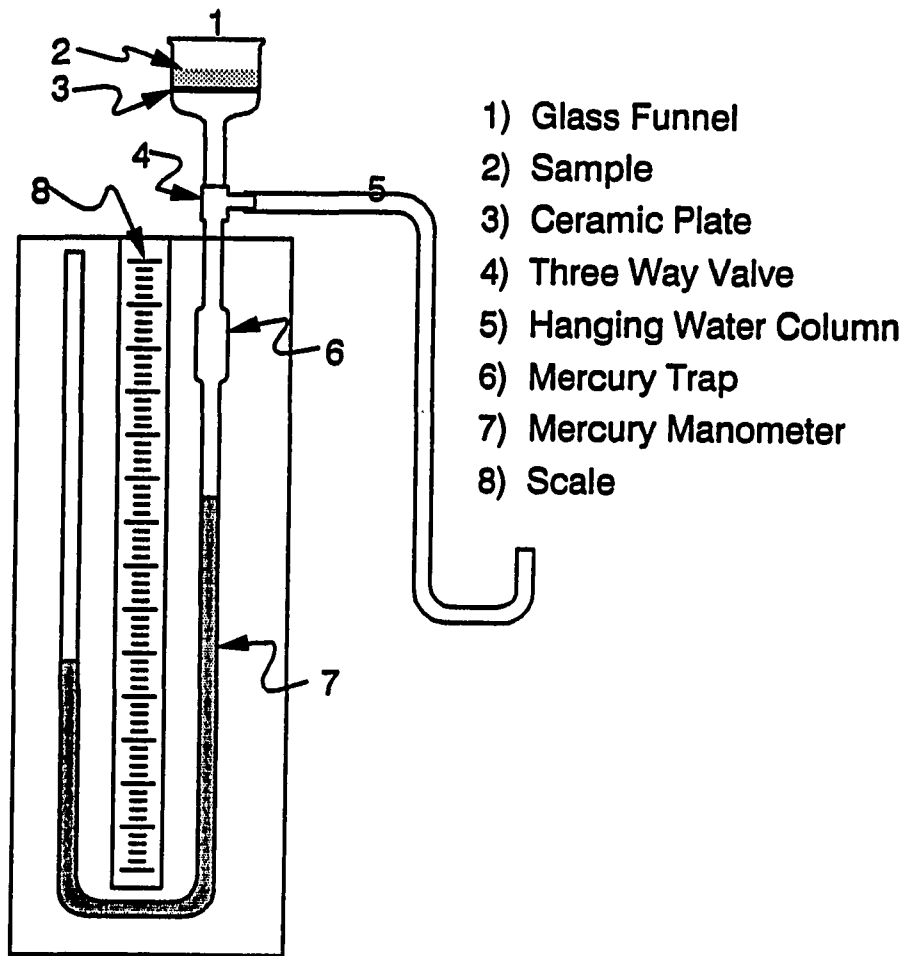


Figure 4.4 Schematic of mercury tensiometer

increased to -800 cm (-80 kPa). Different potentials are generated by allowing different amounts of moisture to evaporate from the sample. Equilibrium is gauged by the cessation of mercury movement.

Ranging further (-300 to -1500 cm; -30 to -150 kPa), such apparatus as pressure plates and pressure membranes are applicable. In this study, a variation on the pressure plate

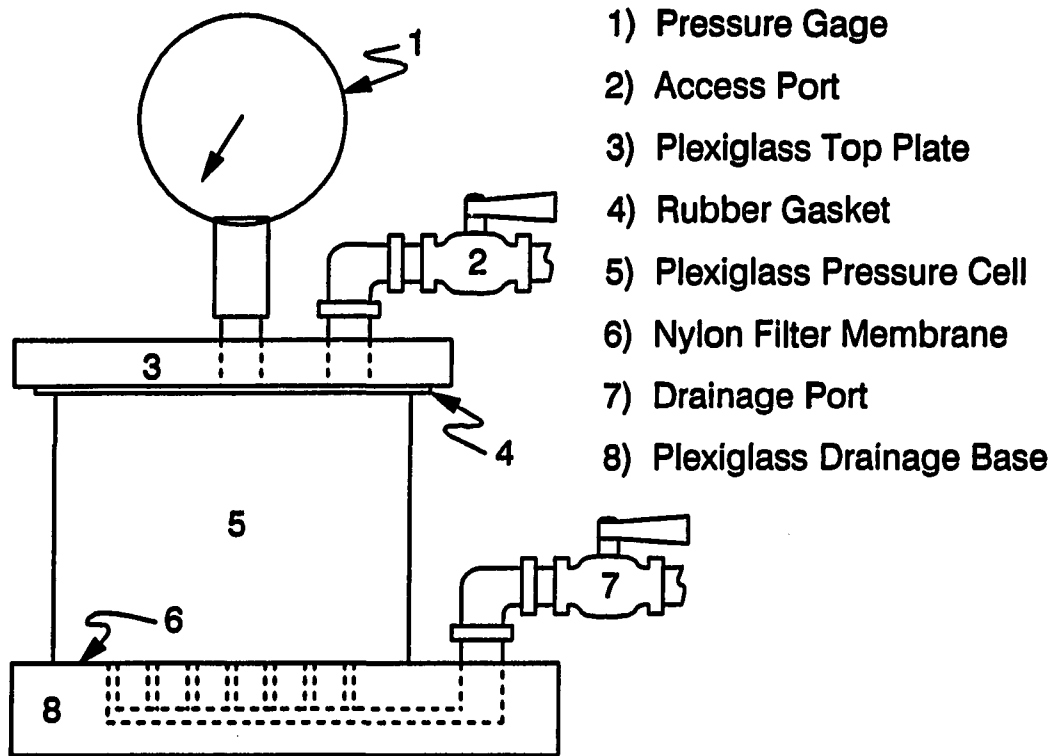


Figure 4.5 Schematic of a pressure plate cell

(Figure 4.5) was used for potentials less than -500 cm (50 kPa). This consisted of a plexiglass base which provided the drainage ports, a fine pore sized nylon filter membrane which served as the pressure plate, a plexiglass pressure chamber, and a top plate fitted with access ports for pressure measurement and application. Different potentials were attained by applying compressed air at different pressures to different samples inside the pressure chamber. Equilibrium was gauged by connecting the drainage port to a burette and observing the level of effluent from the sample. Additional techniques such

as psychrometry and vapor equilibrium can produce equilibrium potentials at much lower potentials (higher suction levels). These methods were not used in this study since most of the moisture in the sands was at high potentials.

4.4 Experimental procedure

As noted in section 4.3, the experimental measurements of the moisture tension relationship were made with three different apparatus. The materials used in this study were previously described in section 3.2.

4.4.1 Sample preparation

Samples were prepared by mixing equal volumes of solid particles and distilled water. The mixture was kneaded repeatedly to minimize the amount of air bubbles in the slurry. This produced a nearly saturated slurry with a void ratio of approximately one. At this void ratio, the slurry could be easily handled and placed in the moisture retention measurement apparatus without undergoing any segregation of particle sizes. After assembling the apparatus and lightly wetting the ceramic plate or nylon filter, the mold was filled with slurry to a height of approximately 2.5 centimeters.

4.4.2 Pressure measurement

Samples in the hanging water column and pressure plate apparatus were desorbed under the preset pressure deficiency. Consolidation of the sample took place under that desorption

pressure by drainage alone. Samples in the tensiometer were initially desorbed with a 50 centimeter hanging water column before switching the valve and connecting the sample to the mercury manometer (see Figure 4.4). Further reduction in the moisture content was accomplished by evaporation. When the tensiometer response approached the desired potential, the sample was covered to impede further evaporation. The sample was kept in this condition until the change in tensiometer response dropped to less than one millimeter over a six hour period. This was taken to be equilibrium and the sample was removed, measured, and weighed prior to being oven dried to determine the moisture content.

Equilibrium in the pressure plate apparatus was monitored by observing the level of effluent in a burette connected to the drainage port. Final potential was calculated as the applied air pressure minus the back pressure from the column of water in the burette. Equilibrium in the hanging water column was monitored by gauging when the water-air meniscus in the glass capillary tube ceased to move.

4.4.3 Density and moisture content measurements

After the equilibrium pressure was recorded, each sample was weighed and measured in the mold to determine total sample mass, height and diameter. Cell diameters (nominal 7.50 cm) were measured directly with a vernier micrometer. Sample heights (generally 2.0 - 2.5 cm) were calculated as the dif-

ference between the total cell height and the average of three measurements from cell top to sample top as measured with the vernier micrometer. These measurements were used to calculate the total (bulk) density of the sample (total mass divided by total volume). The moisture contents of each sample were measured and calculated according to ASTM D-2216. The dry density (dry mass divided by total volume) was then calculated from the bulk density and gravimetric moisture content.

The mean dry densities obtained purely by drainage in the pressure cells (Table 4.2) are similar at about 2 g/cc except for those of the $n = 0.2$ gradation which has a density of 1.81 g/cc. The relative densities of the five materials are in the dense range (Table 3.2) for all except the 0.5 exponent gradation which classifies as medium density. The $n = 0.5$ gradation also had the greatest difference between maximum index density (oven dry) and saturated dry density (cf. Table 3.4). Densities achieved by drainage and the maximum saturated densities attained by the ASTM D-4253 wet method are similar. This suggests that drainage of laterally confined, saturated materials can be an effective method of compaction for well graded sands. In fact, the Naval Facilities Engineering Command Design Manual (NAVFAC DM-7.3, 1983) states that relative densities from 70 to 75% are satisfactory to preclude significant settlements beneath vibratory equipment. The NAVFAC design manual goes on to recommend that injection

Table 4.2 Relative density of moisture retention samples

Gradation Exponent	Mean Dry Density (g/cc)	Relative Density ASTM D-4254	Maximum Saturated Density (g/cc)	Relative Difference (Mean and Saturated)
0.2	1.81	68%	1.82	0.3%
0.4	2.05	70%	2.04	0.6%
0.5	2.04	52%	2.08	1.9%
0.6	2.08	72%	2.22	6.4%
0.8	2.02	65%	2.19	7.6%

pumping coupled with deeper drainage wells which cause downward seepage forces can be an effective means of consolidating loose sand deposits.

However, the percentage difference between the drained and vibrated saturated densities increases significantly as the material becomes more poorly graded. This indicates that poorly graded materials may require application of shear forces in order to achieve high density. This is attributed to the generally higher frictional resistance between large particles which would be more pronounced in uniformly graded materials.

4.4.4 Measurement precision and accuracy

The precision of the equilibrium matric potential measurements in this study vary according to the apparatus. In the hanging water column, the equilibrium potential is measured directly as the difference in height of the sample and

column outlet. The precision is therefore a function of the precision of the height measurement. This is also the case in the tensiometer in which the moisture tension is balanced by the height differential of the mercury column. In this study, measurements in the hanging water column and tensiometer were made with a meter stick graduated in millimeters. This corresponds to a precision of ± 1 millimeter of potential (~ 0.01 kPa) in the hanging water column and approximately ± 14 millimeters (~ 0.14 kPa) in the tensiometer. The differences in the two lie in the specific gravity of the mercury in the tensiometer.

In the pressure plate apparatus, pressures were measured with a calibrated, Bourdon tube gauge, graduated in 2 psi increments. Measurements can be reliably estimated to the 0.2 psi level which provides a precision of ± 140 millimeters (1.4 kPa) in the reported tensions.

The main difficulty and source of experimental error in all of these measurements lies in determining when equilibrium is obtained. With the apparatus used in this study, allowing additional time before taking measurements, which increased the surety of attaining equilibrium, also increased the chances of mechanical difficulties with the experimental apparatus. After several mechanical failures (leaks and gas bubbles in the system), the rate of mercury column movement (tensiometer), discharged volume of liquid (pressure plate), or air-

water meniscus movement in the capillary observation tube (hanging water column) was used to signal impending equilibrium.

Although the range of measurement precision reported here is very narrow, the accuracy of the measurements can not be directly assessed. Indirectly, the accuracy is a function of the care taken to insure that measurements were actually taken after equilibrium had been achieved. This was very closely monitored during the course of this study.

4.5 Curve fitting technique and results

Due to the scatter in the experimental results, nonlinear, least squares regression was used to fit curves to the data. A sigmoidal curve, proposed by van Genuchten (1980), was used. The nonlinear, least squares regression technique, described in section 3.3.5 was used to generate the parameters for the equation. In this case, van Genuchten's equation was specified as the user defined function:

$$\theta = \frac{\theta_s - \theta_r}{(1 + \alpha^n h^n)^m} + \theta_r \quad (4.2)$$

in which θ is the volumetric moisture content, θ_s and θ_r are the saturated and residual volumetric moisture contents and α , n , and m are empirical curve fitting parameters. Since the volumetric moisture content can also be stated in terms of

gravimetric moisture content, ω , or saturation level:

$$\theta = \frac{\omega G}{1 + e} = \frac{S e}{1 + e} \quad (4.3)$$

van Genuchten's equation can also be stated as:

$$\omega = \frac{\omega_s - \omega_r}{(1 + \alpha^n h^n)^m} + \omega_r \quad (4.4)$$

in terms of gravimetric moisture content, or:

$$S = \frac{1 - S_r}{(1 + \alpha^n h^n)^m} + S_r \quad (4.5)$$

in terms of the saturation level, where the subscripts s and r continue to refer to the saturated and residual moisture levels.

Of the five parameters used in this model, the saturated volumetric or gravimetric moisture content is easily calculated from the specific gravity and average density of the samples. Nonlinear, least squares regression was then used to minimize the sum of the squares of the residuals in order to produce the other four parameters.

4.5.1 Analysis of the parameters α , n , and m

Figures 4.6, 4.7, and 4.8 show the sensitivity of the moisture characteristic curve to the three curve fitting parameters used in the sigmoidal equation of van Genuchten.

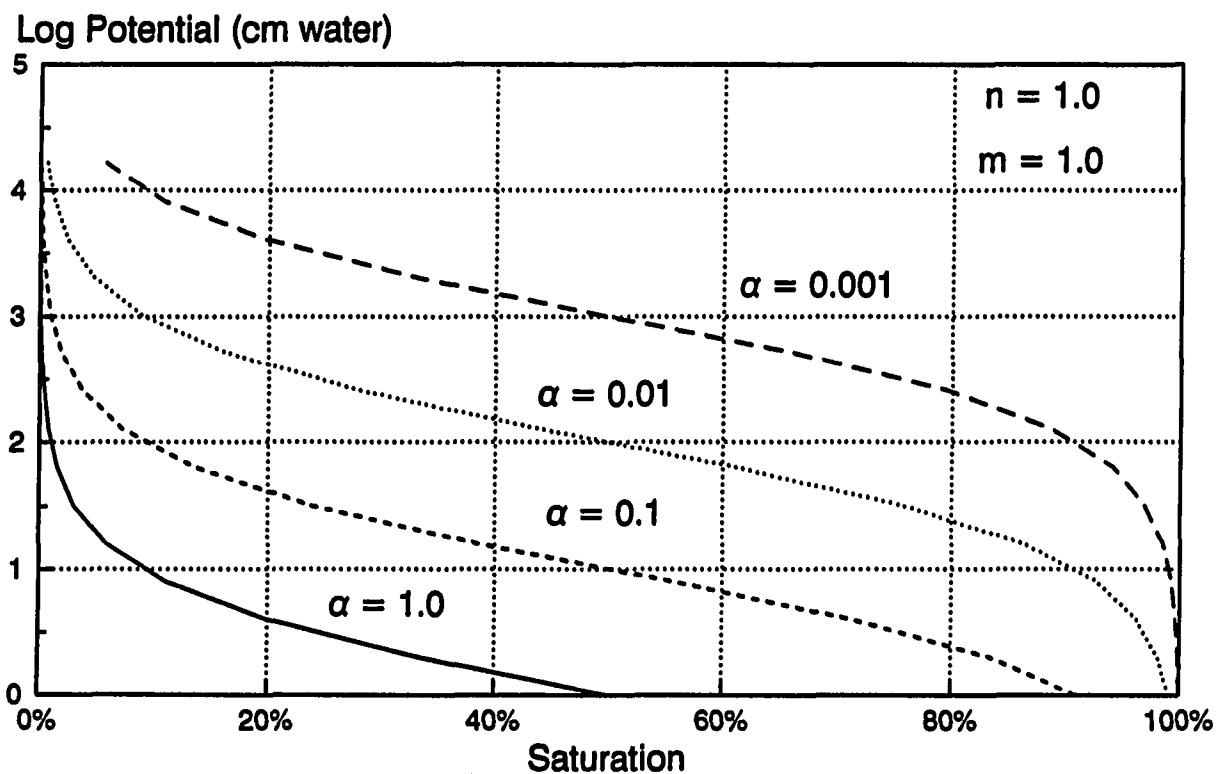


Figure 4.6 Sensitivity of van Genuchten's equation to changes in the parameter α

Decreasing values of α increase the potential at any given saturation level (Figure 4.6). Increasing values of the exponent, n , produce flatter slopes in the funicular moisture range (Figure 4.7).

The exponent, m , also affects the slope of the moisture characteristic curve (inversely to parameter n) and the location of the upper and lower flex points (Figure 4.8).

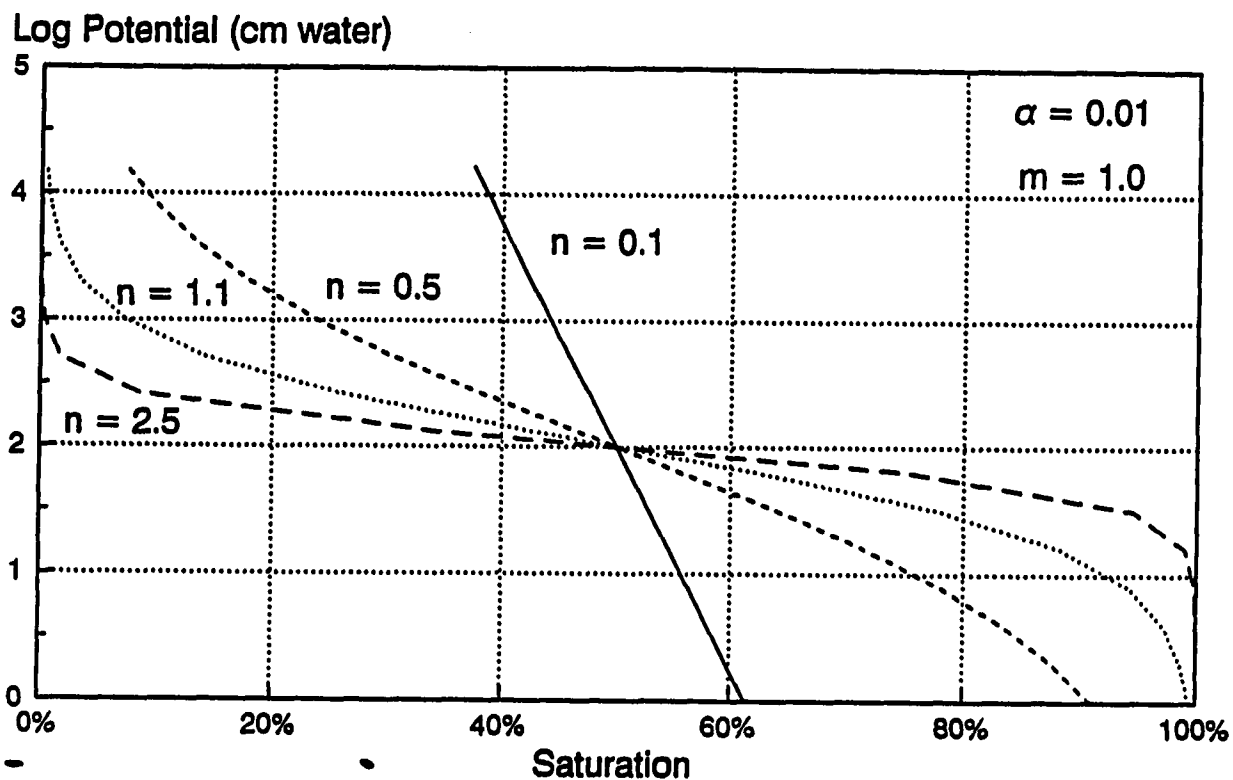


Figure 4.7 Sensitivity of van Genuchten's equation to changes in the parameter n

4.6 Experimental results and discussion

The curve fitting technique described in section 4.5 was used to fit the data obtained from the experimental study. The four curve fitting parameters generated for the van Genuchten equation as well as the sum of squares (F) are summarized in Table 4.3. These fitted curves were used for the analyses presented in this and the following chapter.

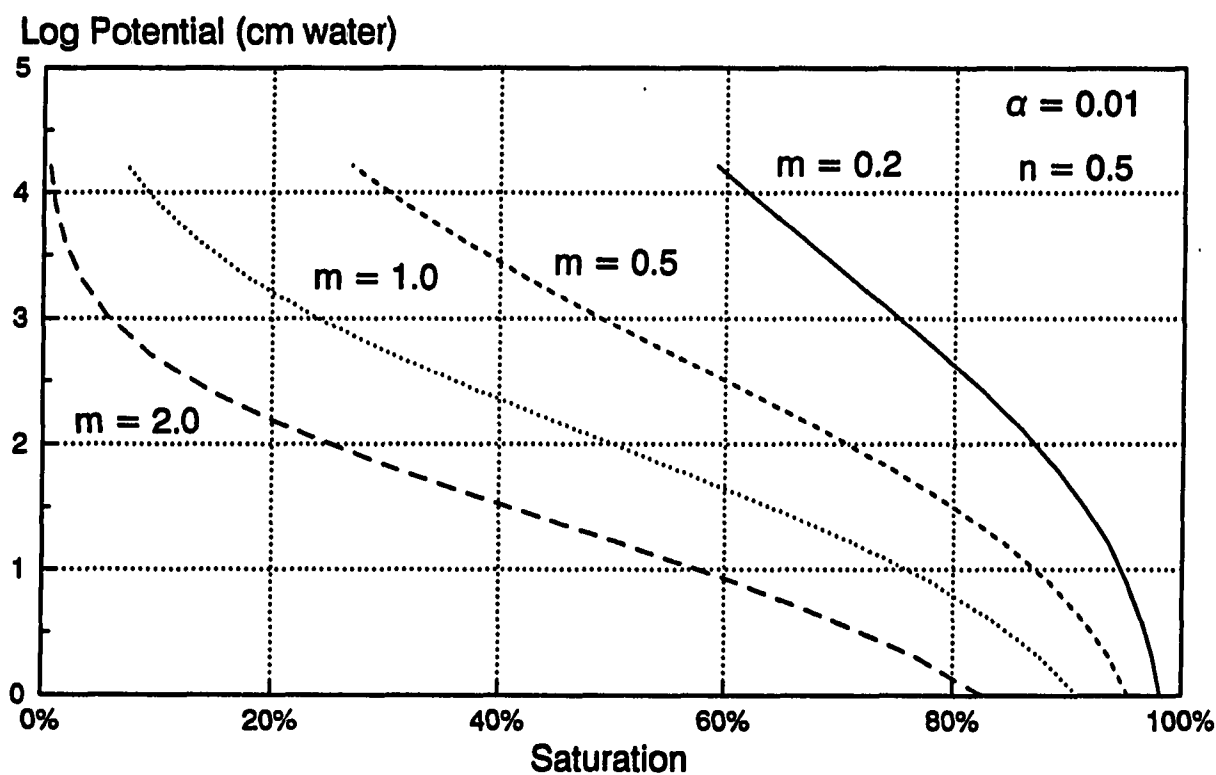


Figure 4.8 Sensitivity of van Genuchten's equation to changes in the parameter m

Table 4.3 Regression analysis of moisture characteristic data

Sand	θ_s	θ_r	α	n	m	F
0.2	0.326	0.0737	5.41E-3	3.92	0.417	7.97E-4
0.4	0.238	0.0728	4.62E-4	1.10	10.0	6.40E-4
0.5	0.242	0.0480	4.21E-4	0.90	10.0	8.85E-4
0.6	0.228	0.0453	2.26E-2	1.31	0.687	3.28E-4
0.8	0.250	0.0432	9.33E-2	7.50	0.087	3.58E-4

Figures 4.9 and 4.10 present data and fitted curves for the five gradations of sand in units of both matric potential (cm H₂O) and pressure deficiency (kPa). Figures 4.9, 4.10, and Table 4.4 show that gradation has a decided effect on the moisture characteristic curve. For the five gradations, an increasing gradation exponent yields decreased values of air entry and upper flex point pressure which is indicative of a larger pore structure. Also, the materials with gradation exponents of 0.4, 0.5, and 0.6 have steeper slopes in the funicular range indicating a wider range of pore sizes in that range than for either the 0.2 or 0.8 gradations. The logarithmic potential scale in Figure 4.10 magnifies the high potential (low suction) portion of the moisture retention curve allowing closer inspection of this section. The more uniform gradations have more indistinct air entry flex points. Consideration of this observation in light of Iowa DOT specifications (1984) for drainable sub-base and porous backfill materials, which specify coarse gradations with little fines (high gradation exponents), indicates that this type of gradation may actually require a slight positive head to become fully saturated. Due to the very low suction levels throughout the upper funicular range, these materials would make very good capillary water barriers under pavements. In addition, they would provide good drainage layers under the low head conditions found in pavement sub-bases.

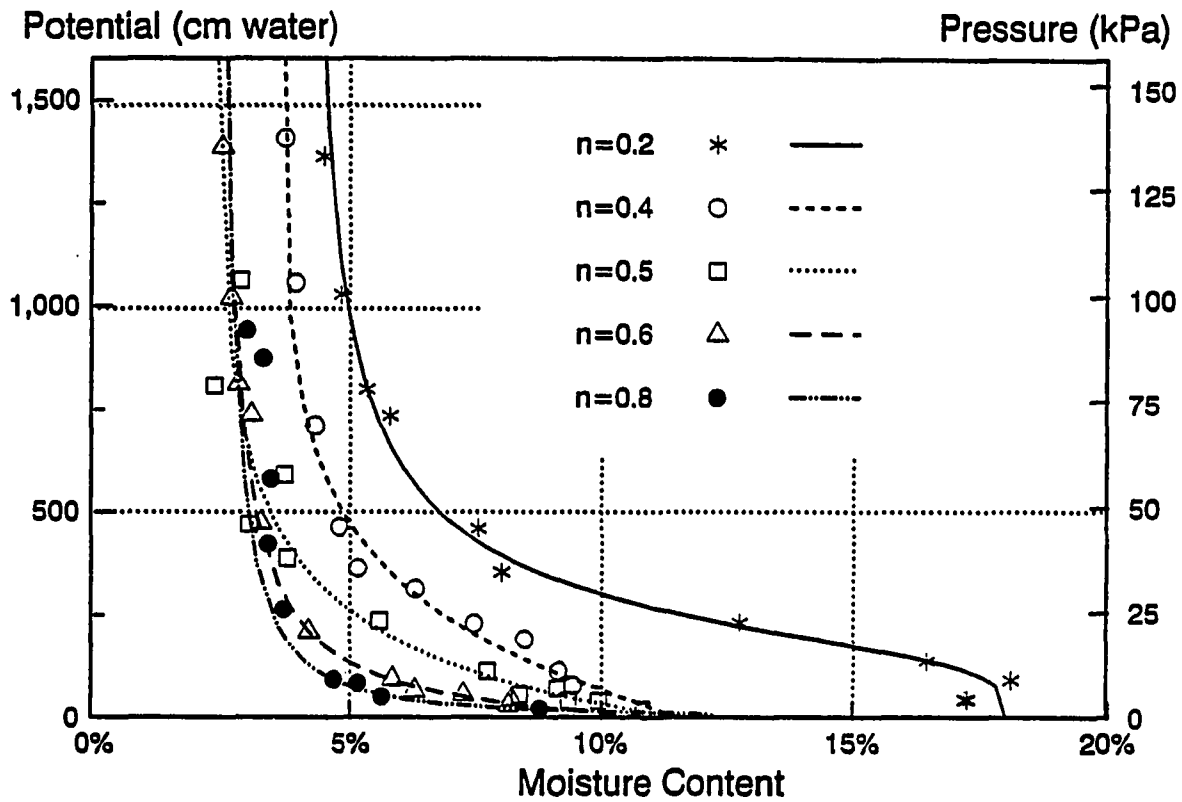


Figure 4.9 Moisture retention data and fitted drainage curves for five sand gradations

Table 4.4 Moisture characteristic data

Sand	Residual Gravimetric Moisture Content	Saturated Gravimetric Moisture Content	Air Entry Pressure cm H ₂ O (kPa)	Upper Flex Point Pressure cm H ₂ O (kPa)
0.2	4.06%	18.0%	130 (12.8)	840 (82.4)
0.4	3.55%	11.6%	60 (5.9)	800 (78.4)
0.5	2.35%	11.8%	39 (3.8)	670 (65.7)
0.6	2.18%	11.0%	23 (2.3)	253 (24.8)
0.8	2.13%	12.3%	10 (1.0)	80 (7.8)

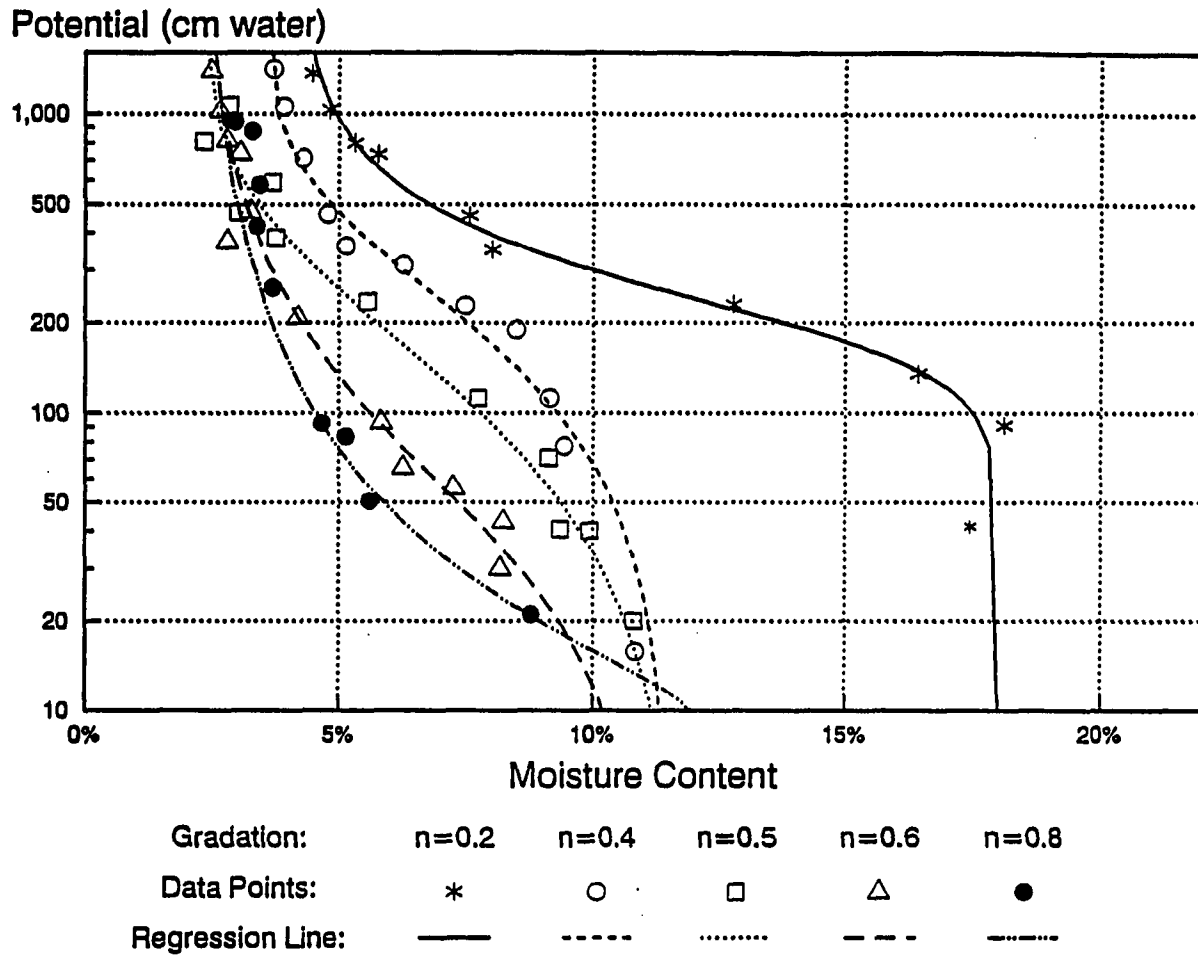


Figure 4.10 Semi-logarithmic presentation (pF) of moisture retention data and fitted drainage curves for five sand gradations

5. COMPARISON OF PARTICLE AND PORE SIZE DISTRIBUTIONS

5.1 Introduction

In the previous chapter, the size of individual pores was related to the matric potential based on the capillary rise equation (eq. 4.1). Also, the shape of the moisture characteristic curve was shown to be dependent on gradation, density, and moisture history.

This chapter describes the relationship used to calculate the pore size distribution from the results of the moisture retention tests. The pore size distributions are then shown to be related to the curvature of the gradations tested. Finally, a conceptual model is developed which allows estimates of pore size distribution to be made for other materials under given conditions of gradation, density and history.

5.2 Calculations of pore size distribution

The capillary tube model of pore size and the moisture retention data were used to generate estimates of pore size distribution since these could be readily generated from the existing moisture retention data.

The capillary rise equation (eq.4.1) can be rewritten to provide a relationship between capillary tube diameter and height of rise (potential) of liquid in the tube. Substituting values for the constants and simplifying:

$$h \text{ (in cm.)} = - \frac{2.98}{d \text{ (in mm.)}} \quad (5.1)$$

where the height of rise, h , is measured in centimeters of water and the tube, or pore diameter, d , is measured in millimeters. Substituting this relationship into equations 4.2, 4.4, or 4.5 allows transformation of the moisture retention relations to cumulative pore size distribution functions. Recalling that saturation is the ratio of the volume of water in the pores to the total volume of the pores, the saturation level then represents the relative volume of water held in the pores at a given level of potential. For the drainage condition, the saturation level represents the relative pore volume attributable to pores with equivalent diameters smaller than the diameter calculated by equation 5.1. Thus the saturation calculated by equations 4.5 and 5.1 becomes the cumulative distribution function for the equivalent pore diameter. The percentage of the pore volume in a given range, or frequency, is then calculated as the difference in the saturation levels calculated for the diameters bounding the range. Pore size distributions were calculated for each of the five materials with the parameters developed for the fitted moisture characteristic curves presented in chapter 4. This crude model of pore structure allows estimates of the pore size distribution for comparison with the particle size distributions used.

5.2.1 Limitations of the capillary tube model

The capillary tube model assumes that all pores of a given size drain at the same pressure deficiency. For this to occur, there could be no constrictions between large pores in the interior of the sample and the exterior. It is probable that large pores in the interior of the sample are surrounded by smaller pores and therefore would not be drained at the same pressure which drains large pores at the exterior of the sample. These larger pores would actually drain when the largest pore to which they are connected was drained. Therefore, the volume of water held in the sample at a given level of pressure includes some water held in pores larger than indicated by the capillary rise equation. Pore size distributions calculated on the basis of drainage curves will therefore attribute the volume of large, enclosed pores to the size of the largest pore enclosing it. Thus the calculated pore size distribution is shifted toward smaller equivalent diameters in comparison to the actual pore size distribution.

5.3 Discussion of pore size distributions

Comparison of Figures 3.1 and 5.1 in which the cumulative particle and pore size distributions are plotted indicates that the slopes of the pore size distributions calculated according to equations 4.5 and 5.1 and the curvature of the particle size distribution curves are related. The most well graded material ($n = 0.2$) has the most uniform pore size

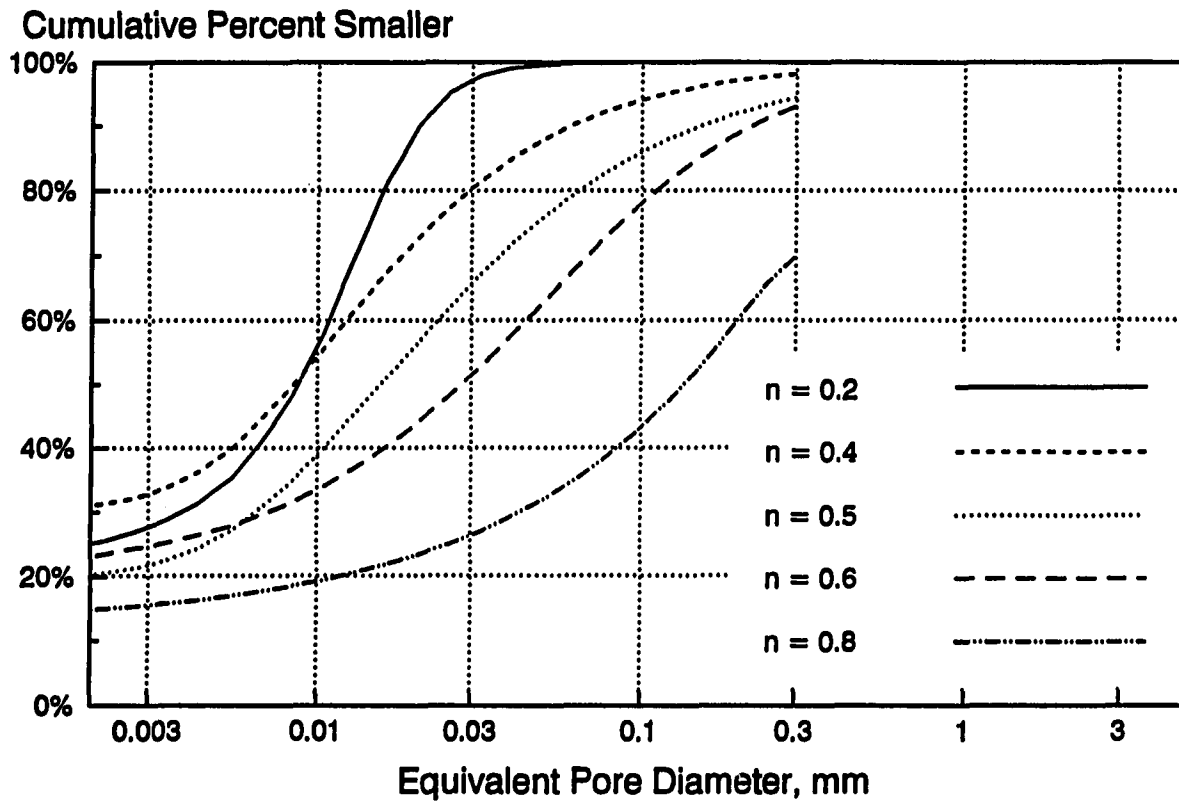


Figure 5.1 Cumulative pore size distributions according to equations 4.5 and 5.1

distribution. The most poorly graded material ($n = 0.8$) has the highest volume of large pore sizes. All pore size distributions in Figure 5.1 are truncated above 0.298 mm, which corresponds to a matric potential of 10 cm. of water because no moisture tension measurements were made at potentials greater than 10 cm. Those particle gradations which produced the highest densities ($n = 0.4$ and 0.5) have pore size distributions with curvatures nearly identical to their particle size distributions. The pore size distribution of the $n = 0.6$

gradation has a flatter slope than its particle size distribution, tending toward that of the $n = 0.8$ gradation but without as high a volume of large pores.

The particle size frequency diagrams in Figure 5.2 show the increasing coarseness of the gradations with increasing exponent value. However, the pore size frequency diagrams in Figure 5.3 emphasize the points made in the preceding paragraph. These frequency diagrams show only the distribution of equivalent pore diameters greater than 0.002 mm. The $n = 0.2$ gradation, with very evenly distributed particle size frac-

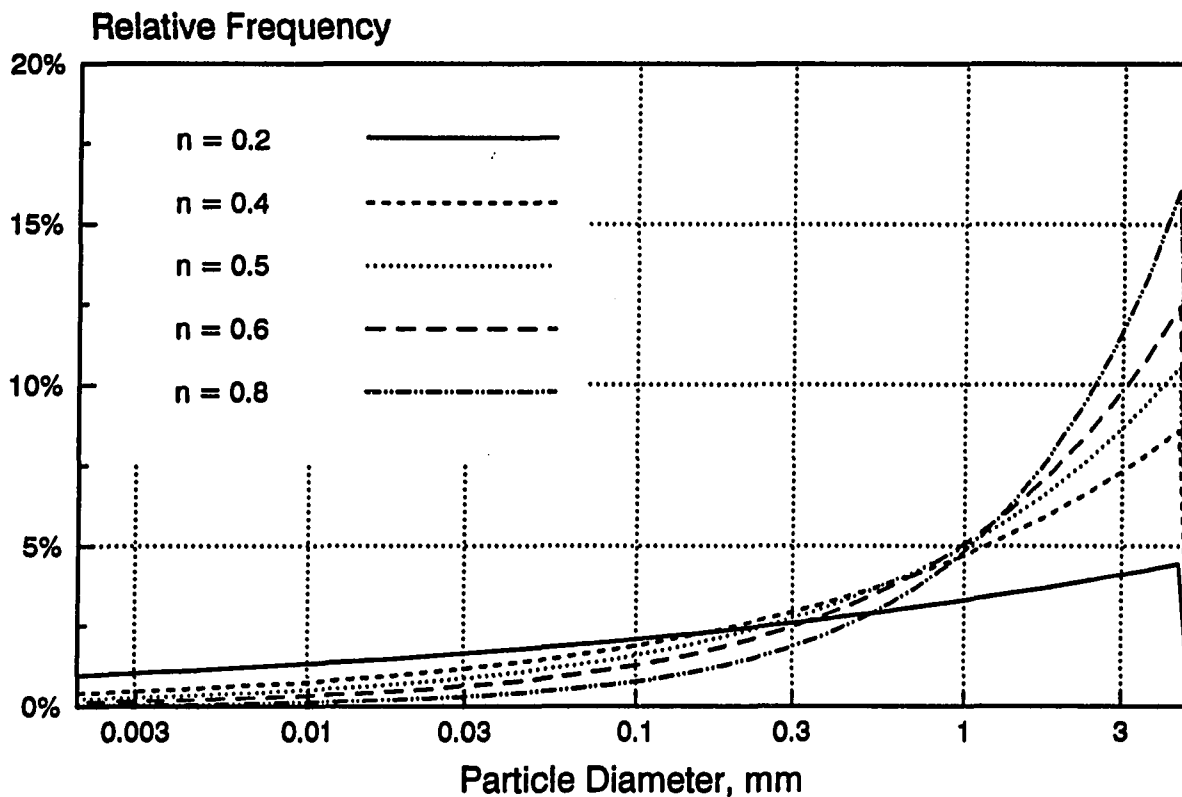


Figure 5.2 Particle size frequency distribution

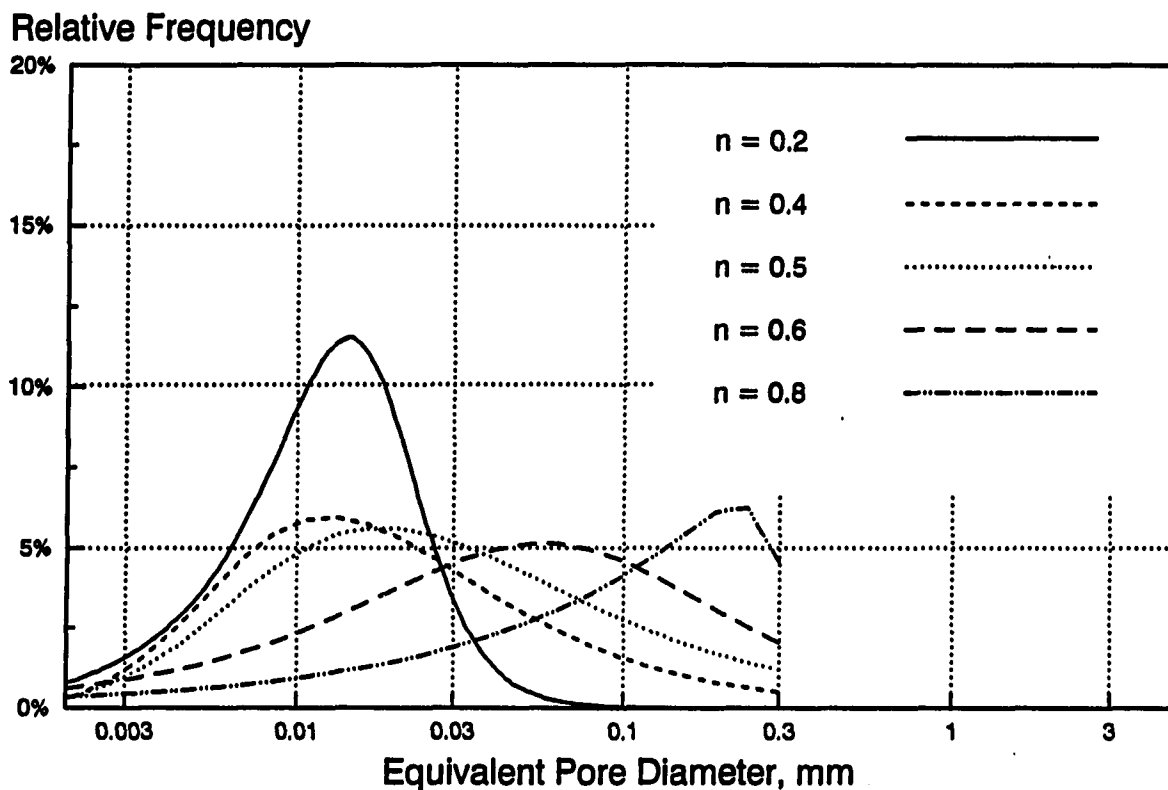


Figure 5.3 Pore size frequency distributions

tions, has the finest pore size distribution with a modal diameter of 0.013 mm. The two gradations which exhibited the highest maximum densities ($n = 0.4$ and 0.5) have very similarly distributed pore sizes with modal diameters of 0.012 and 0.018 mm respectively. The $n = 0.6$ gradation, which has a fairly uniform pore size distribution, has a modal pore diameter of 0.055 mm. The $n = 0.8$ gradation exhibits a distinctively greater concentration of larger pores with a mode greater than 0.225 mm. The overlap of the modal diameters for

the $n = 0.2$ and 0.4 gradations is due primarily to the higher void ratio of the $n = 0.2$ gradation. The range of void ratios for the other gradations was from 0.30 to 0.33 . The $n = 0.2$ gradation was tested at a void ratio of 0.48 . This serves to emphasize the effect of compaction on pore size distribution in addition to the effects of gradation.

Figure 5.3 does not show the frequency distribution of pores with equivalent diameters smaller than 0.001 mm because of the limited pressures used in the moisture retention experiments. The calculated total percentages of pore volume in pores smaller than 0.001 mm are:

$n = 0.2$	23%
$n = 0.4$	31%
$n = 0.5$	20%
$n = 0.6$	22%
$n = 0.8$	14%

The relatively large pore volumes in pores with equivalent diameters less than 0.002 mm. may be due, in part, to the absence of particles finer than 0.002 mm. Apart from these volumes, the largest pore volumes occurred in the 0.01 to 0.1 mm. equivalent diameter range for all except the $n = 0.8$ gradation, two orders of magnitude lower than the range of largest particle concentration.

Analysis of the mercury porisimetry data provided by Badger and Lohnes (1973) for compacted loess at six different densities shows that the largest volume of pores occurred in the 0.001 to 0.01 mm. diameter range. This is within one

order of magnitude of the maximum particle size (0.01 mm.). The loess, however, is a very uniformly graded material ($n > 1.0$). This corroborates the observation that the pore size distributions of very uniformly graded particulates have a large fraction of the pore volume in pores with equivalent diameters in the same range as the majority of the particle diameters.

Figure 5.4 presents the relationship between the equivalent pore diameters at the upper and lower flex points of the

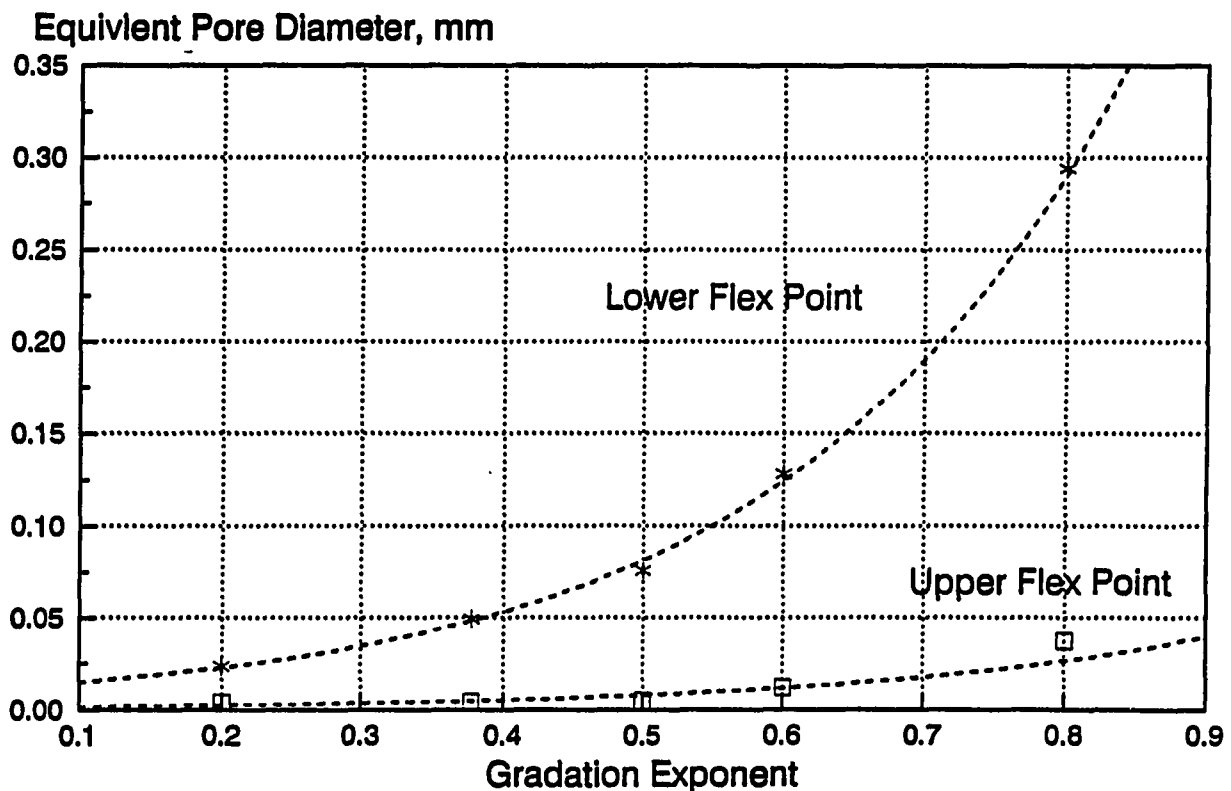


Figure 5.4 Relationship between equivalent pore diameters at the moisture characteristic curve flex points and gradation exponents

moisture characteristic curves and the gradation exponents. The range of equivalent pore diameters in the funicular moisture range increases dramatically as the particle size distribution becomes more uniform.

The lines shown in Figure 5.4 are from equations of the form $y = ae^{bx}$, generated by linear regression of the exponential transform of the data. For the limited data, the "a" parameters differ by a factor of ten (lower: 9.7E-3 vs. upper: 9.9E-4) and the "b" parameters are nearly identical (lower: 4.2 vs. upper: 4.1). This suggests a strong connection between the curvature of a particle size distribution curve and its pore size distribution.

Figure 5.5 shows the calculated volumes attributed to the capillary, funicular and pendular moisture states. As expected from the pore size distributions, the $n = 0.8$ gradation could hold the largest percentage of capillary water. Since capillary water is the easiest to drain, this substantiates drainable sub-base specifications which call for materials with steep gradation curves with little or no fines. In all cases, the pendular water volume is between 25 and 35% of the total pore volume. This narrow range is associated with the relatively narrow range of equivalent pore diameters calculated for the upper flex points and the very similar volumes of pores in the minus 0.001 mm. diameter range.

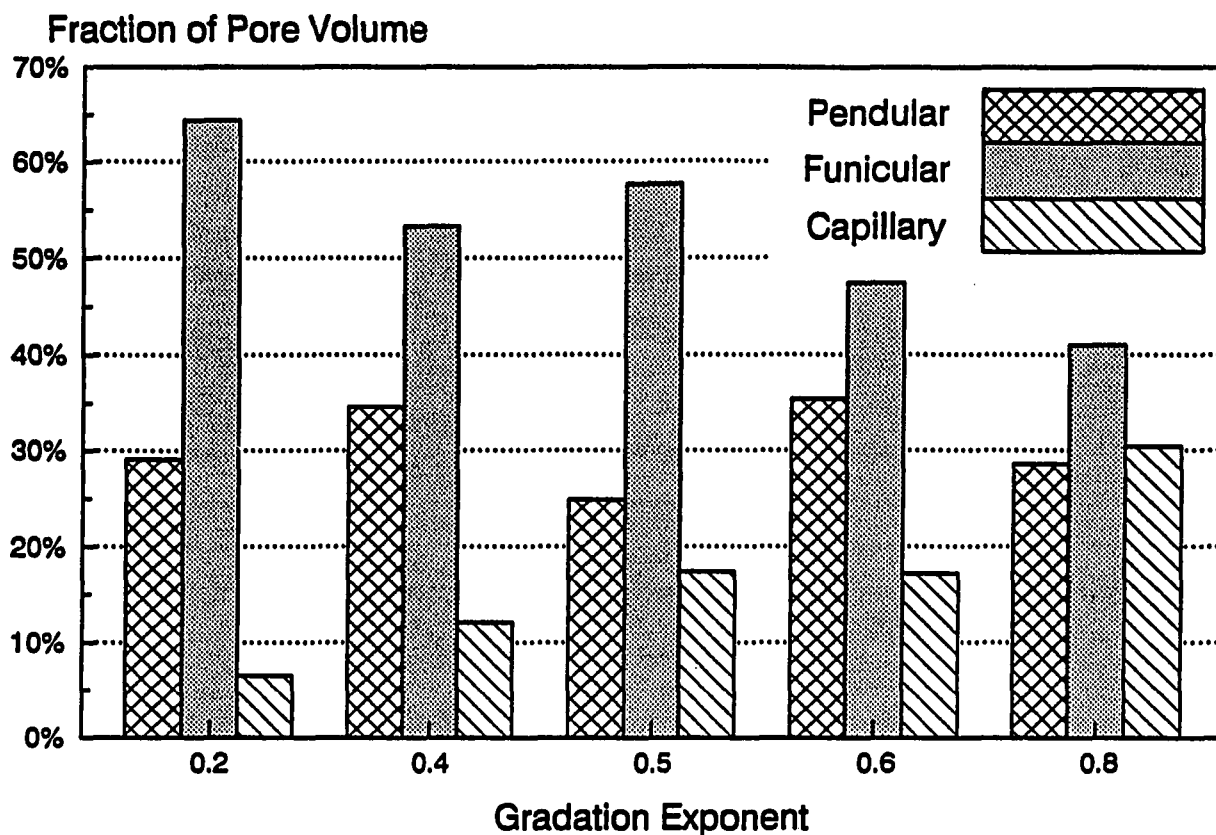


Figure 5.5 Fraction of pore volume attributable to the pendular, funicular, and capillary moisture ranges

5.4 Conceptual model of pore and particle size distributions

For particulate materials with gradations which can be modeled according to equation 3.1 (generally applicable to manufactured or crushed materials), the pore size distribution and therefore the moisture characteristic curve have been shown to be functions of the density and curvature of the gradation. In a dense condition, gradations with exponents from 0.4 to 0.6 exhibit widely distributed pore sizes centered

approximately two orders of magnitude smaller than the maximum particle size. They therefore exhibit steeper funicular range slopes in moisture characteristic curves. Well graded materials exhibit more uniform pore size distributions two to three orders of magnitude smaller than the maximum particle size. Poorly graded materials exhibit larger pores with monosized materials exhibiting uniform pore size distributions in the same order of magnitude as the particle size. As relative density decreases, pore size distributions shift toward higher pore volumes at larger equivalent diameters.

6. EQUIVALENT PORE PRESSURES IN PARTIALLY SATURATED SYSTEMS

6.1 Introduction

Chapter two introduced the effective stress equation first proposed by Terzaghi for saturated soils and the pore pressure term, u . For two phase systems (dry or saturated), the pore pressure is obviously equal to the gas or liquid pressure and in most dry systems the gas pressure is equal to atmospheric pressure (zero gauge pressure). However, when applying this equation to partially saturated (three phase) materials, defining what the actual pore pressure is becomes a problem.

The liquid pressures were previously shown to decrease as the level of saturation decreases (chap. 4) and to exhibit different rates of change in pressure in different moisture regimes. In the capillary moisture state where the voids are full or nearly full of fluid, the pressure decreases drastically with very little change in the moisture content. In the funicular range where both the liquid and gas phases are continuous throughout the voids, the pressure decreases less dramatically as moisture content decreases. Finally, in the pendular state, the moisture is no longer continuous and the pressures in the remaining fluid decrease extremely rapidly with very little change in the moisture content. Since the liquid pressures change inversely to liquid distribution and continuity, it is appropriate to consider the rationale behind

treating the three phases with an equation based on continuum mechanics principles.

6.2 Continuum mechanics approach

Classical soil mechanics theories and applications are based on the concepts of continuum mechanics. Thus, the inhomogeneous and discontinuous materials which make up the earth's crust are modeled as homogeneous, continuous bodies because experience has shown that the predictions of continuum mechanics are generally correct. By selecting a large enough scale, the inhomogeneities and discontinuities become indistinct and small irregularities are smoothed over. Therefore, the use of the effective stress concept assumes that the stress state in partially saturated particulate materials can also be modeled with continuum mechanics principles.

The effect of particle size distribution on the number of interparticle contacts was introduced in chapter two. It is only at these individual grain to grain contact points that the solid phase is even remotely continuous. Bishop and Eldin (1950) have shown that the actual area of solid contact is typically as low as 0.03% of the total cross sectional area. The actual contact point effective stresses are therefore extremely high and yet the effective or solid phase stresses are modeled on a total cross sectional area basis. This provides a general, averaged stress parameter for the solid phase.

In order to reconcile the variations in distribution and continuity of the liquid and gas phases with the continuum mechanics approach, the effective stress equation for partially saturated soils (eq. 2.1) treats the pressures in the pore fluid(s) as averaged values, acting on the entire cross sectional area. In this form, the equation depends on measurements of both the pore air and water pressures plus knowledge of the relationship between saturation level and the value of the parameter X .

The actual fluid and gas phase pressures are then treated as what may be termed an "equivalent pore pressure" made up of a combination of fluid and gas phase pressures related by a proportionality parameter. Thus, the equivalent pore pressure, u^* , may be expressed as (Skempton, 1960):

$$u^* = u_a - X(u_a - u_w) \quad (6.1)$$

In nearly saturated, or capillary moisture systems, the saturation level itself is often used as the proportionality factor. However, in three phase systems using saturation level as the proportionality factor in equation 2.1 produced poor agreement between the results of saturated, consolidated undrained (CU) triaxial tests with pore pressure measurements and unsaturated, CU tests with both air and liquid pressure measurements (Bishop and Eldin, 1950; Aitchison and Donald, 1956).

Further, the concept of an equivalent pore pressure in materials with saturation levels in the pendular moisture range can not be addressed with proportionality factors. The pressures in this moisture region are so low that they can not easily be measured with the techniques normally associated with triaxial tests. Because of this, the proportionality factor, X , is undefined in the pendular moisture range. The traditional, geotechnical approach has been to neglect the negative pore pressures in this moisture region as inconsequential to the stability of naturally occurring soils. However, the normal range of moisture contents for many bulk solid materials, such as coal, is in the pendular moisture range and these materials owe much of their apparent cohesive properties to this pendular moisture.

Because the bonding forces due to pendular moisture can contribute significantly to the strength and compressibility behavior of some materials it is necessary to have some means of estimating an equivalent pore pressure in this moisture region if the effective stress concept is to be used.

6.3 Micromechanical approach

An alternate method to account for the contribution of negative fluid pressures to the strength of partially saturated materials is to model the individual forces on discrete particles and then extrapolate the model from the microscopic to macroscopic scale. Rumpf's (1958) model of tensile

strength in agglomerates bound by liquid bonds was introduced in chapter two and is presented here as an example of the micromechanical approach.

Rumpf (1958) developed a model of the tensile strength of agglomerates which accounts for either localized bonding at contact points or bonding due to pressures in partly to fully saturated voids. From considerations of a randomly packed, monosized system of spheres, Rumpf developed equations relating the strength and size of a single, pendular bond to the particle size and porosity. The contributions to the strength of the pendular bond arise from both the pressure deficiency of the liquid held in the pendular bridge as well as the interfacial forces in the liquid-gas membrane. An equation for the size of each pendular bridge was generated from the assumed geometry, assumptions about the relationship between porosity and number of contact points, and the amount of moisture in the system.

A second model accounts for the tensile bonding of fully filled voids (capillary moisture state). In this model the capillary rise equation (eq. 4.1) is used as the basis to develop a relationship between the tensile strength, particle size and shape, surface tension, and porosity. The introduction of a particle size and shape function to represent pore diameter is based on the work of Carman (1941); (see also section 4.1).

These two models are micromechanical in scale, but, to be useful in a field dominated by continuum mechanics, the results must be extrapolated to the larger, macromechanical scale. In the pendular model, the statistically random orientation of the contact forces allows the summation of these forces across an arbitrary plane to be transformed into a stress state on that plane. Also because of the random orientation and arbitrary nature of the chosen plane, this stress could be taken as an equivalent, isotropic pore pressure when seen on the macroscopic scale. The capillary model is a direct stress model and requires no statistical scale up to be applicable on the continuum scale. These models, when used jointly describe the tensile strength of particulates on a total stress basis (section 2.2 and Figure 2.1).

6.4 Resolution of effective and total stress concepts

Reexamination of Figure 2.1 and the total stress approach to apparent cohesion in light of the effective stress concept for unsaturated materials indicates that the total and effective stress representations of shear strength need not be exclusive. The effective stress concept assumes that the shear stress intercept of the Mohr envelope is an inherent *property*, not parameter, of the material and that the envelope is unique for the material at a given density. Negative pore pressures vary with moisture content, but this variation does not produce different Mohr envelopes; the variation in pore

pressure simply causes variation in the effective normal stress.

The total stress models of tensile strength predict the contribution of the void fluid to the cohesive strength of the material. Since the predicted tensile strength according to these models can be calculated for moisture bonding alone, the tensile strength can be equated with the equivalent, negative pore pressure for a given material at a specified density and moisture content. In this manner the total and effective stress models can be reconciled.

6.4.1 Equality of tensile stress and equivalent pore pressure

As an example, consider an unsaturated, noncohesive, particulate specimen undergoing shear in a triaxial test with no applied, confining stress (unconfined test). The material possesses no "true" cohesion and would therefore have a Mohr envelope which intersects the normal stress axis at zero shear stress (Figure 6.1, "effective stress envelope"). The tensile strength intercept, σ_t , is the origin of the "total stress envelope". The failure condition Mohr's circle for the total stress case is labeled "T". The confining stress for the total stress case is zero and the intersection of the Mohr's circle and failure envelope occurs at a shear stress of τ_f .

If the tensile strength is in fact equal to the equivalent negative pore pressure, u^* , the effective confining stress according to equation 2.3 is equal to the absolute

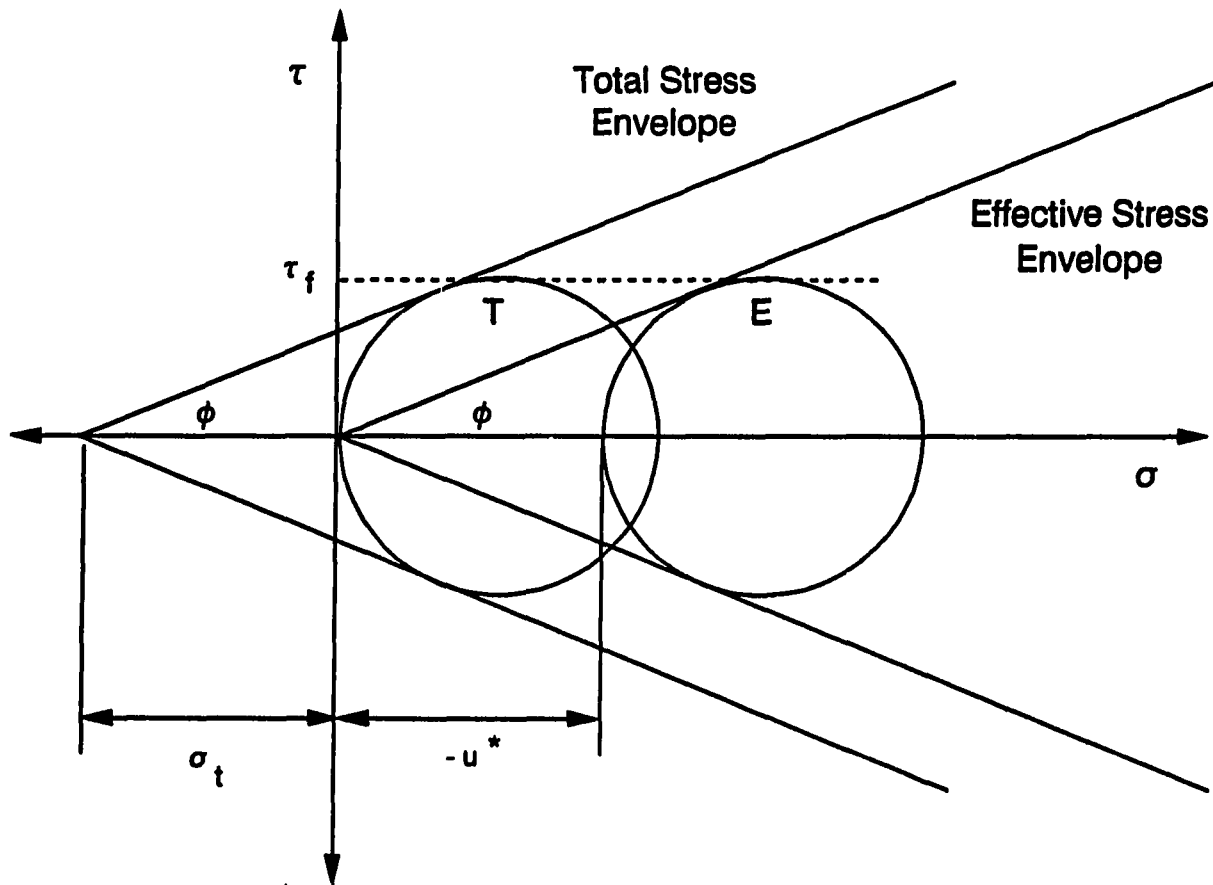


Figure 6.1 Total and effective stress representation of unconfined compressive strength for noncohesive materials

value of u^* . This would then generate the failure Mohr's circle labelled "E" which is shifted to the right on the compressive stress axis. However, the intersection of the effective stress Mohr's circle with the effective stress envelope

still occurs at a shear stress of τ_f , as did the total stress representation. Both representations of stress state produce the same shear stress at failure and can therefore be equated by the effective stress concept.

This simple analysis is predicated on the assumption that the negative pressures in the fluid phase are the same at failure as in the initial sample. This is a very simplistic assumption and is only valid for materials which undergo no volume change during shear. However, for materials which undergo either consolidation or dilation during shear, the same changes in equivalent pore pressure or tensile strength are expected independent of the representation of stress state. Therefore, viewing the tensile strength in the total stress system as the equivalent pore pressure in an effective stress system reconciles the two approaches. Moreover, this approach allows the use of tensile strength models to predict and explain equivalent pore pressures.

6.5 Equivalent pore pressure model

The tensile strength-equivalent pore pressure model used in this research is based on the previously cited work of Rumpf and Schubert. The full derivation of the model is found in Levorson (1991); a summary of the salient points is provided here.

The development of the model assumes that the mechanisms of stress transfer between solid particles by the pore fluid

can be categorized according to the moisture state or region. Therefore, the capillary state in which the pores of the particulate system are fully or nearly full of fluid is modeled with one equation. The equivalent pore pressure in the pendular state is modeled on the basis of an assumed geometry in which the moisture is seen as existing as pendular rings at the contact points between solid particles. The funicular moisture state is not directly modeled because the geometry of the liquid-gas-solid structure is too complex. However, the funicular state can be envisioned as a transition state between the pendular and capillary states and can therefore be modeled by superimposing systems composed of discrete pendular rings and fully saturated capillaries. The equivalent pore pressure can then be modeled as pendular rings and fully saturated capillaries in direct proportion to the amount of fluid in excess of the pendular-funicular transition.

6.5.1 Capillary state model

When the void volume is completely filled with fluid, the pressure in the fluid is the pore pressure. Capes (1980) and Schubert (1984) have shown that for saturation levels above 90% the equivalent pore pressure can be stated as:

$$u_c^* = S \cdot p_c \quad (6.2)$$

where p_c is the negative fluid pressure. Restating the capillary rise equation (eq. 4.1) in terms of the hydraulic radius (R) of the pores rather than the diameter (Carman, 1948):

$$p_c = \frac{T \cos \delta}{R} \quad (6.3)$$

Further, the hydraulic radius can be stated in terms of the volumetric specific surface (S_v , the ratio of particle surface area to volume) and the void ratio of the system (Levorson, 1991):

$$R = \frac{e}{S_v} \quad (6.4)$$

Restating volumetric specific surface in terms of a mean particle size (x_{sv}) and shape factor (ψ_{sv}), equation 6.3 becomes:

$$p_c = \frac{T \psi_{sv} \cos \delta}{e x_{sv}} \quad (6.5)$$

For spheres, ψ_{sv} (the ratio of particle surface area to volume) is equal to six. Carman (1941) and Newitt and Conway-Jones (1958) report that irregularly shaped sand particles exhibit surface to volume shape factors of 6.5 to 8. Schubert (1984) reports that these values are only valid for materials

made up of a narrow range of particle sizes and that ψ_{sv} may vary from 1.9 to 14.5 for wider particle size distributions.

For materials with $\delta = 0^\circ$, the equivalent pore pressure in the capillary moisture state becomes:

$$u_c^* = \frac{ST\psi_{sv}}{e x_{sv}} \quad (6.6)$$

6.5.2 Pendular state model

In the pendular state, the moisture is assumed to exist as pendular bridges between particles at the grain to grain contacts. The forces transmitted by the bridges are divided into those transmitted by the gas-liquid meniscus and those caused by the negative pressure in the fluid. Therefore, since the magnitude of the force is dependent on the size of the bridge, the volume of each bridge is stated as a function of the amount of fluid in the system, the number of contact points where bridges could form (dependent on the density of the system), the particle size and shape, and the contact angle between the solids and fluid. The volume of a single, representative bridge is then used to determine the minimum cross sectional area and circumference of the bridge and its internal and external radii.

The pressure of the fluid is estimated from the double curvature form of the capillary rise equation, which is

$$p_p = T \left(\frac{1}{r_i} - \frac{1}{r_o} \right) \quad (6.7)$$

for $\delta = 0^\circ$, where p_p is the pressure in a pendular bridge, and r_i and r_o are the internal and external radii. This pressure is multiplied by the minimum cross sectional area of the bridge to obtain the limiting adhesion force due to the negative pressure. Similarly, the surface tension of the gas-liquid interface is multiplied by the circumference of the bridge to obtain the limiting adhesion force transmitted by the boundary. Summing the two force components yields an expression for the force transmitted by a single bridge (A_L):

$$A_L = T \cdot x_{sv} \cdot F_A \quad (6.8)$$

where F_A is a dimensionless function incorporating terms and variables developed from the volume, area, circumference, and pressure calculations above.

This adhesion force is a vector term representative of the average, pendular, adhesion force in the system. Due to the statistically random orientation of all adhesion vectors in the system, the macroscopic stress state can be modeled as isotropic. Further, the distribution and orientation of these forces on any arbitrary plane can be resolved to yield the equivalent pore pressure equation for the pendular state:

$$u_p^* = \frac{T F_A}{e X_{sv}} \quad (6.9)$$

6.5.3 Funicular state model

Since the equivalent pore pressures in the funicular state are modeled as a combination of the pendular and capillary models, the boundary saturation levels must first be defined. Haines (1930) calculated the saturation levels at which pendular bonds should begin to coalesce and form funicular bonds in systems composed of monosized spheres. For a closely packed system, the saturation level at the pendular-funicular transition (S_b) was 12% and that for a loosely packed system was 6%. Baver (1956) presents a number of moisture characteristic curves for a wide range of soil gradations which show transition saturation levels between 5 and 45%. Coarse and uniform soils exhibited low transition saturation levels while finer and more distributed gradations exhibited higher transitions. In uniform gradations the transition is instantaneous and the moisture characteristic curve has a very pronounced flex point. Materials with widely distributed particle sizes exhibit broad transition zones with high radii of curvature. Figures 4.9 and 4.10 show that the transition is very gradual in the materials used in this research. As stated previously, the pendular-funicular tran-

sition was taken to occur at the point of maximum curvature in the moisture characteristic curve. This point occurs at a slightly higher moisture content than the residual moisture content.

Alway and McDole (1917) showed that the residual moisture content was between two and three times higher than the hygroscopic moisture content for a wide variety of soils and sands. They defined hygroscopic moisture content as the dry weight basis moisture content of a sample in equilibrium with air at a relative humidity of 99%. If we then take the transition moisture content to be three times the hygroscopic moisture content (w_H), the saturation level at the pendular-funicular transition (S_p) becomes:

$$S_p = \frac{3 w_H G_s}{e} \quad (6.10)$$

It was previously stated that several researchers have found that the saturation level at the capillary-funicular transition (S_c) occurs between 90 and 100%. For this research, the transition used in the model was arbitrarily set at 95% on the basis of the experimental moisture retention curves in chapter 4.

The equivalent pore pressure in the funicular range is modeled as the sum of prorated pendular and capillary pressures. The equivalent pendular (u_p^* from eq. 6.9) and capil-

lary (u_c^* from eq. 6.6) pressures are calculated at their respective transitions (S_p and S_c) and are prorated linearly to zero at the other transition. Thus, the individual components become:

$$u_{p'}^* = u_p^* \left(\frac{S_c - S}{S_c - S_p} \right) \quad (6.11)$$

$$u_{c'}^* = u_c^* \left(\frac{S - S_p}{S_c - S_p} \right) \quad (6.12)$$

If the material has an open, drainable pore structure, the equivalent pore pressure would follow the trend shown by the dotted line labeled $u_{p'}^*$ in Figure 6.2. For materials with finer pore size distributions, the equivalent pore pressure would follow the trend of the solid line in the funicular range which is the sum of the two components.

6.5.4 Parameters for the equivalent pore pressure model

In practice this model requires estimates or measurements of the specific surface or mean particle size, hygroscopic moisture content, surface tension, contact angle, moisture content and state of packing of the material (void ratio or porosity). All other parameters and intermediate, calculated values are derived from these input parameters.

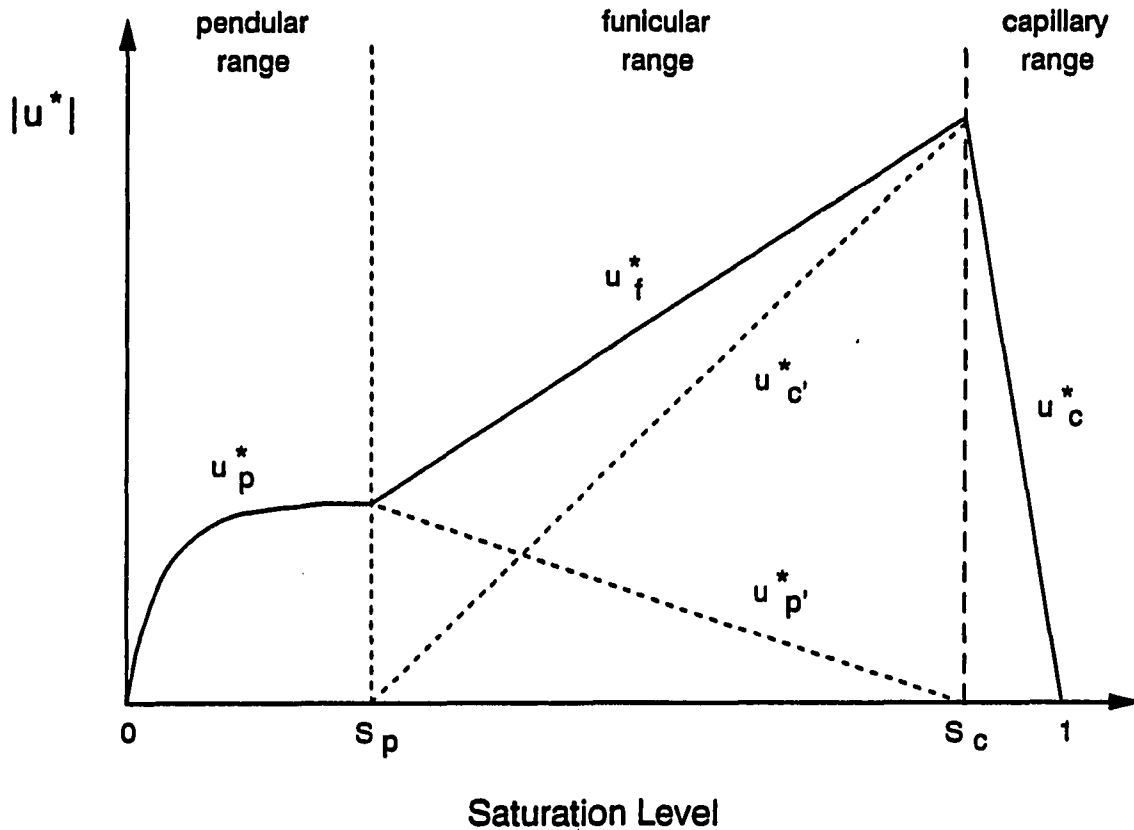


Figure 6.2 Diagram of the equivalent pore pressure model as a function of saturation level

6.6 Estimates of specific surface mean diameter

As stated in section 6.5.1, the volumetric specific surface can be restated in terms of a mean particle size (x_{sv}) and shape factor (ψ_{sv}). Hogg (1978) presents a method for

estimating a specific surface based mean particle size by integrating the particle size density function times the ratio ψ_{sv}/x_{sv} from the smallest size (d) to the top size (D). For the single curvature gradations used in this research, the integration yields (Hogg, 1978):

$$x_{sv} = \frac{n-1}{n} \left(\frac{D^n}{D^{n-1} - d^{n-1}} \right) \quad (6.13)$$

Alternatively, the measured air entry pressures from the moisture retention curves can be substituted for u_c^* in equation 6.6 which can then be solved for x_{sv} .

6.6.1 Comparison of mean diameters

Mean particle diameters were calculated according to equation 6.13 for the five gradations. These values were used in equation 6.6 to calculate the equivalent pore pressure at the funicular-capillary transition (p_c) for comparison with the measured air entry pressures (p_e) of the moisture characteristic curves (cf. Table 4.4). The values of the other variables used in this analysis were: saturation (S) = 95%, surface tension (T) = 0.073 N/m, shape factor (ψ_{sv}) = 6.5, and void ratio (e) calculated from the average density of the moisture retention samples (cf. Table 4.2). Mean particle diameters were also calculated with equation 6.6 and the measured air entry pressures. Both diameters, the calculated

air entry pressures and the measured air entry pressures are presented in Table 6.1.

Table 6.1 Comparison of predicted and measured values

Gradation	x_{sv} (eq. 6.13) (mm)	p_c (eqs. 6.6 & 6.13) (kPa)	p_e (Table 4.2) (kPa)	x_{sv} (p_e & eq. 6.6) (mm)
n = 0.2	0.079	11.7	12.8	0.072
n = 0.4	0.112	12.9	5.9	0.245
n = 0.5	0.159	8.9	3.8	0.372
n = 0.6	0.218	7.1	2.3	0.671
n = 0.8	0.404	3.4	1.0	1.372

Other than for the $n = 0.2$ gradation, there is a two to threefold difference between the predicted and measured pressures and particle sizes. Because the model is very sensitive to the particle size estimate and those derived from the measured air entry pressures, p_e , provide a way to calibrate the model, the values derived from the measured air entry pressures (last column of Table 6.1) are used from here on.

7. COMPRESSIVE STRENGTH IN PARTIALLY SATURATED MATERIALS

7.1 Introduction

The objective of this phase of the research was to examine the shear strength of the five gradations as a function of the gradation and fluid pressures. Unconfined compressive strength tests were performed on compacted samples of each material over the full range of saturation levels and these measured strengths were compared to strengths predicted on the basis of the equivalent pore pressure model.

7.2 Shear strength as a function of negative pore pressure

The shear strength of particulate materials can be described by the Coulomb equation:

$$\tau = c + \sigma \tan \phi \quad (\text{cf. eq. 2.5})$$

in which τ is the shear stress at failure, c is the cohesion or shear strength under zero applied normal stress, σ is the normal stress on the plane of failure, and $\tan \phi$ is the slope of the shear stress-normal stress relationship. The angle of internal friction is normally designated as ϕ .

In terms of total stresses, the equivalent pore pressure term developed in the preceding chapter becomes the normal stress intercept of the Mohr-Coulomb diagram (cf. Fig. 2.1). The equivalent pore pressure is related to the cohesion term in Equation 2.5 by

$$c = -u^* \cdot \cot \phi \quad (7.1)$$

This representation of the stress state is often called apparent cohesion since the cohesion produced by the moisture tension induced pore pressures is as transient in nature as the moisture content of the material.

The major (σ_1) and minor (σ_3) principal stresses at failure for this total stress condition can be related to the intrinsic or tensile stress intercept (equivalent pore pressure) by:

$$\sigma_1 (1 - \sin \phi) - 2 u^* \sin \phi + \sigma_3 (1 - \sin \phi) \quad (7.2)$$

Or for the unconfined compression (f_c) case in which the minor principal stress (σ_3) is equal to atmospheric pressure:

$$f_c = \sigma_1 = 2 u^* \frac{\sin \phi}{1 - \sin \phi} \quad (7.3)$$

In granular materials the effective stress value of cohesion in equation 2.5 is insignificant and is ignored hereafter. This reduces equation 2.5 to a one parameter relationship between shear strength and normal stress. For the case of pore air pressures equal to atmospheric pressure, equation 2.5 can be written as:

$$\tau = \bar{\sigma} \tan \bar{\phi} = (\sigma - u^*) \tan \bar{\phi} \quad (7.4)$$

in terms of effective stresses or total stress and equivalent pore pressures. This concept was developed in section 6.4 (see also Figure 6.1).

Therefore, the failure stress on either a total stress or effective stress basis is a function of the equivalent pore pressure of the partially saturated material and its friction angle. Assuming that the equivalent pore pressure is the same at failure as it is in the initial state, the equivalent pore pressure estimated by the model in chapter six can be used to estimate the major principal stress at failure if the friction angle of the material is known.

7.2.1 Relationship between friction angle and initial density

It has been well established that there exists a relationship between the peak friction angle of sands and gravels and the initial density of the material prior to shear (Taylor, 1948; Rowe, 1962). The friction angle increases as initial density increases. This is illustrated in Figure 7.1 in which Rowe showed that the friction angle of a medium fine sand increased from its lowest value of slightly less than 32° in its loosest state to 40° in a dense state. The constant volume friction angle, ϕ_{cv} , for the loose state (shown as the solid square) is the lower bound of friction angle for this sand since looser samples will consolidate during shear and reach a constant volume condition at high strains. The ultimate shear stress then corresponds to the peak shear stress

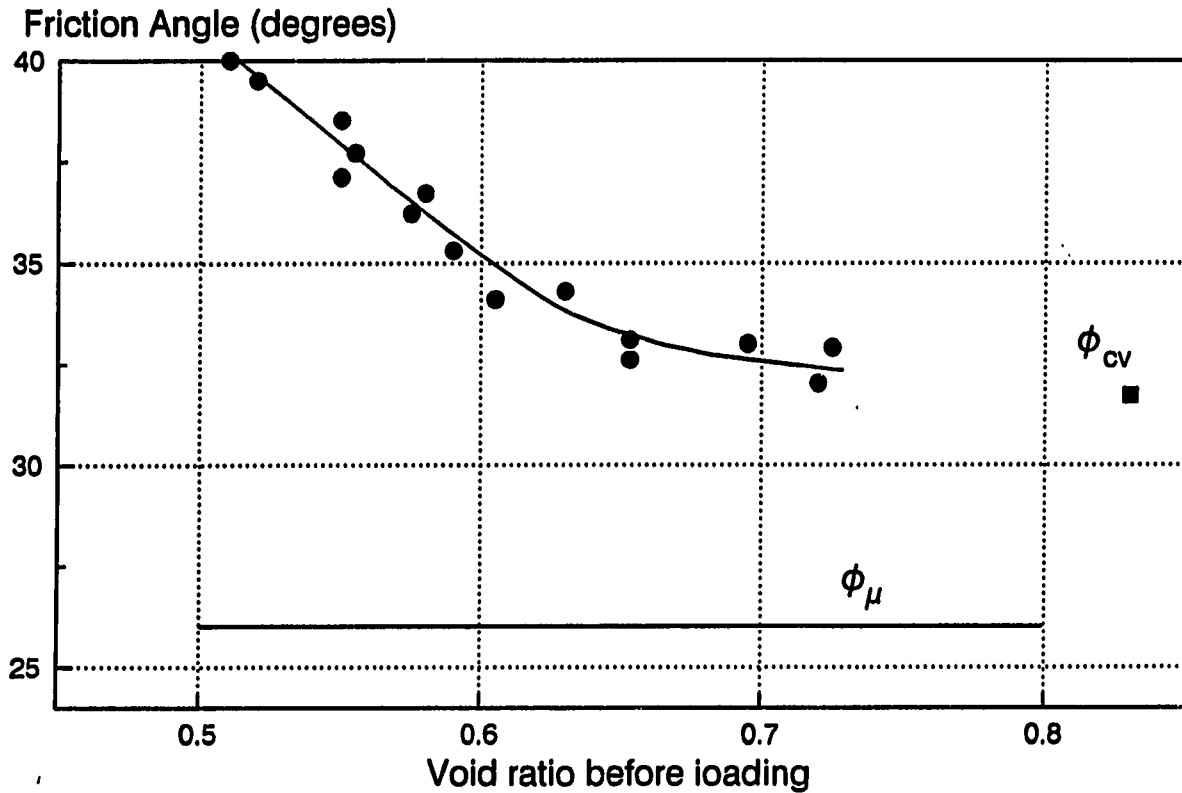


Figure 7.1 Relationship between initial void ratio and friction angle for a medium fine sand (Rowe, 1962)

condition. Also shown in the figure is the particle to particle friction angle, ϕ_{μ} , which represents purely sliding friction without the rolling and interlocking components which are present in the lumped parameter, ϕ .

This relationship was determined for the $n = 0.2$ and $n = 0.8$ gradations from direct shear tests on oven dry samples (Figure 7.2). These gradations (the finest and coarsest) were chosen to represent probable upper and lower bounds for the friction angle - void ratio relationship. Samples were tested

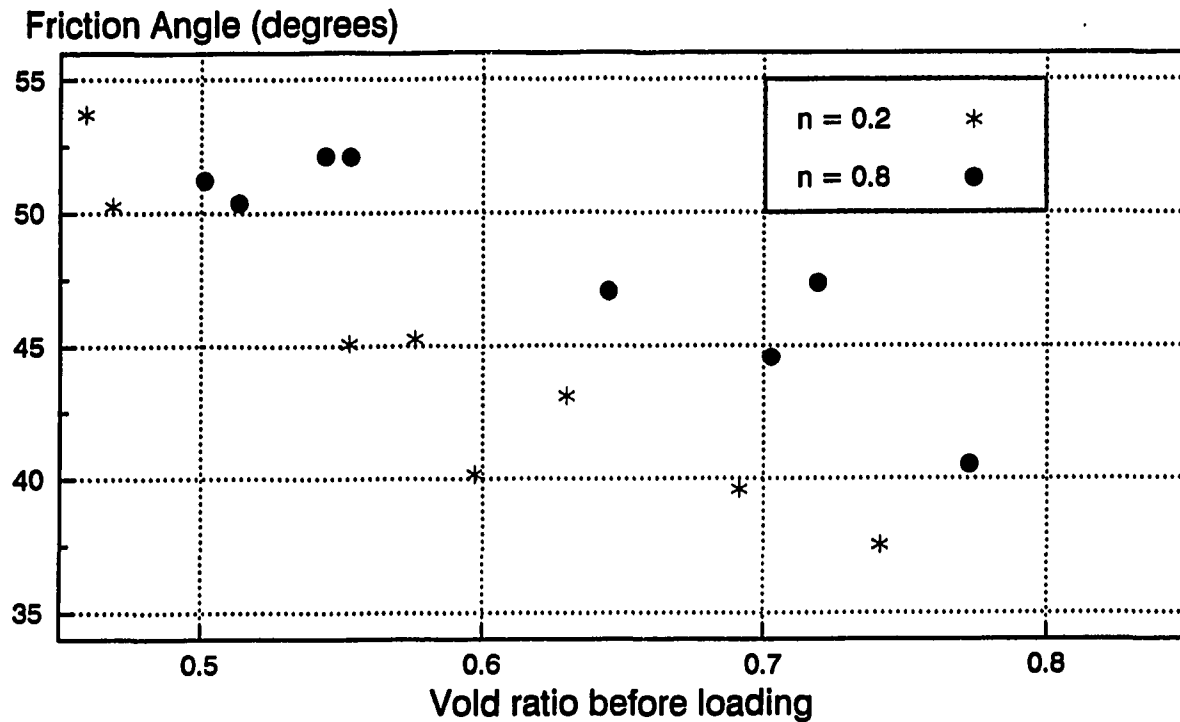


Figure 7.2 Relationship between initial void ratio and friction angle for $n = 0.2$ and $n = 0.8$ gradations

at void ratios from 0.4 to 0.8 and resulted in a range of friction angles from 37° to 54° . Assuming that these results do provide the upper and lower bounds to the friction angle - void ratio relationship, and further, assuming that the relationship varies linearly with gradation exponent, a relationship between friction angle, void ratio, and gradation exponent was generated by linear regression of the data and linear interpolation between these bounds (equation 7.5).

$$\phi = 77.8 - 8.8n + 29.3ne - 59.7e \quad (7.5)$$

This equation was used in equation 7.3 to allow for variation of friction angle with void ratio in the strength model.

7.2.2 Limitations of the model

In addition to the variability of friction angle which can be modeled empirically, an important assumption in the failure prediction model is that the pore pressure at failure is the same as the initial pore pressure. For this to occur, the void ratio at failure would have to be the same as the initial void ratio; there could be no net volume change. Consolidation and dilation could occur prior to failure, but the final volume would have to be the same as the initial.

Researchers who have measured volume change and pore pressures in partially saturated soils during undrained shear have shown that the volumetric strains and pore pressures during shear are inversely related (Bishop and Blight, 1963). That is, consolidation is accompanied by increased pore pressures and dilation by decreased pore pressures. This stems from the effect of volume change on the pore structure of the material (cf. chapters 4 and 5).

Bishop and Blight (1963) present the results of several undrained triaxial shear tests on partially saturated, compacted soils which indicate that during the initial stages of shear loading (less than 5% axial strain) slight consolidation is accompanied by an increase (less negative) in pore water pressures. The results also indicate that the closer the

initial pore water pressure is to atmospheric pressure, the greater is the increase for the same amount of consolidation. When viewed as a function of the continuity and quantity of the pore liquid, greater increases should be expected in materials initially at higher saturation levels. Thus, at low saturation levels, the change in pore water pressure is not as great as at high saturation levels. As dilation begins to occur in the failure zone, the pore water pressures decrease (become more negative). Bishop and Blight's results show that the pore pressure eventually decreases to lower values than the initial pressures, but at high axial strains (greater than 15%). The higher the confining stress, the higher the axial strain at which the pore pressures become less than the initial. Therefore, the use of the constant volume assumption in the equivalent pore pressure model is extremely simplistic and must be considered a limitation when used to predict failure stresses.

7.3 Comparison of measured and predicted strengths

Further validation of the equivalent pore pressure model was conducted by comparing the results of unconfined compression tests on remolded samples of the five gradations with predictions of strength according to equations 7.3 and 7.5. The equivalent pore pressures were modeled by equations 6.6, 6.9, 6.11, and 6.12.

7.3.1 Experimental method

Variable moisture contents were achieved by mixing increasing amounts of deionized water with samples of the five sand-silt mixtures. The moist material was then placed into a steel mold (5.2 cm in diameter by 10.8 cm tall) in three equal lifts. Each lift was compacted under a static load of 9.75 kg. This produced vertical stresses of 45 kPa in each lift. The surfaces of the two lower lifts were scarified with a spatula before placing the next lift in order to provide better continuity between lifts. After compaction, each specimen was extruded from the mold, weighed, measured and placed in a Soiltest, Inc. unconfined compression load frame. Failure loading was accomplished by raising the sample against a proving ring mounted in the load frame. The samples were unjacketed and open to the atmosphere during testing. Failure stresses were calculated as the maximum load which the sample was able to carry divided by the initial cross sectional area of the sample. In addition to failure load, the observations of the technician performing the tests were recorded for each sample. Observations included the shape of the deformed and failed sample, the distribution and apparent condition of moisture flow during compaction and loading, the occurrence of any cracks or irregularities in the sample before failure, and qualitatively, the amount of vertical and lateral strain which occurred during loading.

The unconfined compressive strength test was chosen because it is a relatively easy test to conduct and many tests can be conducted in a short period of time. All of the tests reported in this chapter were conducted within a three week period by one technician. The test does have its limitations however. There is no measurement of volume change during shear when usingunjacketed specimens and at low saturation levels in which the apparent cohesion is small, the samples are extremely sensitive to handling stresses and collapse under their own weight before testing.

7.3.2 Presentation of results

Figures 7.3, 7.4, and 7.5 present the experimental data for the five gradations and envelopes generated by the previously described model (labeled model A) and a modified model (model B) which is described later. Each strength test is shown as an individual data point and the model envelopes are shown as lines. Figure 7.5 presents both the data (solid circles) and an alternate strength calculation (open circles) which is discussed later. The data and the technician's observations are tabulated in Appendix C.

As mentioned previously, the unconfined strengths were calculated from the maximum applied load and the initial cross sectional area. The saturation levels were calculated from the measured moisture contents, mass, volume, and specific gravity. The theoretical curves were generated for a constant

Unconfined Strength, kPa

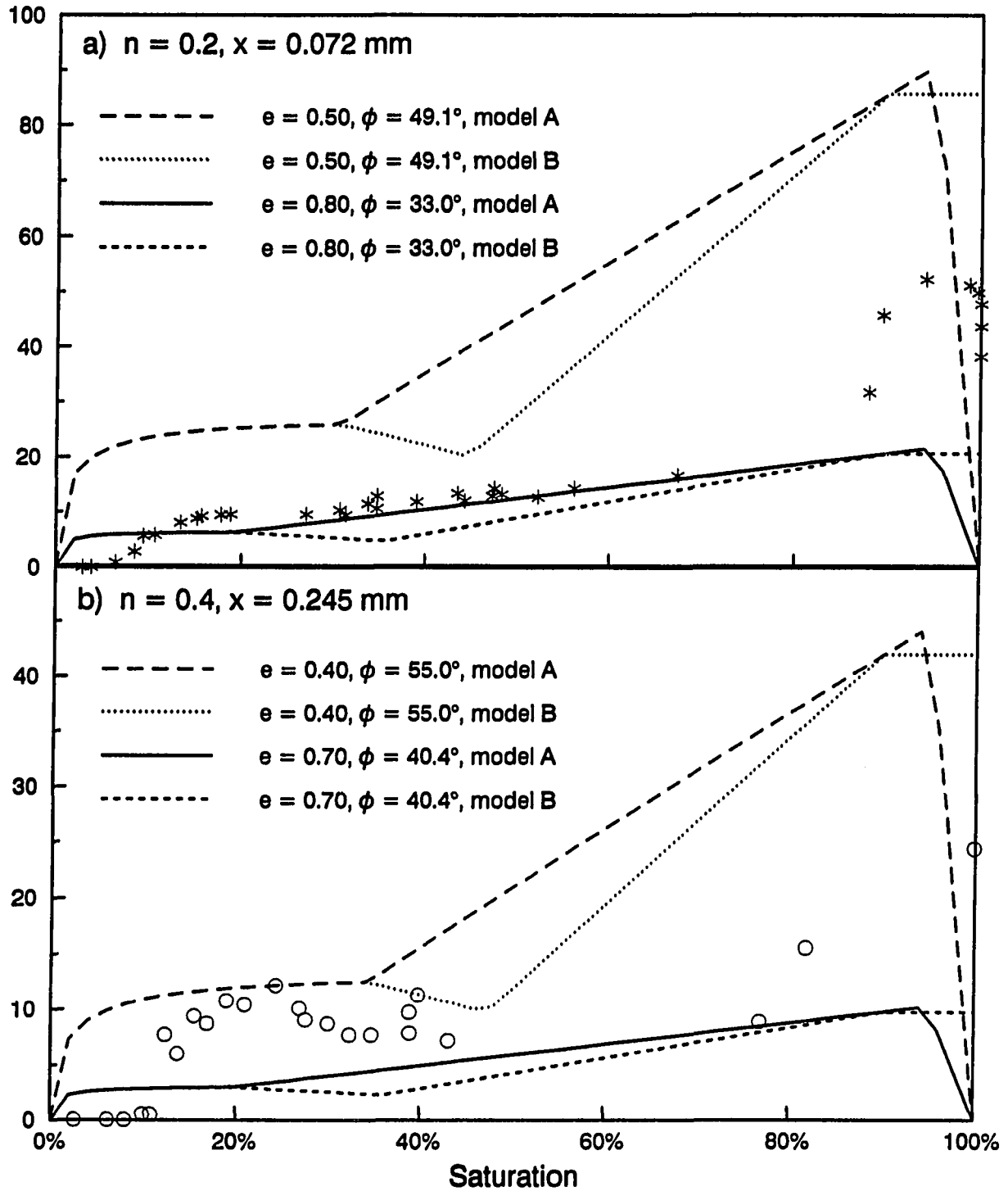


Figure 7.3 Measured and predicted strengths ($n = 0.2$ & 0.4)

Unconfined Strength, kPa

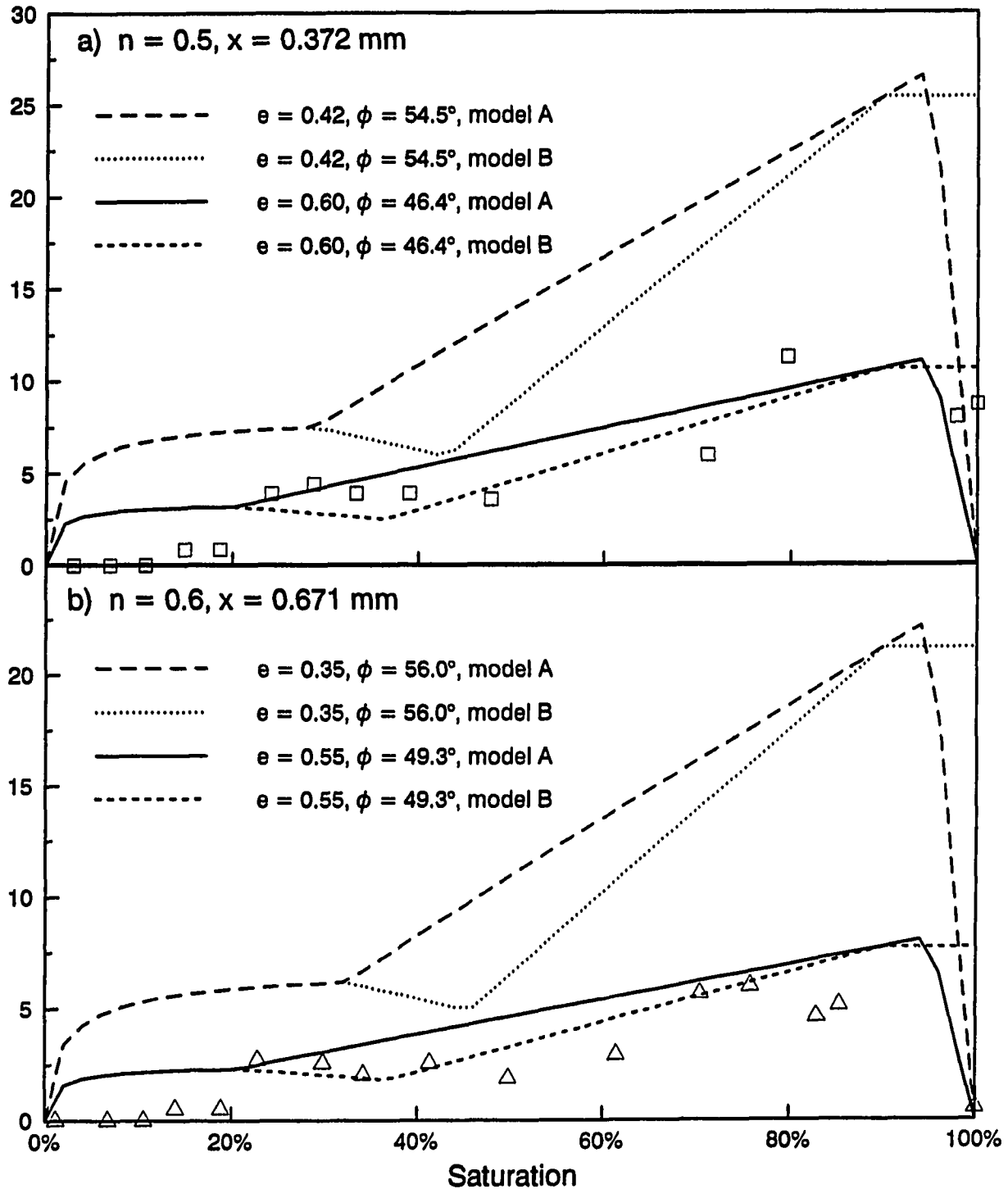
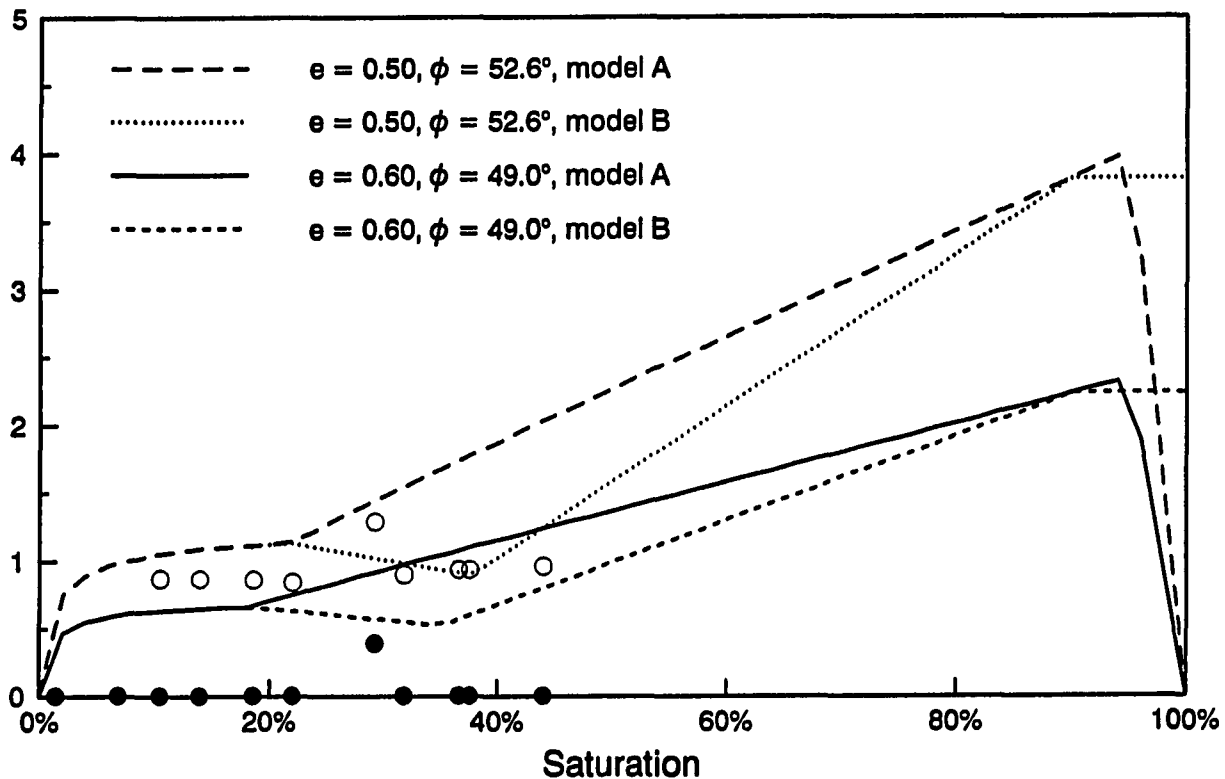


Figure 7.4 Measured and predicted strengths ($n = 0.5$ & 0.6)

Unconfined Strength, kPa ($n = 0.8, x = 1.372 \text{ mm}$)Figure 7.5 Measured and predicted strengths ($n = 0.8$)

void ratio and friction angle condition. The void ratios used were the average plus and minus one standard deviation of all void ratios for tests on a given gradation. The friction angles used were generated by equation 7.5.

Examination of the maximum strengths obtained indicates that gradation does have a dramatic impact on the apparent cohesion of granular materials. The $n = 0.2$ gradation exhibited a maximum unconfined strength of 52.1 kPa; $n = 0.4$, 24.4 kPa; $n = 0.5$, 11.3 kPa; $n = 0.6$, 6.0 kPa; and $n = 0.8$, 0.4

kPa. In addition, the shape of the strength-saturation relationship varies with gradation. The $n = 0.2$ gradation exhibits a decided "hump" in the upper funicular and capillary range (above 85% saturation). The strengths in the capillary range are approximately twice that of the pendular range, however, the location of this trend shifts to lower saturation levels with increasing gradation exponent. The trend also broadens and becomes less distinct for the more uniform gradations. The $n = 0.8$ gradation samples were unable to retain moisture above 50% saturation and therefore no strength tests were conducted above that saturation level.

The second set of data points shown in Figure 7.5 were calculated by adding half of the mass of the sample to the failure load (to zero in the case of samples which failed during handling). The rationale for this stems from the definition of failure stress used in plotting Figures 7.3 through 7.5. In these figures, failure stress was defined as the maximum applied load divided by initial cross sectional area. This neglects the body forces of the sample itself which is the common approach in soils testing. However, as previously observed, the samples which failed prior to loading did have some cohesion due to the negative pore pressures. By adding half of the weight of the sample we assume that this weight is also a driving force causing failure. This correction increases the failure stress by approximately one kilo-

pascal which is negligible compared to the loads applied to the finer materials, but is a substantial contribution for the lower strength, high gradation exponent materials.

The model "A" envelopes (denoted in the figures as solid and long-dashed lines) predict a more gradual increase in strength than was exhibited by the experiments. Also, model A predicts that the pore pressures in the capillary range increase to zero at full saturation, therefore unconfined strength decreases to zero. This is true for a saturated sample in contact with and at the same elevation as a free water surface, but is not true for a saturated sample surrounded by the atmosphere as we have in the experimental work. These two observations instigated modifications to the original pore pressure model as follows.

7.3.3 Modifications to model A

The funicular pore pressure model (section 6.5.3) was founded on the assumption that the equivalent pore pressures in this range of moisture content could be modeled as proportioned pendular and capillary pressures. Equations 6.11 and 6.12 were developed to do the proportioning and the results were summed. Reexamination of this assumption in light of the experimental results indicates that the two mechanisms may act independently. Rumpf (1962) and Schubert (1975, 1984) state that this is a possibility which may better fit some materials, however, Schubert (1975) claims that summing the two

components yields the best fit for the greatest number of materials. It should be noted however, that Schubert bases this claim on tests of materials which are much finer than those tested here ($0.002 \text{ mm} < x < 0.070 \text{ mm}$). Pietsch (1984), in a review of Rumpf's and Schubert's experimental work, shows several graphs which corroborate the hypothesis that treating the two mechanisms separately produces a better fit for coarser materials.

Therefore, as an alternative (model B), the funicular range is modeled as proportioned pendular and capillary bonding according to equations 6.11 and 6.12 without the summation used in model A. The envelopes based on this assumption are also shown in Figures 7.3 through 7.5 as dotted and short-dashed lines. This interpretation predicts that the strength in the lower funicular range decreases to a minimum before increasing in the capillary range. This has been shown to occur in crushed coals with fairly uniform (high exponent) gradations and maximum particle sizes greater than 2.36 mm (Van Weelden and Lohnes, 1991; Levorson and Lohnes, 1993). No mechanistic explanation for this observed phenomena or the model assumption is presently available. The modeling technique simply attempts to follow the observed strength response.

To rectify the differences between the capillary range predictions of model A and the observed strengths, model B was

formulated as a step function at 100% saturation in which the equivalent pore pressure is simply fixed at 90% of the calculated air entry pressure (equation 6.5) for the saturation range from 90 to 100%. The value of 90% was chosen on the basis of experimental results presented by Schubert (1984) and those of this research. As with the funicular range modification, this is a purely empirical modification to the original pore pressure model.

7.3.4 Direct comparison of predictions and data

In addition to the calculated envelopes shown in Figures 7.3 through 7.5, models A and B were used to predict the strength of each test from the measured moisture content and void ratio. Comparisons of strengths less than 20 kPa are presented in Figure 7.6 a&b. The predicted values are graphed on the ordinate and the measured strengths on the abscissa. The diagonal line in each graph is the line of perfect agreement between predicted and experimental results. As the figures show, both models tend to overpredict the strengths of samples with measured strengths less than 6 kPa. In the 6 to 15 kPa range of measured strengths, both models underpredict the strengths, but the trends have much less scatter than at lower measured strengths. The funicular range differences in models A and B are also clearly pointed out in these figures. Model B provides a much tighter trend of predictions, located at the lower bound of the model A predictions.

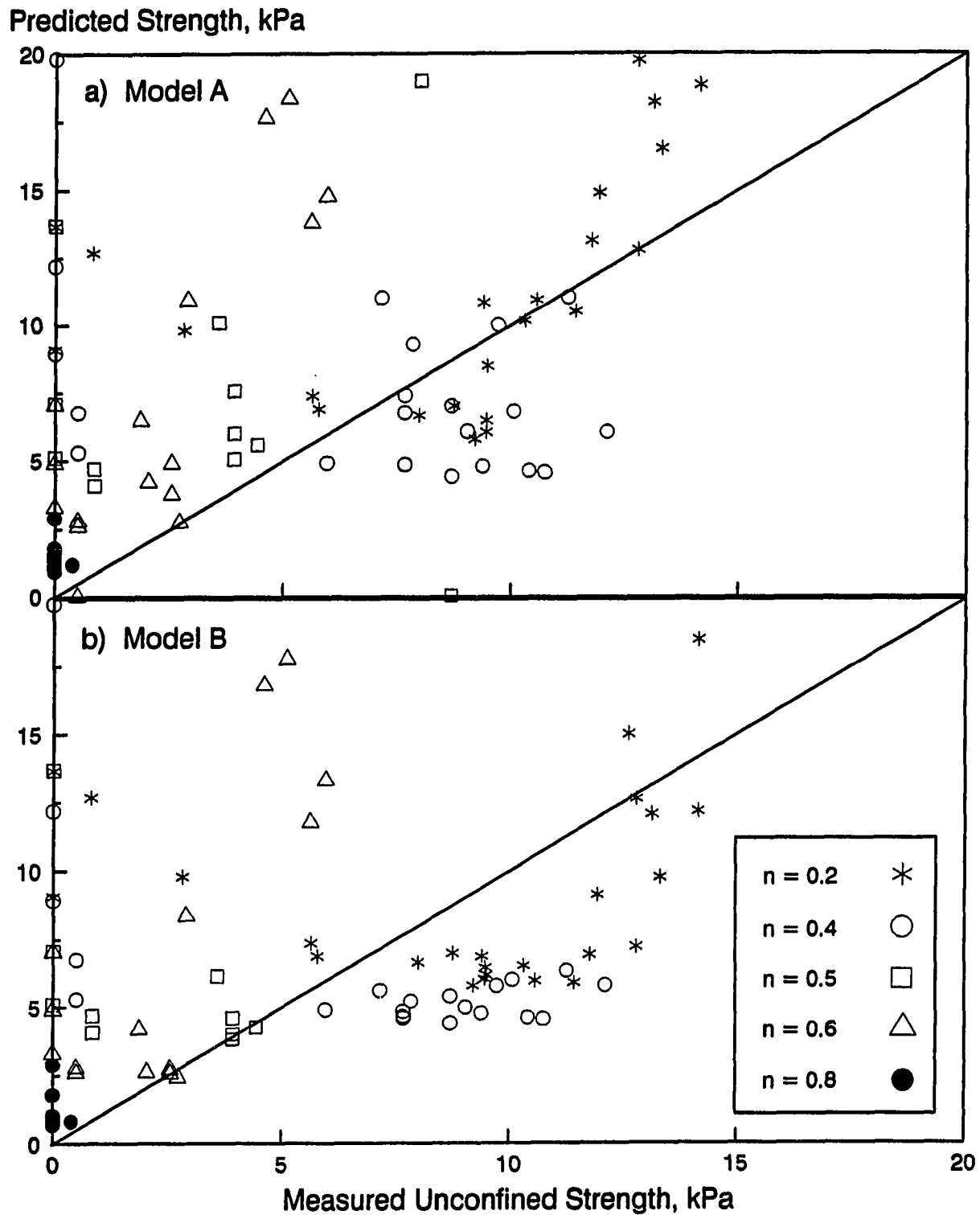


Figure 7.6 Comparison of model predictions and data

There are also nine tests not shown in this figure (eight from $n = 0.2$ and one from $n = 0.4$) which had measured strengths greater than 20 kPa. Model A overestimated three of the nine by a factor of two and underestimated the rest by variable amounts. Model B overestimated the strengths of all tests by up to three times.

7.4 Discussion

A possible explanation for the poor agreement in the low strength range was partly explained before. The notes taken during testing (Appendix C) indicate that the majority of the low moisture content tests failed prior to loading, either during extrusion or handling. This indicates that the samples did indeed have some apparent cohesion, but that the handling stresses were great enough to cause failure and therefore the failure strength remains unknown. This is a limitation due to the choice of testing method.

Figure 7.7 shows the comparison of the two models and the measured strengths for those tests which were conducted on samples with saturation levels between 10 and 60%. As stated previously, the measured strengths at saturations less than 10% may be discounted due to the testing method. Also, the upper funicular and capillary range strengths showed a high degree of variability which is discussed subsequently. Examination of the two graphs in Figure 7.7 indicates that both models do a fair job of prediction in this saturation range.

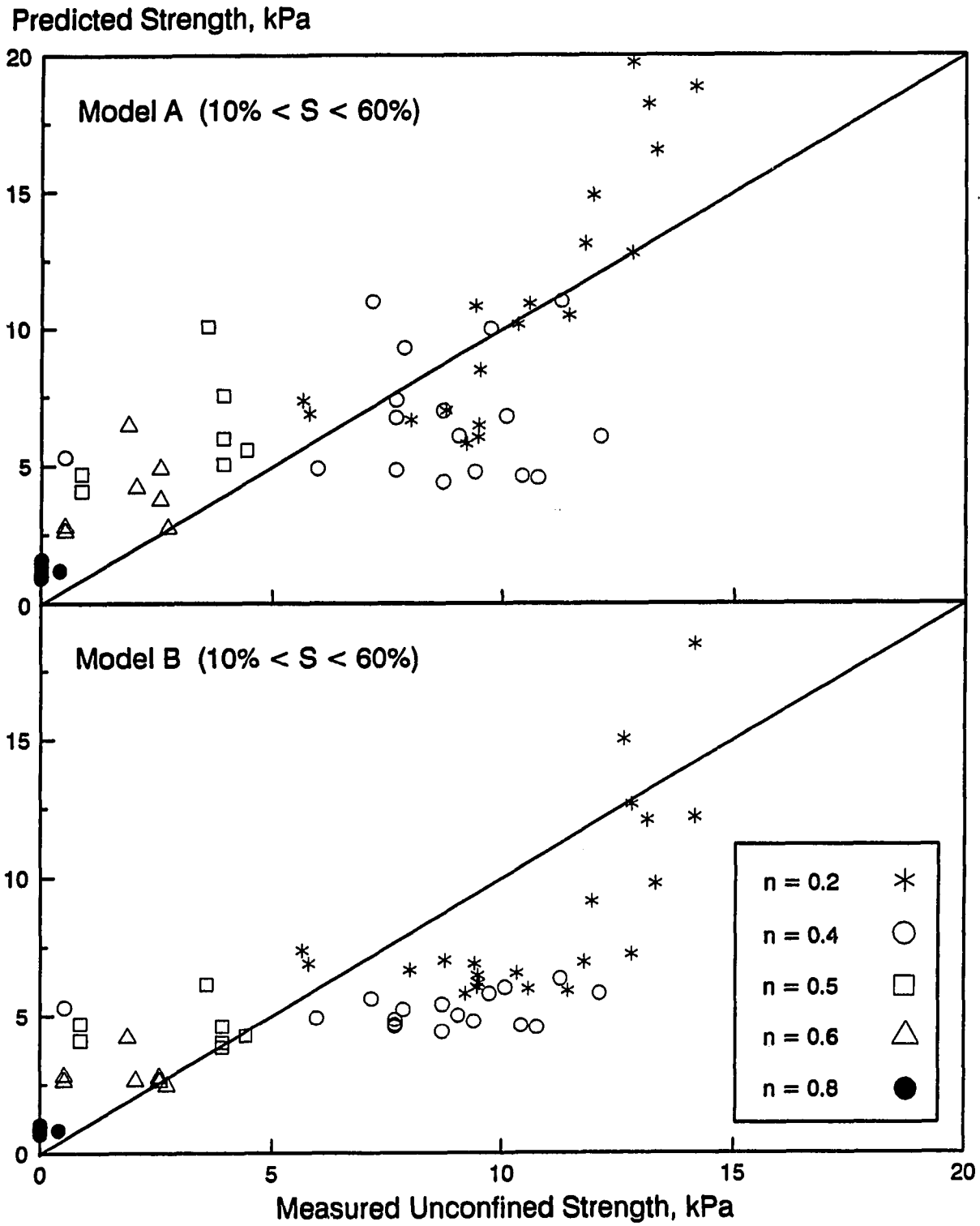


Figure 7.7 Comparison of models and data for 10% < S < 60%

Closer examination points out that model B provides a better fit for the higher gradation exponent materials ($n = 0.5$ and 0.6 particularly). Model A fits the finer sized gradations better than model B. There is more scatter, but model A does not consistently underpredict strength for the fine gradations as does model B.

The poor agreement of the experimental data and model predictions at high saturation levels can be partly explained by the moisture holding capacity of the high gradation exponent materials. Examination of the moisture retention curves of Chapter 4 and the volumes attributed to the capillary and funicular moisture ranges found in Figure 5.5 indicates that the $n = 0.6$ and $n = 0.8$ gradations hold water at very low tensions in the higher saturation ranges. They also hold a greater percentage of water in the capillary moisture range. Observations during the experiments indicate that moisture was slowly flowing from the samples during application of the shear load. This indicates that the initial negative pore pressures in the samples were not constant during shear and that the pore pressures actually became neutral or positive. The assumption of constant pore pressures during shear is obviously not a good assumption in the coarser materials. This leads to a conclusion that coarse materials may only be capable of retaining pendular moisture during shear and necessitates a reevaluation of the pore pressure-strength model.

The poor agreement at high saturation levels in the finer gradations and the qualitative observations of deformation and volume change during testing further indicate that the constant volume assumption used in the prediction is faulty. Figure 7.8 presents a summary of the observations of failure mode and deformation behavior. At low saturation levels, failure occurred at very low strains and in many cases was preceded by the formation of vertical cracks at the exterior of the sample. These tests are labeled "brittle" in Figure 7.8. In these tests the constant volume assumption seems to be

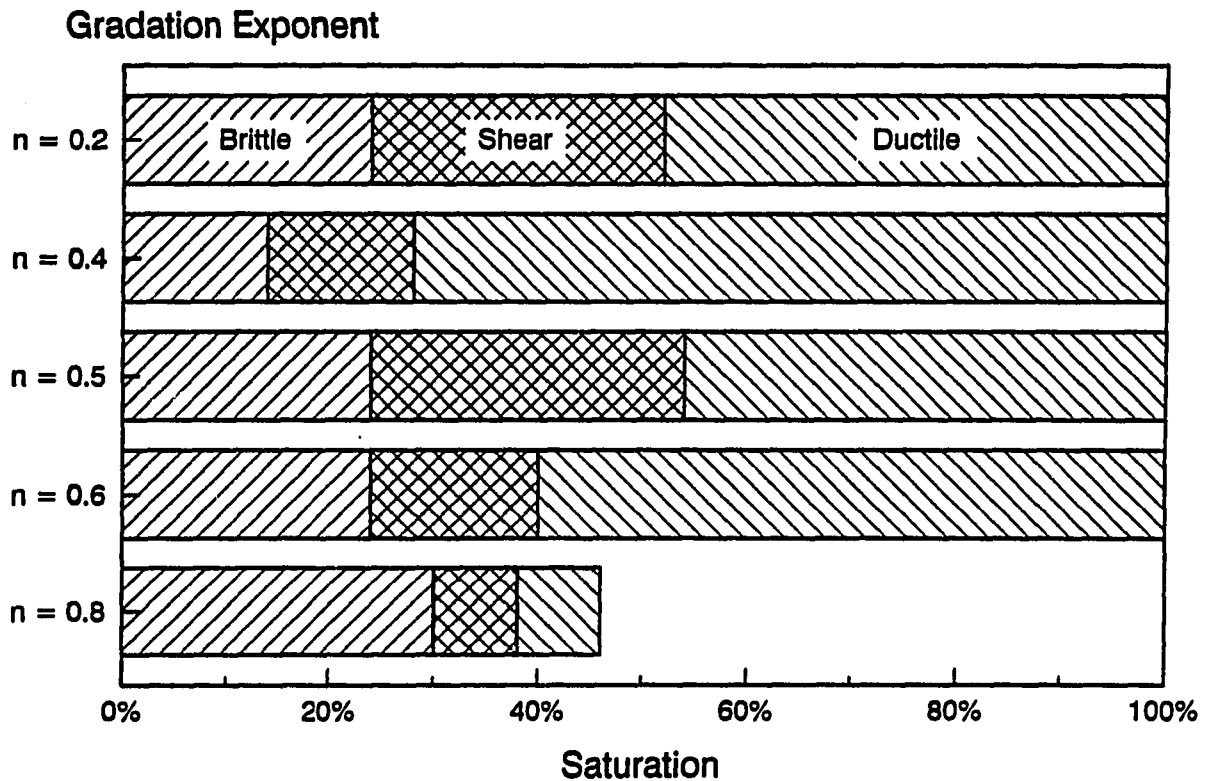


Figure 7.8 Summary of failure mode observations from unconfined strength tests

fairly valid. In the mid saturation range the failure mode was primarily a single shear plane running diagonally through the sample. These failures also occurred at low strains. At higher saturation levels, however, loading was accompanied by high vertical and lateral strains and the failure mode was more ductile. In all gradations, the void ratios at these high saturation levels were very low which would suggest that the deformation was dilational. This dilation (increasing void ratio) would cause the fluid pressures to become more negative and the saturation level to decrease. The net effect is to increase the equivalent pore pressures (become more positive) and therefore decrease the shear strength. Interestingly, the observations of the technician indicate that in the $n = 0.5, 0.6,$ and 0.8 gradations moisture was draining from the samples which indicates either neutral pore pressures or enough dilation of the larger pores so that they are no longer able to hold moisture. Conversely, the $n = 0.2$ and 0.4 gradations retained all of the pore fluid as they deformed. These observations also coincide with the shapes of the moisture retention curves presented in chapter 4.

8. DISCUSSION OF EXPERIMENTAL AND MODELING RESULTS

It has been shown that the density of granular materials under both vibratory and static compaction conditions is both a function of the initial density of the sample and the resistance to compaction afforded by the fluid phase pressures. The magnitude of the compacted density is also affected by the gradation of the material.

During vibration of an externally loaded system, the load is also vibrating. This causes the normal stress due to the load to pulsate, increasing and decreasing with each cycle. For sands to densify, adhesional and frictional bonds must be broken to allow movement of the particles and void filling to occur. In dry sands the adhesional forces are negligible to nonexistent and therefore the frictional resistance, which is proportional to the normal stress, also fluctuates with the vibratory load. As the normal stress decreases during the "up" phase of the cycle, the inertial force of the particles becomes greater than the resistance and the particles move and fill voids.

As moisture is added to the system (pendular state) the moisture provides adhesional forces which increase the normal stresses between particles and thus the frictional resistance to movement. The adhesion of a single pendular ring is a one dimensional force vector between particles but can be considered isotropic when viewing a large enough control volume with

randomly oriented contact vectors. Thus the vibrational energy which causes compaction of a dry system can not cause the same amount of compaction in a moist system because the frictional resistance to movement is increased.

In the capillary moisture range, the adhesional component of interparticle bonding becomes isotropic rather than one dimensional because the pore volumes are nearly, to completely, filled with fluid. The pressure in the fluid is higher (less negative) than in either the pendular or funicular ranges but there is more of it. The isotropic nature of the pore pressures increases the frictional resistance by increasing the normal stresses and increases the tangential or shearing stresses at the contacts. A further possibility in pore systems saturated to greater than 80% is that the pulsating load can cause alternating positive and negative pressures in the system. If the pressures approach atmospheric or actually go positive, this decreases the frictional resistance drastically by reducing the normal stresses between the particles. In essence, this causes cyclic liquefaction of the material.

In the funicular range, the pores become more and more filled with fluid. The finer pores are first saturated; increases in moisture content cause filling of larger and larger pores. At those points of contact in large pores, the pendular analogy of adhesional and frictional resistance continues to govern. However, in the saturated, fine pores,

the saturated capillary analogy governs on the microscopic scale. Thus, increases in density accompanied by increases in moisture above the pendular-funicular transition can be explained by microscopic scale liquefaction of small volumes within the sample due to pulsating normal loads which cause reduction in the local fluid tension.

8.1 Shear strength

The shear strength of partially saturated materials has been shown to depend on the density, friction angle and equivalent pore pressure of the material. The friction angle is a function of the initial density. The initial density is a function the equivalent pore pressures and the gradation. Therefore, the strength of remolded, partially saturated materials can be said to be primarily a function of the moisture tension which has been shown to depend highly on the gradation of the material.

8.1.1 Empirical model

Since the primary range of interest in remolded particulate materials is the pendular moisture range, an empirical fit to the pendular model (eq. 6.9) was performed. It was observed that equation 6.9 produced nearly hyperbolic results for constant void ratio conditions. The equation was rewritten in dimensionless form and linear regression of the hyperbolic transform produced an equation for the equivalent pendu-

lar pore pressure in terms of the saturation level:

$$u_p^* = \frac{ST}{ex(0.03 + 0.5S)} \quad (8.1)$$

where S is the saturation level (equal to $w \cdot G \cdot e^{-1}$), T is the surface tension of water, e is the void ratio, and x is the mean particle size. Use of this equation with T in newtons per meter and x in mm returns u_p^* in kPa. This equation can be used in any of the strength equations presented in the previous chapter to provide an estimate of the equivalent pore pressure in the pendular moisture range.

9. APPLICATION TO COAL HANDLING

9.1 Introduction

Over 600 tons of coal are burned annually in U.S power plants. Historically, individual power plants would contract with specific mining operations to buy coal from that one source. This allowed the plant to be designed specifically to handle that coal. The advent of world wide marketing of coal and improvements in transportation have produced a situation in which a single plant may burn coals from many different sources, each with vastly different mechanical properties. In addition, environmental concerns about smokestack emissions have prompted eastern utilities to blend low sulfur western coals with high sulfur eastern coals or to switch wholly to low sulfur coals to meet new "Clean Air" regulations. This requires the designs or retrofits for bins, bunkers, conveyors, hoppers, chutes and other components of the handling system to be capable of dealing with coals with a vast range of mechanical behavior. An example of the problems this can cause is given by Arnold, et al. (1992). A western utility purchased enough deep-mined Utah coal for a 30 day test burn after satisfying themselves that the coal met the same performance criteria for boiler operations as their usual Powder River Basin coal. After 10 days the test burn was abandoned because excess fines and moisture caused plugging in the plant's bins and feeders. In many cases, problems such as

this have resulted in adding redundant systems in order to maintain the flow of coal to the boilers which results in added capital costs.

To address these problems, the Electric Power Research Institute began funding research in 1987 to develop a predictive model of the behavior of crushed coal in power plant handling systems. The ultimate aim of this research is to provide coal-fired power plant personnel, coal buyers, shippers, and vendors with a means of indexing or classifying the "handleability" of any given coal. This can then be compared to facility constraints either for use as an accept/reject criterion or as a warning of potential problems.

9.2 The handleability index

A handleability index is used to compare the behavior of different materials during flow through the handling system. The indices which have been developed to date fall into two basic categories: material indices and hopper indices. As the names suggest, a material index characterizes the flow behavior independent of the handling system and a hopper index characterizes the flow behavior in a specified system. Because a material index is independent of the handling system, the index must be compared to an index of limiting points in the handling system to provide an estimate of possible handling problems. Hopper indices are often generated by test devices with geometric configurations for specific hopper

applications. Therefore, a different index must be determined for each different handling system.

The handleability index chosen for this research (Bradfield, 1989) is based on the widely used hopper design theory of Jenike (1961, 1964). In the calculation for the minimum hopper opening needed to promote mass flow in a bin, the unconfined strength, f_c , of the ensiled material is divided by the total unit weight, γ (producing units of length). This ratio is multiplied by factors which are functions of the geometry and material properties of the hopper. The ratio of f_c to γ was chosen as a material handleability index, HI. Thus, the design equation itself combines a material index with systems constraints and the hopper opening dimension may be viewed as a hopper index.

9.3 Summary of EPRI experimental project

Measurements of unconfined strength, f_c , and bulk density were performed on 26 coals with ranks ranging from lignite to low volatile bituminous and one anthracite silt. Maximum particle size ranged from 2.36 mm to 37.5 mm and gradation exponents ranged from 0.35 to 0.90 for the 53 different gradations tested. The specific gravities of the materials varied between 1.31 and 1.78 with the majority near 1.4. Each coal was tested at two to four moisture contents under isotropic consolidation stresses of 10, 30, and 50 kPa. This program produced a data base containing the results of over 500 tests.

The following general and specific conclusions are drawn from the experimental data.

- A single gradation of coal at a specified consolidation stress exhibits a maximum unconfined strength at an intermediate moisture content. For eastern bituminous coals, this occurs at $11 \pm 3\%$ moisture content (Levorson and Lohnes, 1993).
- The handleability index, HI, of a given coal responds in nearly the same way to increases in moisture content as unconfined strength.
- The major variables affecting the strength and handleability of crushed coal are moisture content, gradation, and density.
- At a given moisture content coals with higher maximum particle size exhibit lower void ratios.
- For coals with maximum particle sizes less than 6.3 mm, void ratio increases as moisture content increases.
- For coals with maximum particle sizes greater than 6.3 mm, void ratio remains constant as moisture content increases.
- For coals with gradation exponents less than 0.5, void ratio increases as moisture content increases.
- For coals with gradation exponents greater than 0.5, void ratios become highly variable as moisture content increases.
- The maximum HI for a given coal is a function of void ratio and therefore, is dependent on gradation, moisture

content and consolidation stress. However, the maximum HI for a given coal does not always occur at the lowest void ratio (densest state).

- At a given moisture content, HI increases as void ratio, maximum particle size, and gradation exponent decrease.
- For maximum particle sizes less than 6.3 mm, HI increases as moisture content increases.
- For maximum particle sizes greater than 6.3 mm, HI exhibits considerable variability as moisture content increases.

9.4 Handleability classification

The first attempts to produce a handleability classification system which predicts handling problems on the basis of the previously mentioned variables (Van Weelden and Lohnes, 1991; Lohnes and Levorson, 1992) were made by empirically grouping the results of the experimental study. In the tentative classification system which was produced, the handling behavior of eastern bituminous coals was classified according to the amount of fines (-0.5 mm) and moisture (Figure 9.1). In Figure 9.1 the data are grouped according to three ranges of HI (less than 0.2 meters, 0.2 m to 0.5 m, and greater than 0.5 m). These ranges were tentatively recommended to represent bounds between free flowing, possibly problematic, and highly problematic coals. The HI bounds were established on the basis of pilot scale hopper test results (Arnold et al., 1992) but have not yet been validated by plant experience.

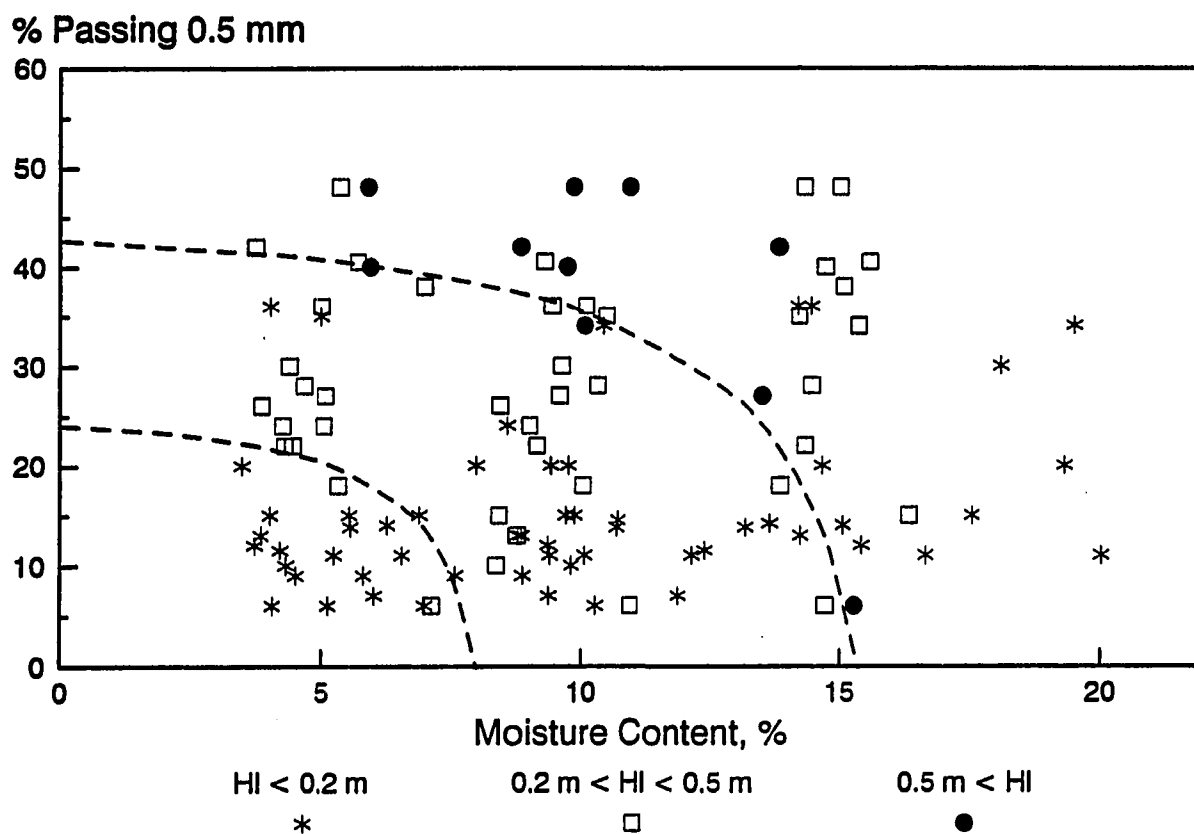


Figure 9.1 Initial handleability classification (from Lohnes and Levorson, 1992)

The fines and moisture content boundaries were conservatively chosen on the basis of the experimental results and represent lower bounds to the handleability index. It is possible for coals with high fines and moisture contents to exhibit free flowing behavior, but the combination increases the probability that handling problems would occur.

9.4.1 Modifications to the classification system

Using the simplified, empirical model presented in chapter eight, the handleability index can be stated as a function of the moisture content (ω), specific gravity (G), void ratio (e), particle size (x), surface tension (T), and friction angle (ϕ). Of these, the specific gravity and surface tension vary within a small range compared to the other variables and therefore can be treated as constants. An evaluation of the variability of friction angle in coals (Van Weelden, 1991) indicates that friction angle may vary from 30 to 55°. Insufficient data exist to define the relationship between friction angle and void ratio for different coal gradations. The value of friction angle used in the following analyses is therefore held constant at 45°. The other three variables were identified previously as those most important in describing the variability in HI. In this formulation, the handleability index (HI) can be written as:

$$HI = \frac{f_c}{\gamma} = \frac{\frac{\omega GT}{e^2 x \left(0.03 + 0.5 \frac{\omega G}{e} \right)} \frac{2 \sin \phi}{1 - \sin \phi}}{\frac{G(1 + \omega) \gamma_w}{1 + e}} \quad (9.1)$$

where γ_w is the unit weight of water. This is simplified to:

$$HI = \frac{2T}{x\gamma_w} \frac{\omega}{1 + \omega} \frac{1 + e}{e} \frac{1}{(0.03e + 0.5\omega G)} \frac{\sin \phi}{1 - \sin \phi} \quad (9.2)$$

Further, the moisture content, void ratio, and friction angle functions can be replaced by power function approximations of the form ax^b in which a and b are empirical fitting parameters and x is the variable. Power function approximations were developed for the expected ranges of these variables and were inserted into equation 9.2. Rewriting equation 9.2 with T equal to 0.073 N/m , $G = 1.4$, and $\gamma_w = 9.81 \text{ kN/m}^3$:

$$HI = \frac{\omega^{0.94} \phi^{2.3}}{118338 e^{0.65} x (0.03 e + 0.7 \omega)} \quad (9.3)$$

A comparison of the predicted value of HI versus the measured value for 115 tests on eastern bituminous coals at a consolidation stress of 50 kPa over the previously given ranges of moisture content and gradation is presented in Figure 9.2. In this analysis, the particle size for which 20% of the mass of material is finer (d_{20}) was substituted for the mean particle size in equation 9.3 based on empirical observation of the resulting fit. From this, the mean particle size can be expressed in terms of the top size and exponent as:

$$x = D (0.2)^{\frac{1}{n}} \quad (9.4)$$

where x and D are in millimeters as before.

Regression analysis of the comparison yielded a slope of 1.113, an intercept of 0.053, and a correlation coefficient of

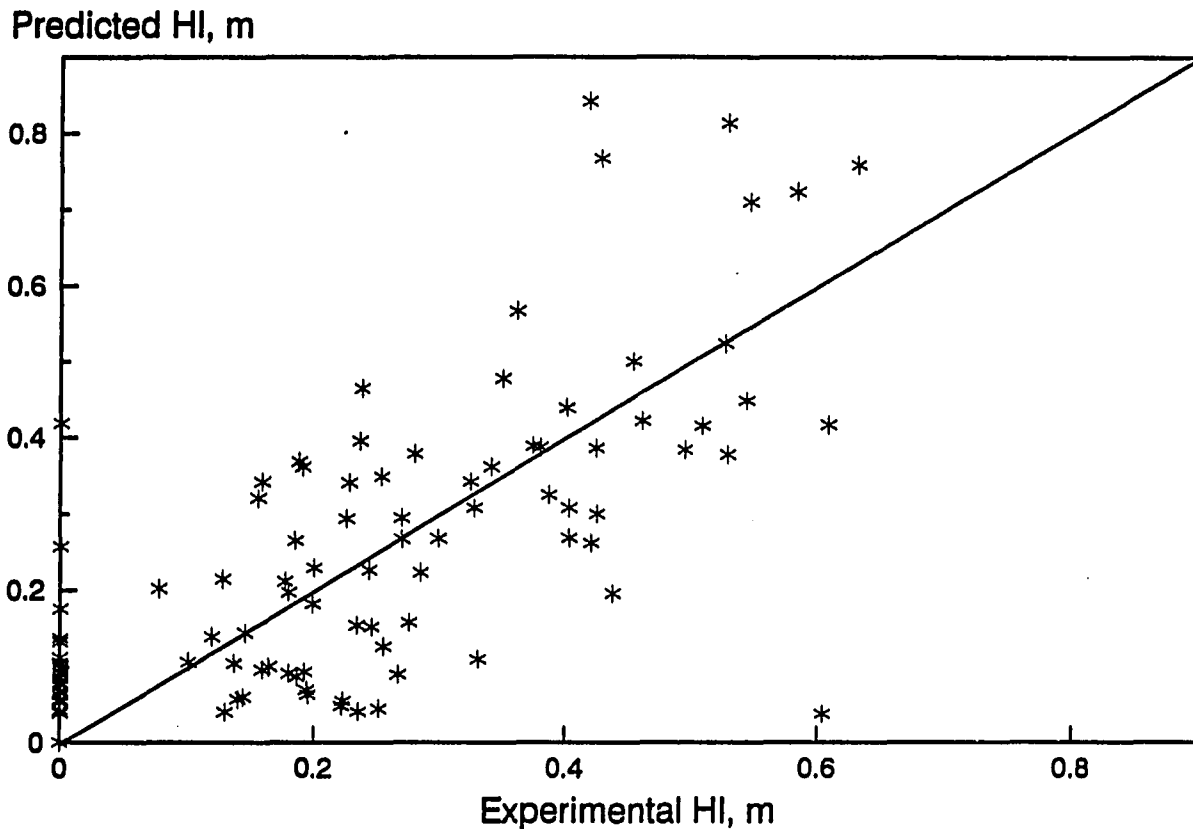


Figure 9.2 Comparison of predicted (eq. 9.3) and experimentally determined values of handleability index (HI)

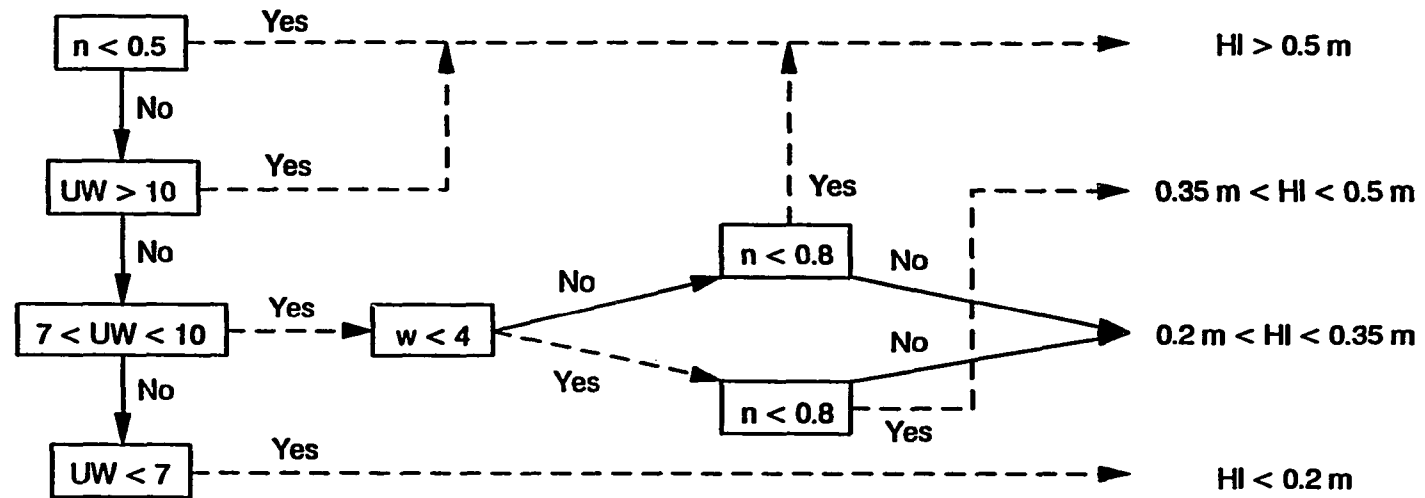
0.598. Compared to the perfect agreement line (slope = 1.0 and intercept = 0.0) for 113 degrees of freedom, the regression slope and intercept are not significantly different at the 95% level.

Assuming this analysis to constitute validation of the simplified model, equation 9.3 was used to develop a revised handleability classification which accounts for variation in top size, gradation exponent, total unit weight, and moisture content. As in the previous analysis, the friction angle was

held constant at 45°. The resulting classification is presented in Figures 9.3 and 9.4. Significantly, top size and gradation exponent are the major differentiating variables in the decision diagram. Moisture content plays only a minor differentiating role.

As the figures illustrate, the finer the top size and the more well graded the material, the more difficult it will be to handle. Since the top size and curvature of the gradation are controllable variables, set by the crusher operation, the most basic recommendation which can be made is to maintain better control of crushing and sizing operations to minimize the production of well graded materials. This in itself will promote better handleability. Secondly, since total unit weight is very important, especially in finer coals, maintaining moisture contents at levels which promote bulking would also promote better handleability.

2 - 4 mm
top size



4 - 8 mm
top size

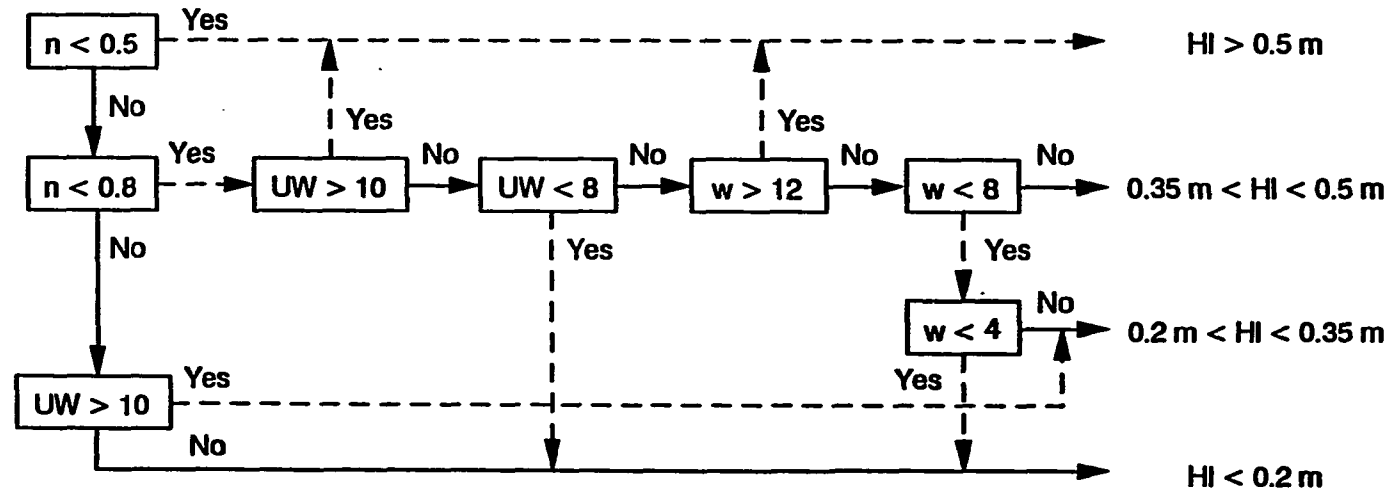
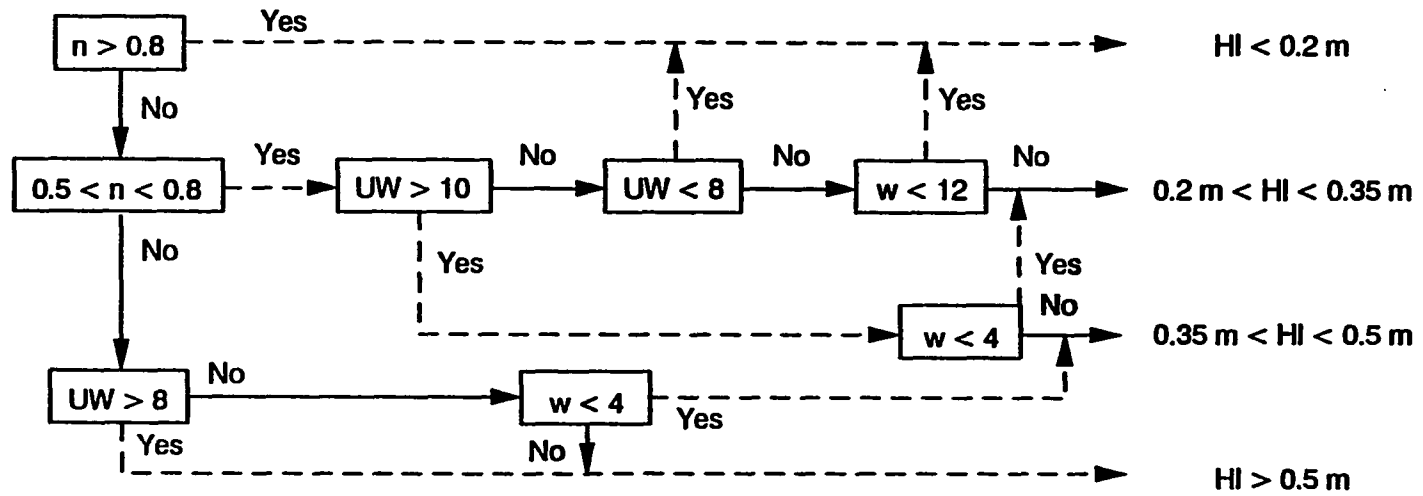


Figure 9.3 Handleability index classification flowchart for topsize less than 8 mm
(n = gradation exponent, UW = unit weight-kN/cu.m., w = moisture content-%)

8 - 12 mm
top size



> 12 mm
top size

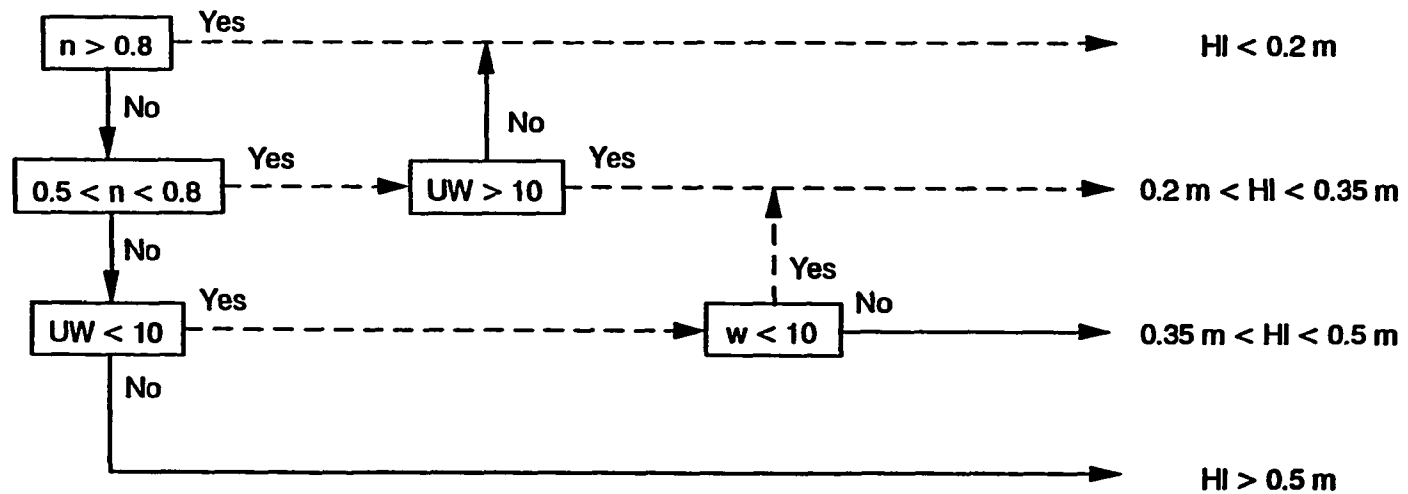


Figure 9.4 Handleability index classification flowchart for topsize greater than 8 mm
(n = gradation exponent, UW = unit weight-kN/cu.m., w = moisture content-%)

10. CONCLUSIONS

The following conclusions are drawn from the experimental and analytical studies presented in this thesis.

- The exponent value in the Talbot equation (eq. 2.6) can be used as a characterizing number for the mechanical behavior of single curvature particle size distributions.
- Single curvature gradations produce significantly lower dry densities (higher void ratios) at exponents less than 0.4 than more uniformly graded materials under the same compactive energy.
- Granular materials compacted at low moisture contents can exhibit relative densities as low as 15%.
- More uniform gradations exhibit less change in density due to bulking than well graded materials.
- The mechanism of bulking can be explained in terms of the effective stresses and negative pore pressures associated with different moisture ranges.
- The mechanical response in these ranges is closely related to the moisture characteristic curve of the material.
- The effect of changes in density and the resulting changes in pore size distribution on the shape of the moisture characteristic curve is qualitatively described for both compaction and desiccation.
- For a constant maximum particle size, increasing gradation exponent causes decreased air entry pressure and higher

(less negative) fluid pressures in the funicular moisture range. It also causes steeper slopes in the funicular range of the moisture characteristic curve. This indicates a broader distribution of pore sizes in the funicular range.

- Increased gradation exponent also causes higher pore volumes in the capillary range and lower pore volumes in the funicular range.
- The pore size distribution was shown to increase in mode and deviation with increasing gradation exponent.
- A model for the equivalent pore pressure in unsaturated granular media is developed from micromechanical arguments for use in effective stress analyses.
- A rationale for equating total stress analyses, in which apparent cohesion is a function of the moisture content, and effective stress analyses, in which there is no cohesion, is developed.
- Experimental determination of the strength of granular materials due to negative pore pressures shows that the gradation exponent has a significant effect on the magnitude of shear strength.
- The correlation between predicted strengths based on a mean particle size obtained from the measured air entry pressure and the measured strengths emphasizes the bond between negative pore pressure and shear strength in unsaturated materials. This also underscores the value of moisture reten-

tion testing in geotechnical applications for both predictive modeling and qualitative explanation of mechanistic behavior.

- The equivalent pore pressure model coupled with Coulomb's equation is shown to provide reasonable agreement with experimental results in the 10 to 60% saturation range. The poor agreement above 60% saturation is explained, in part, by the effect of volume changes during shear.

- As the gradation exponent increases, the unconfined strength response in the capillary moisture range is shown to be highly variable. It is hypothesized that the negative pore pressures at failure should actually be modeled as purely pendular in nature for uniformly sized gradations.

- A simplification of the equivalent pore pressure model is presented and applied to the problem of crushed coal handling. The algebraic form of this model emphasizes the multivariate nature of handling problems.

- The simplified model provides a means of evaluating the sensitivity of the handleability index to changes in the seven major variables. Those shown to be most important are the gradation parameters, top size and curvature.

- The resulting classification system for predicting handling problems emphasizes the controlling influence of gradation (both top size and curvature).

10.1 Recommendations for application and further development

This research has shown that the mechanical behavior of unsaturated granular media is highly dependent on the gradation of the material. Even though changes in density can be qualitatively predicted on the basis of gradation and moisture content, the actual value of density can not yet be predicted from gradation. Continued work with gradations which can be modeled by mathematical functions may provide a predictive model of compacted density based solely on gradation, moisture content, and compaction energy.

The differences that gradation causes in moisture retention relationships points out the value of these tests as an aid in developing design and acceptance criteria for granular bases. To make this a practical tool, the moisture tension test cell should be designed to serve as a compaction mold as well as a pressure cell. This would require a very robust pressure plate capable of withstanding either the impact or vibratory stresses of compaction. Further, the pressure apparatus should be capable of providing accurate pressures in the range from zero to two or three atmospheres. With an apparatus such as this, a single saturated specimen could be equilibrated at successively higher levels of air pressure, with either volumetric or gravimetric determination of moisture content at each pressure level. This would produce an entire moisture retention curve from a single sample.

The poor correlation of the predicted and measured strengths in the upper funicular and capillary moisture ranges was due, in part, to the constant volume assumption used in the model. The equivalent pore pressure model is highly sensitive to variations in both void ratio and mean particle size. Because the void ratio is present in the calculations of both pendular and capillary (and therefore funicular) pressures, the void ratio term could be replaced by a constitutive relationship for volume change as a function of strain. This would allow more realistic modeling of the changes in equivalent pore pressures during loading.

The handleability classification system presented here is based on laboratory investigations and theoretical analysis and must be considered a tentative classification. The handleability classes and the limits placed on the decision variables need to be verified by plant experience. The major limitation of this classification system is its dependence on estimates of the total unit weight. Therefore, research should be devoted to methods of estimating or measuring the in situ total unit weight of materials in handling systems for both at rest and flow conditions. Direct transmission nuclear methods such as those used for determining density and moisture content in soils have been well developed for some time and may prove useful in this application as well.

REFERENCES

- The Aggregate Handbook. 1991. R. D. Barksdale, ed. National Stone Association, Washington D. C.
- Aitchison, G. D. 1956. The circumstances of unsaturation in soils with particular reference to the Australian environment. Proc. 2nd Australian-New Zealand Conf. Soil Mech. and Found. Engrg. pp. 173-191.
- Aitchison, G. D. 1960a. Effective stresses in multi-phase systems. Proc. 3rd Australian-New Zealand Conf. Soil Mech. and Found. Engrg. pp. 209-212.
- Aitchison, G. D. 1960b. Relationships of moisture stress and effective stress functions in unsaturated soils. Proc. Conf. Pore Pressure and Suction in Soils. Butterworths, London. pp. 47-52.
- Aitchison, G. D. and I. B. Donald. 1956. Effective stresses in unsaturated soils. Proc. 2nd Australian-New Zealand Conf. Soil Mech. and Found. Engrg. pp. 192-199.
- Allam, M. M. and A. Sridharan. 1987. Stresses present in unsaturated soils. Jour. Geotech Engrg. 113(11):1395-1399.
- Alway, F. J. and G. R. McDole. 1917. Relation of the water-retaining capacity of a soil to its hygroscopic coefficient. Jour. Agric. Res. 9:27-71.
- Andreasen, A. H. M. and J. Andersen. 1930. Ueber die Beziehung zwischen Kornabstufung und Zwischenraum in Produkten aus losen Kornern (mit einigen Experimenten). Kolloid Zeitschrift. 50:217-228.
- Arnold, B. J., C. D. Harrison, and R. A. Lohnes. 1992. Coal handleability - Addressing the concerns of the electric utility industry. Mining Engineering. 44(1):84-89.
- Ashton, M. D., D. C. H. Cheng, R. Farley, F. H. H. Valentin. 1965. Some investigations into the strength and flow properties of powders. Rheological Acta. 4:206-218.
- Ayer, J. E. and F. E. Soppett. 1965. Vibratory compaction: I, Compaction of spherical shapes. Jour. Am. Ceramic Soc. 48(4):180-183.

- Ayer, J. E. and F. E. Soppett. 1966. Vibratory compaction: II, Compaction of angular shapes. Jour. Am. Ceramic Soc. 49(4):207-210.
- Badger, W. W. 1972. Structure of friable Iowa loess. Ph.D. Dissertation. Iowa State University, Ames.
- Badger, W. W. and R. A. Lohnes. 1973. Pore structure of friable loess. Highway Research Record. 429:14-23.
- Baver, L. D. 1956. Soil Physics. Third Edition. John Wiley and Sons, Inc., New York. 489 pp.
- Bell, W. C. 1958. An introduction to the vibratory compaction of powders. in Ceramic Fabrication Processes. W. D. Kingery, ed. Tech. Press (MIT) and John Wiley and Sons, Inc., New York. pp. 74-78.
- Bishop, A. W. 1959. The principal of effective stress. Teknisk Ukeblad. 39:850-863.
- Bishop, A. W. and G. E. Blight. 1963. Some aspects of effective stress in saturated and partly saturated soils. Geotechnique. 13(3):177-197.
- Bishop, A. W. and G. Eldin. 1950. Undrained triaxial tests on saturated sands and their significance in the general theory of shear strength. Geotechnique. 2:13-32.
- Bo, M. K., D. C. Freshwater, and B. Scarlett. 1965. The effect of particle size distribution on the permeability of filter cakes. Trans. Inst. Chem. Engrs. 43:T228-T232.
- Bradfield, B. E. 1989. Assessment of the flowability of a crushed coal by triaxial testing. M. S. Thesis. Iowa State University, Ames.
- Briggs, L. J. 1897. The mechanics of soil moisture. U.S. Dept. Agric. Bur. Soils. Bull. 10.
- Buckingham, E. 1907. Studies on the movement of soil moisture. U.S. Bur. Soils. Bull. 38.
- Capes, C. E. 1980. Particle Size Enlargement. Elsevier, New York. 192 pp.
- Carman, P. C. 1938. Fundamental principles of industrial filtration. Trans. Inst. Chem. Engrs. 16:168-188.

- Carman, P. C. 1941. Capillary rise and capillary movement of moisture in fine sands. *Soil Sci.* 52:1-14.
- Cheng, D. C. H. 1968. The tensile strength of powders. *Chem. Eng. Sci.* 23:1405-1420.
- Coulson, J. M. 1949. The flow of fluids through granular beds: effect of particle shape and voids in streamline flow. *Trans. Inst. Chem. Engrs.* 27:237-257.
- Croney, D., and D. Coleman. 1960. Pore pressure and suction in soil. *Proc. Conf. Pore Pressure and Suction in Soils.* Butterworths, London. pp. 31-73.
- Edlefsen, N. E., and A. B. C. Anderson. 1943. Thermodynamics of soil moisture. *Hilgardia.* California Agricultural Experiment Station, University of California, Berkeley. 15(2):1-298.
- Evans, P. E. and R. S. Millman. 1964. The vibratory packing of powders. *Powder Metallurgy.* Iron and Steel Inst. and Inst. of Metals, London. 7(13):50-63.
- Fredlund, D. G. 1979. Second Canadian Geotechnical Colloquium: Appropriate concepts and technology for unsaturated soils. *Canadian Geotech. Jour.* 16:121-139.
- Gardner, W. 1920. The capillary potential and its relation to soil-moisture constants. *Soil Sci.* 10:357-359.
- Graton, L. C. and H. J. Fraser. 1935. Systematic packing of spheres with particular relation to porosity and permeability. *Jour. Geology.* 43:785-909.
- Gray, W. A. 1968. *The Packing of Solid Particles.* Chapman and Hall, Ltd., London. 134 pp.
- Griffiths, F. J., and R. C. Joshi. 1989. Change in pore size distribution due to consolidation of clays. *Technical Note. Geotechnique.* 39(1):159-167.
- Haines, W. B. 1930. Studies in the physical properties of soils. V. The hysteresis effect in capillary properties, and the modes of moisture distribution associated therewith. *Jour. Agric. Sci.* 20:97-116.
- Hogentogler, C. A. 1936. Essentials of soil compaction. *Proc. Highway Res. Bd. Nat. Res. Council, Washington D. C.* pp. 309-316.

- Hogg, R. 1978. Measurement of size distributions of cement. Short Course on Cement Manufacturing Technology. The Pennsylvania State University, University Park, PA.
- Horn, H. M. 1960. An investigation of the frictional characteristics of minerals. Ph.D. Dissertation. Univ. of Illinois, Urbana.
- Jenike, A. W. 1961. Gravity flow of bulk solids. Utah Engineering Experiment Sta. Bull. 108.
- Jenike, A. W. 1964. Gravity flow of solids. Utah Engineering Experiment Sta. Bull. 123.
- Jennings, J. E. B. 1960. A revised effective stress law for use in the prediction of the behavior of unsaturated soils. Proc. Conf. Pore Pressure and Suction in Soils. Butterworths, London. pp. 26-30.
- Jennings, J. E. B. and J. B. Burland. 1962. Limitations to the use of effective stresses in partly saturated soils. Geotechnique. 12(2):125-144.
- Jury, W. A., W. R. Gardner, and W. H. Gardner. 1991. Soil Physics. Fifth Edition. John Wiley and Sons, Inc., New York. 328 pp.
- Kahaner, D., C. Moler, and S. Nash. 1989. Numerical Methods and Software. Prentice Hall, Englewood Cliffs, NJ. 495 pp.
- Kaspar, C. N. 1988. Some geotechnical properties and dehydration characteristics of five volcanic-ash-derived soils of Hawaii. M. S. Thesis. Iowa State University, Ames.
- Kocova, S. and N. Pilpel. 1973. The tensile properties of mixtures of cohesive powders. Powder Technology. 7:51-67.
- Lambe, T. W. 1960. Structure of compacted clay. Trans. ASCE. 125:682-705.
- Lambe, T. W. and R. V. Whitman. 1969. Soil Mechanics. John Wiley and Sons, Inc., New York. 553 pp.
- Levorson, S. M. 1991. The role of moisture and packing in the strength of coal filter cake. M. S. Thesis. Iowa State University, Ames.

- Levorson, S. M., and R. A. Lohnes. 1993. Coal handling and the role of moisture. Proc. Coal Handling Systems: The State of the Future III, Pensacola, Florida.
- Lohnes, R. A. and S. M. Levorson. 1992. Handling characteristics of coal. Final Report submitted to CQ, Inc., Homer City, PA by Iowa State Mining and Mineral Resources Research Inst. and Iowa State Univ. College of Engineering. Iowa State University, Ames. 97 pp.
- Linger, D. A. 1963. Effect of vibration on soil properties. Highway Research Record. 22:10-22.
- Livneh, M., J. Kinsky, and D. Zaslavsky. 1970. Correlation of suction curves with the plasticity index of soils. Jour. of Materials. JMLSA. 5(1):209-220.
- Manegold, E., R. Hofmann, and K. Solf. 1931. Ueber Kapillar-Systeme XII (1). Kolloid Zeitschrift. 55:142-159.
- Manegold, E., and W. Von Engelhardt. 1933. Ueber Kapillar-Systeme XII (2 & 4). Kolloid Zeitschrift. 62:285-294, 63:12-25, 63:149-154.
- Matyas, E. L. and H. S. Radhakrishna. 1968. Volume change characteristics of partly saturated soils. Geotechnique. 18:432-448.
- McBride, J. F., R. Horton, and M. L. Thompson. 1987. Evaluation of three Iowa soil materials as liners for hazardous-waste landfills. Proc. Iowa Acad. Sci. 94:73-77.
- McGreary, R. K. 1961. Mechanical packing of spherical particles. J. Am. Cer. Soc. 44(10):513-522.
- Nagaraj, T. S., A. Vatsala, and B. R. Srinivasa Murthy. 1990. Change in pore size distribution due to consolidation of clays. Discussion in Geotechnique. 40(2):303-309.
- Newitt, D. M. and J. M. Conway-Jones. 1958. A contribution to the theory and practice of granulation. Trans. Inst. Chem. Eng. 36:422-442.
- Olson, R. E. 1963. Effective stress theory of soil compaction. J. Soil Mech. and Found. Div., Proc. ASCE. 89(SM2):27-45.
- Orr, C. 1966. Particulate Technology. Macmillan Co., New York. 562 pp.

- Pietsch, W. 1984. Agglomerate bonding and strength. Handbook of Power Science and Technology. M. E. Fayed and L. Otten, eds. Van Nostrand Reinhold Company, Inc., New York. pp. 231-252.
- Proctor, R. R. 1933. Fundamental principles of soil compaction. Engineering News Record. McGraw-Hill Publ. Co., Inc., New York. 111:286.
- Richards, L. A. 1928. The usefulness of capillary potential to soil-moisture and plant investigations. Jour. Agric. Research. 37:719-742.
- Richards, L. A. and L. R. Weaver. 1944. Moisture retention of some irrigated soils as related to soil-moisture tension. Jour. Agric. Research. 69:215-235.
- Rowe, P. W. 1962. The stress-dilatancy relation for static equilibrium of an assembly of particles in contact. Proc. Roy. Soc. A269:500-527.
- Rumpf, H. 1958. Grundlagen und methoden des granulierens. Chemie-Ing. Tech. 30(3):144-158.
- Rumpf, H. 1962. The strength of granules and agglomerates. Agglomeration. W. A. Knepper, ed. John Wiley, New York. pp. 379-418.
- Rumpf, H. and E. Turba. 1964. Uber die zugfestigkeit von agglomeraten bei verschiedenen bindenmechanismen. Ber. Dtsch. keram. Ges. 41(2):78-84.
- Russell, E. R. and J. L. Mickle. 1971. Correlation of suction curves with the plasticity index of soils. Jour. of Materials. JMLSA 6(2):320-331.
- Salter, P. J. and J. B. Williams. 1965. The influence of texture on the moisture characteristics of soils: I. A critical comparison of techniques for determining the available-water capacity and moisture characteristic curve of a soil. Jour. Soil Sci. 16:1-15.
- Schubert, H. 1975. Tensile strength of agglomerates. Powder Technology. Elsevier Sequoia S. A., Lausanne. 11:107-119.
- Schubert, H. 1984. Capillary forces - modeling and application in particulate technology. Powder Technology. Elsevier Sequoia S. A., Lausanne. 37:105-116.

- Skempton, A. W. 1960. Effective stress in soils, concrete and rocks. Proc. Conf. Pore Pressure and Suction in Soils. Butterworths, London. pp. 4-16.
- Soil Dynamics, Deep Stabilization, and Special Geotechnical Construction. Design Manual 7.3. 1983. Dept. of the Navy, Naval Facilities Engineering Command, Alexandria, VA.
- Standard Specifications for Highway and Bridge Construction. 1984. Iowa Dept. of Transportation, Ames, Iowa.
- Taylor, D. W. 1948. Fundamentals of Soil Mechanics. John Wiley and Sons, Inc., New York. 700 pp.
- Terzaghi, K. 1936. The shearing resistance of saturated soils and the angle between the planes of shear. Proc. First Int. Conf. Soil Mech. 1:54-56.
- Terzaghi, K. and R. B. Peck. 1948. Soil Mechanics in Engineering Practice. John Wiley and Sons, Inc., New York. 566 pp.
- Thompson, M. L., J. F. McBride, and R. Horton. 1985. Effects of drying treatments on porosity of soil materials. Soil Sci. Soc. Am. J. 49:1360-1364.
- Tsunakawa, H. and R. Aoki. 1972. Tensile strength of wet granular materials. Kagaku Kogaku. 36(3):281-286.
- Tuncer, E. R. 1976. Engineering behavior and classification of lateritic soils in relation to soil genesis. Ph.D. Dissertation. Iowa State University, Ames.
- Tuncer E. R., R. A. Lohnes, and T. Demirel. 1977. Desiccation of soils derived from volcanic ash. Transportation Research Record, Trans. Res. Bd. 642:44-49.
- van Genuchten, M. Th. 1980. A closed-form equation for predicting the hydraulic conductivity of unsaturated soils. Soil Sci. Soc. Am. J. 44:892-898.
- Van Weelden, S. K. 1991. Determining the flow properties of coal by triaxial testing. M. S. Thesis. Iowa State University, Ames.

- Van Weelden, S. K. and R. A. Lohnes. 1991. Triaxial testing for determining handling characteristics of coal. Proc. Coal Handling Systems: The State of the Future II, Pensacola, Florida.
- Versluys, J. 1917. Die kapillaritat der boden. Int. Mitteilungen fur Bodenkunde. 7:117-140.
- Westman, A. E. R. and H. R. Hugill. 1930. The packing of particles. J. Am. Cer. Soc. 13:767-779.
- White, H. E. and S. F. Walton. 1937. Particle packing and particle shape. J. Am. Cer. Soc. 20:155-166.

ACKNOWLEDGEMENTS

I am deeply indebted to my wife, Janice, and children for their support and encouragement. Grateful thanks are extended to my major professor, Dr. Robert Lohnes, and members of the committee for their interest and counsel.

This work was supported by the Electric Power Research Institute through a grant from CQ, Inc. of Homer City, PA, administered by the Iowa State Mining and Mineral Resources Research Institute. The findings, opinions, recommendations, and conclusions expressed in this thesis are those of the author and do not necessarily reflect the views of the sponsors or administrators.

APPENDIX A: MOISTURE-DENSITY DATA

Gradation: D = 4.75 mm, n = 0.2
 Maximum index density = 1.97 g/cc
 Minimum index density = 1.55 g/cc

Test #	Moisture Content	Dry Density g/cc	Saturation Level	Relative Density
79	0.00%	1.968	0.00%	100.0%
44	0.30%	1.927	2.03%	91.8%
45	0.30%	1.938	2.07%	93.9%
47	3.11%	1.622	12.70%	21.0%
48	5.73%	1.618	23.28%	20.0%
64	8.76%	1.649	37.32%	28.2%
65	12.35%	1.763	63.12%	56.8%
66	15.25%	1.859	91.76%	78.2%

Gradation: D = 4.75 mm, n = 0.4
 Maximum index density = 2.26 g/cc
 Minimum index density = 1.70 g/cc

Test #	Moisture Content	Dry Density g/cc	Saturation Level	Relative Density
6	0.00%	2.243	0.00%	97.7%
5	0.00%	2.224	0.00%	95.1%
11	0.19%	2.225	2.42%	95.2%
12	0.47%	2.180	5.36%	88.9%
13	0.92%	2.091	8.63%	75.6%
14	1.67%	1.878	10.41%	38.4%
15	2.69%	1.797	14.54%	21.8%
16	3.70%	1.782	19.54%	18.8%
18	4.14%	1.796	22.36%	21.5%
7	5.20%	1.809	28.69%	24.3%
8	5.20%	1.797	28.11%	21.7%
19	5.81%	1.829	33.16%	28.5%
20	6.84%	1.894	43.69%	41.3%
21	7.28%	1.993	55.83%	59.3%
39	7.64%	2.041	64.47%	67.4%
40	8.20%	2.108	79.65%	78.1%
9	9.43%	2.132	96.76%	81.8%
38	9.44%	2.078	86.10%	73.5%
22	10.09%	2.093	94.96%	75.8%
23	10.19%	2.084	94.01%	74.3%
41	10.56%	2.073	95.14%	72.6%
10	9.84%	2.129	100.00%	81.3%
24	11.62%	2.051	100.00%	69.0%
25	12.52%	2.014	100.00%	62.8%
26	12.41%	2.018	100.00%	63.6%

Gradation: D = 4.75 mm, n = 0.5
 Maximum index density = 2.35 g/cc
 Minimum index density = 1.78 g/cc

Test #	Moisture Content	Dry Density g/cc	Saturation Level	Relative Density
27	0.37%	2.216	4.68%	80.7%
28	2.58%	1.865	15.68%	16.9%
29	5.00%	1.883	31.35%	20.8%
30	7.05%	2.162	77.55%	72.4%
31	8.12%	2.209	100.02%	79.6%
32	8.55%	2.188	100.01%	76.4%

Gradation: D = 4.75 mm, n = 0.6
 Maximum index density = 2.25 g/cc
 Minimum index density = 1.74 g/cc

Test #	Moisture Content	Dry Density g/cc	Saturation Level	Relative Density
80	0.00%	2.165	0.00%	86.6%
33	0.28%	2.184	3.24%	89.6%
34	2.70%	1.892	17.21%	35.5%
35	5.26%	1.990	40.14%	55.3%
36	7.16%	2.142	74.97%	82.7%
37	7.31%	2.270	100.00%	100.0%

Gradation: D = 4.75 mm, n = 0.8
 Maximum index density = 2.19 g/cc
 Minimum index density = 1.68 g/cc

Test #	Moisture Content	Dry Density g/cc	Saturation Level	Relative Density
46	0.11%	2.105	1.04%	86.7%
49	1.95%	1.971	14.36%	63.4%
50	3.79%	1.910	24.92%	51.7%
51	5.87%	1.922	39.46%	54.1%
56	6.28%	1.974	46.47%	64.0%
53	7.79%	2.122	78.08%	89.4%
54	8.40%	2.190	100.00%	100.0%

APPENDIX B: MOISTURE RETENTION DATA

Gradation: D = 4.75 mm, n = 0.2
 Mean dry density = 1.81 g/cc
 Relative density = 68%

Moisture Content	Potential		Apparatus*
	cm H ₂ O	kPa	
4.46%	1361.5	133.5	P
4.82%	1028.5	100.8	P
5.32%	798.7	78.3	P
5.78%	732.2	71.8	P
7.55%	459.2	45.0	P
8.01%	351.5	34.5	P
12.80%	229.7	22.5	T
16.43%	135.7	13.3	T
18.09%	88.0	8.6	H
17.18%	40.0	3.9	H
17.24%	40.0	3.9	H

*Note: P = Pressure Plate, T = Tensiometer,
 H = Hanging Water Column

Gradation: D = 4.75 mm, n = 0.4
 Mean dry density = 2.05 g/cc
 Relative density = 70%

Moisture Content	Potential		Apparatus
	cm H ₂ O	kPa	
3.69%	1406.0	137.9	P
3.90%	1055.0	130.5	P
4.28%	710.0	69.6	P
4.77%	463.1	45.4	T
5.14%	362.2	35.5	T
6.28%	312.5	30.6	T
7.47%	227.8	22.3	T
8.48%	189.9	18.6	T
9.14%	112.2	11.0	T
9.43%	77.3	7.6	H
10.86%	15.8	1.5	H

Gradation: D = 4.75 mm, n = 0.5
 Mean dry density = 2.04 g/cc
 Relative Density = 52%

Moisture Content	Potential		Apparatus
	cm H ₂ O	kPa	
2.83%	1061.5	104.1	P
3.68%	590.5	57.9	P
3.73%	386.6	37.9	P
5.57%	235.1	23.1	T
7.73%	112.0	11.0	T
9.12%	70.6	6.9	H
9.35%	40.5	4.0	H
9.94%	40.0	3.9	H
10.83%	20.0	2.0	H

Gradation: D = 4.75 mm, n = 0.6
 Mean dry density = 2.08 g/cc
 Relative density = 72%

Moisture Content	Potential		Apparatus
	cm H ₂ O	kPa	
2.47%	1384.5	135.8	P
2.65%	1019.5	100.0	P
2.78%	813.6	79.8	P
3.04%	736.2	72.2	P
3.23%	472.7	46.4	P
4.17%	208.9	20.5	T
5.83%	90.0	8.8	H
6.27%	65.5	6.4	H
7.25%	56.0	5.5	H
8.22%	40.0	3.9	H
8.16%	30.0	2.9	H

Gradation: D = 4.75 mm, n = 0.8
 Mean dry density = 2.02 g/cc
 Relative density = 65%

Moisture Content	Potential		Apparatus
	cm H ₂ O	kPa	
2.50%	945.4	92.7	P
3.26%	874.2	85.7	P
3.41%	580.2	56.9	P
3.35%	421.8	41.4	P
3.72%	272.3	26.7	T
4.65%	92.5	9.1	H
5.13%	83.3	8.2	H
5.61%	50.0	4.9	H
8.77%	21.0	2.1	H

APPENDIX C: UNCONFINED STRENGTH DATA

Notation: Ext = Failure during extrusion
 Br = Brittle failure - failure at small strain
 V Cr = Vertical cracks observed prior to failure
 Sh = Well developed shear plane at failure
 Bu = Bulging or barrelling prior to failure:
 large strains vertically and laterally
 H2O = Water draining from sample prior to failure

Gradation: D = 4.75 mm, n = 0.2

Test #	Unconfined Strength kPa	Moisture Content %	Dry Density g/cc	Comments
1	0.00	0.62%	1.71	Ext
2	0.00	0.97%	1.60	Ext
3	0.00	1.49%	1.66	Ext
4	2.82	2.16%	1.60	Br
5	5.65	2.66%	1.53	Br
6	5.79	3.07%	1.52	Br
9	8.75	4.38%	1.52	Br
10	9.21	4.78%	1.48	V Cr, Br
14	9.46	5.35%	1.49	V Cr, Br
16	9.47	5.56%	1.50	Br, Sh
23	9.50	7.86%	1.51	Sh
24	10.31	8.64%	1.53	V Cr, Br
25	9.41	8.67%	1.54	V Cr, Sh
27	10.57	9.84%	1.53	Sh
28	12.80	9.34%	1.56	V Cr, Bu
29	11.43	9.65%	1.52	V Cr, Sh
33	13.31	11.41%	1.58	Sh
35	11.95	12.09%	1.55	Sh
36	14.17	12.20%	1.59	Bu, V Cr
37	13.14	12.64%	1.58	Bu, V Cr
39	12.63	13.27%	1.60	Bu, V Cr
40	14.17	13.84%	1.62	Bu, V Cr
41	12.80	14.20%	1.61	Bu, V Cr
43	16.56	15.26%	1.67	Bu
44	31.58	15.73%	1.82	Bu, Sh
45	45.59	15.20%	1.85	Bu
46	49.68	15.72%	1.89	Bu
47	52.08	15.36%	1.87	Bu, Sh
48	51.05	15.38%	1.90	Bu
49	39.44	15.37%	1.90	Bu
50	43.54	14.20%	1.95	Bu
51	47.64	13.43%	1.98	Bu
52	38.07	13.44%	1.98	Bu

Gradation: D = 4.75 mm, n = 0.4

Test #	Unconfined Strength kPa	Moisture Content %	Dry Density g/cc	Comments
1	0.00	0.37%	1.94	Ext
2	0.00	1.05%	1.84	Ext
3	0.00	1.53%	1.77	Ext
4	0.50	2.11%	1.71	Br
5	0.50	2.50%	1.66	Br
6	7.68	2.93%	1.64	V Cr, Br
8	5.97	3.23%	1.65	V Cr, Br
9	9.38	3.68%	1.64	V Cr, Sh
11	8.70	4.11%	1.63	V Cr, Sh
12	10.75	4.55%	1.64	V Cr, Sh
13	10.41	4.99%	1.64	V Cr, Sh
14	12.12	5.31%	1.70	V Cr, Bu
15	10.07	5.73%	1.71	V Cr, Bu
16	9.04	6.19%	1.68	Bu, V Cr
17	8.70	6.48%	1.70	Bu, V Cr
18	7.68	7.23%	1.68	Bu, Sh
19	11.26	7.65%	1.77	Bu, Sh
20	7.68	7.62%	1.69	Bu
21	9.73	7.75%	1.75	Bu
22	7.85	8.21%	1.77	Bu
23	7.85	8.02%	1.73	Bu
24	7.16	8.53%	1.76	Bu
25	6.65	9.10%	2.26	Bu, Sh
26	8.87	10.18%	1.98	Bu
27	15.53	10.42%	2.00	Bu, H2O
28	24.41	7.66%	2.23	Bu
29	13.48	7.15%	2.26	Bu, H2O

Gradation: D = 4.75 mm, n = 0.5

Test #	Unconfined Strength kPa	Moisture Content %	Dry Density g/cc	Comments
1	0.00	0.41%	1.96	Ext
2	0.00	1.26%	1.80	Ext
3	0.00	2.20%	1.73	Ext
4	0.85	3.13%	1.72	Br
5	0.86	4.11%	1.69	Br
6	3.92	4.99%	1.73	Br, V Cr
7	4.43	5.92%	1.73	V Cr, Bu
9	3.92	6.90%	1.73	Bu, V Cr
10	3.92	7.65%	1.76	Bu, V Cr
11	3.58	8.80%	1.80	Bu, Sh
12	5.97	10.31%	1.94	Bu, Sh
13	11.26	10.33%	2.00	Bu, H2O
14	8.02	10.50%	2.31	Bu, H2O
15	8.70	6.67%	2.34	Bu, H2O

Gradation: D = 4.75 mm, n = 0.6

Test #	Unconfined Strength kPa	Moisture Content %	Dry Density g/cc	Comments
1	0.00	0.17%	1.92	Ext
2	0.00	1.14%	1.85	Ext
3	0.00	2.09%	1.76	Ext
4	0.50	2.93%	1.72	Br
5	0.50	4.02%	1.71	Br
6	2.72	4.88%	1.71	Br, Sh
7	2.55	5.86%	1.76	V Cr, Sh
8	2.04	6.61%	1.77	V Cr, Bu
9	2.55	7.90%	1.78	Bu, V Cr
10	1.87	8.91%	1.82	Bu, Sh
11	2.90	9.27%	1.91	Bu
12	5.97	10.60%	1.96	Bu, Sh
13	5.63	9.84%	1.96	Bu, V Cr
14	4.60	10.53%	2.00	Bu, H2O
15	5.12	10.73%	2.01	Bu, Sh
16	0.50	10.04%	2.12	Bu, H2O

Gradation: D = 4.75 mm, n = 0.8

Test #	Unconfined Strength kPa	Moisture Content %	Dry Density g/cc	Comments
1	0.00	0.21%	1.91	Ext
2	0.00	1.20%	1.82	Ext
3	0.00	2.20%	1.72	Ext
4	0.00	2.98%	1.71	Ext
5	0.00	4.00%	1.70	Sh, Ext
6	0.00	4.77%	1.70	Sh, Ext
7	0.39	6.19%	1.72	Sh
8	0.00	6.98%	1.69	Sh, Ext
9	0.00	7.77%	1.73	Sh, Ext, H2O
10	0.00	7.78%	1.71	Sh, Ext, H2O
11	0.00	9.12%	1.73	Sh, Ext, H2O